

University of Kentucky

UKnowledge

Theses and Dissertations--Chemistry

Chemistry

2022

CELL-ENGINEERED VESICLES FOR THERAPEUTIC DELIVERY AND IMMUNOMODULATORY APPLICATIONS

Khaga Neupane

University of Kentucky, me.rajneupane@gmail.com

Author ORCID Identifier:

 <https://orcid.org/0000-0003-3538-4684>

Digital Object Identifier: <https://doi.org/10.13023/etd.2022.421>

[Right click to open a feedback form in a new tab to let us know how this document benefits you.](#)

Recommended Citation

Neupane, Khaga, "CELL-ENGINEERED VESICLES FOR THERAPEUTIC DELIVERY AND IMMUNOMODULATORY APPLICATIONS" (2022). *Theses and Dissertations--Chemistry*. 170. https://uknowledge.uky.edu/chemistry_etds/170

This Doctoral Dissertation is brought to you for free and open access by the Chemistry at UKnowledge. It has been accepted for inclusion in Theses and Dissertations--Chemistry by an authorized administrator of UKnowledge. For more information, please contact UKnowledge@lsv.uky.edu.

STUDENT AGREEMENT:

I represent that my thesis or dissertation and abstract are my original work. Proper attribution has been given to all outside sources. I understand that I am solely responsible for obtaining any needed copyright permissions. I have obtained needed written permission statement(s) from the owner(s) of each third-party copyrighted matter to be included in my work, allowing electronic distribution (if such use is not permitted by the fair use doctrine) which will be submitted to UKnowledge as Additional File.

I hereby grant to The University of Kentucky and its agents the irrevocable, non-exclusive, and royalty-free license to archive and make accessible my work in whole or in part in all forms of media, now or hereafter known. I agree that the document mentioned above may be made available immediately for worldwide access unless an embargo applies.

I retain all other ownership rights to the copyright of my work. I also retain the right to use in future works (such as articles or books) all or part of my work. I understand that I am free to register the copyright to my work.

REVIEW, APPROVAL AND ACCEPTANCE

The document mentioned above has been reviewed and accepted by the student's advisor, on behalf of the advisory committee, and by the Director of Graduate Studies (DGS), on behalf of the program; we verify that this is the final, approved version of the student's thesis including all changes required by the advisory committee. The undersigned agree to abide by the statements above.

Khaga Neupane, Student

Dr. Christopher I. Richards, Major Professor

Dr. Dong Seng Yang, Director of Graduate Studies

CELL-ENGINEERED VESICLES FOR THERAPEUTIC DELIVERY AND
IMMUNOMODULATORY APPLICATIONS

DISSERTATION

A dissertation submitted in partial fulfillment of the
requirements for the degree of Doctor of Philosophy in the
College of Arts and Sciences
at the University of Kentucky

By
Khaga Raj Neupane
Lexington, Kentucky
Director: Dr. Christopher I. Richards, Professor of Chemistry
Lexington, Kentucky
2022

Copyright © Khaga Raj Neupane 2022
<https://orcid.org/0000-0003-3538-4684>

ABSTRACT OF DISSERTATION

CELL-ENGINEERED VESICLES FOR THERAPEUTIC DELIVERY AND IMMUNOMODULATORY APPLICATIONS

Development of a new kind of drug delivery system (DDS) that could efficiently deliver therapeutics to the cell of interest would allow us to accomplish cell-specific drug delivery while eliminating systemic toxicity. Although nanocarriers including endogenously released extracellular vesicles (EEVs), liposomes, and small molecules seem to be promising drug delivery systems, biological challenges persist for their use in clinical applications. Here, we demonstrate nanovesicles engineered by fragmenting cellular membranes can be exploited as versatile DDSs for therapeutics delivery as well as immunomodulatory functions. Cell-engineered vesicles were produced by cavitating cells using nitrogen gas at high pressure followed by serial centrifugation. Cell-engineered vesicles (CEVs) are smaller in size, can be generated in high yields, easily loaded with both lipophilic as well as hydrophilic cargo, and exhibit cell-targeting specificity both *in vitro* as well as in *in vivo*.

Cell-engineered vesicles generated from immune cells offer additional advantages as immunomodulatory therapeutic agents. Herein, we demonstrate that macrophage-engineered vesicles (MEVs) generated from macrophages, immune effector cells, can modulate the physiological states of immune cells including macrophages and microglia. While MEVs generated from anti-inflammatory (M2) macrophages re-program neurotoxic pro-inflammatory (M1) macrophages towards M2-like phenotype, MEVs generated from M1 macrophages re-polarize M2 macrophages towards an anti-tumor M1-like phenotype. In addition, *in vitro* and *in vivo* delivery of cargo is facilitated by the ability of these vesicles to selectively target the same cell type from which they originated.

Programming cell-engineered nanovesicles through the targeted over-expression of specific membrane-bound ligands transforms them into a more potent immunomodulatory as well as therapeutic delivery platform. We tailored membrane-derived nanovesicles to have unique immunomodulatory features, including the potential to regulate immune cell polarization in both directions. These programmable nanovesicles adorned with certain membrane-bound ligands are capable of targeting particular cell types. Using programmed nanovesicles produced from macrophages enhances immune cell reprogramming to both proinflammatory and anti-inflammatory cells. Additionally, the incorporation of cancer

cell-targeting moieties into the vesicle membrane enhanced the transport and absorption of therapeutically loaded nanovesicles, hence increasing their effectiveness.

KEYWORDS: Exosome, Nanovesicles, Macrophages, Drug Delivery, Cancer Immunotherapy

Khaga Raj Neupane
(Name of Student)

11/09/2022

Date

CELL-ENGINEERED VESICLES FOR THERAPEUTIC DELIVERY AND
IMMUNOMODULATORY APPLICATIONS

By
Khaga Raj Neupane

Dr. Christopher I. Richards

Director of Dissertation

Dr. Dong Seng Yang

Director of Graduate Studies

11/09/2022

Date

DEDICATION

To my family

ACKNOWLEDGMENTS

Firstly, I would like to express my sincere acknowledgement to my advisor, Dr. Christopher I. Richards, for his unwavering guidance and support. He always motivated me to become an independent researcher, execute innovative ideas, and accomplish new results. With his guidance, I was able to complete multiple research projects in a short period of time.

I would also like to thank my committee members, Dr. John Gensel, Dr. Jason DeRouchey, Dr. Samuel G. Awuah, and Dr. Yinan Wei, for their instructive guidance in accomplishing multiple research projects. I am grateful to all my collaborators in the research groups of Professors John Gensel, Jill Kolesar, and Pete Kekenos-Huskey. I am grateful to Dr. Timothy Kooper for training me on bone marrow extraction from mice, Dr. Rob McCorkle, and Dr. David Schweer for *in vivo* xenograft implantation and MEVs administration studies in mice. I want to thank Dr. Jennifer Moylan for allowing me to use the MSD plate reader in her laboratory. I would also like to thank Dr. Jason S. Backus for helping me with ICP-OES experiments. I would like to extend my sincerest thanks to all the current and past members of the Richards research group for their scientific suggestions, help, and collaborations.

My family has always supported me during this journey. I owe them the sincerest acknowledgement in all ways possible. I would like to remember and thank all my teachers who motivated me to become the person I am today.

TABLE OF CONTENTS

ACKNOWLEDGMENTS	iii
TABLE OF CONTENTS.....	iv
LIST OF TABLES	viii
LIST OF FIGURES	ix
CHAPTER 1. INTRODUCTION	1
1.1 Cancer	1
1.2 Therapeutic Approaches for Treating Cancer.....	1
1.2.1 Radiation Therapy.....	1
1.2.2 Chemotherapy	2
1.2.3 Immunotherapy	3
1.2.4 Innovative Cancer Therapies	6
1.3 Tumor Microenvironment.....	7
1.3.1 Macrophage Polarization in the Tumor Microenvironment	10
1.3.2 Role of M2 TAMs in Immune Suppression.....	14
1.3.3 Role of M2 TAMs in Cancer proliferation, Angiogenesis, and Metastasis..	14
1.3.4 Role of M2 TAMs in Resistance to Cancer Therapies	15
1.3.5 TAMs-based Cancer Therapy	18
1.3.6 Reprogramming TAMs for Cancer Immunotherapy	19
1.4 Drug Delivery Systems	22

1.4.1	Liposomes	22
1.4.2	Exosomes	24
1.4.2.1	Cancer Cell Released Exosomes.....	28
1.4.2.2	Immune Cell Released Exosomes.....	28
1.4.3	Cell-Engineered Nanovesicles	31
1.4.3.1	Cancer Cell-Engineered Nanovesicles.....	32
1.4.3.2	Immune Cell-Engineered Nanovesicles.....	32
1.5	Novel Approaches for Generating Cell Engineered Nanovesicles	36
1.5.1	Extrusion.....	36
1.5.2	Filtration-based Method.....	39
1.5.3	Generating Vesicles with Sonication	39
1.5.4	Generating Vesicles with Nitrogen Cavitation	40
CHAPTER 2. MACROPHAGE-ENGINEERED VESICLES FOR THERAPEUTIC DELIVERY AND BIDIRECTIONAL REPROGRAMMING OF IMMUNE CELL POLARIZATION		43
2.1	Summary	44
2.2	Background.....	46
2.3	Methods.....	48
2.4	Results and Discussions.....	55
2.4.1	Characterization of Macrophage Engineered Vesicles (MEVs).....	55
2.4.2	MEV Delivery to Macrophages.....	59
2.4.3	MEVs Reprogram Macrophage Phenotype.....	62

2.4.4	Repolarization of Microglia.....	65
2.4.5	Macrophage Induced Neurotoxicity	68
2.4.6	MEVs for Therapeutic Delivery	70
2.4.7	In vivo Delivery of MEVs to Tumor Xenografts.....	74
2.5	Conclusions.....	74
CHAPTER 3. PROGRAMMING CELL-ENGINEERED VESICLES FOR		
ENHANCED IMMUNOMODULATORY PROPERTIES		75
3.1	Summary.....	75
3.2	Background.....	75
3.3	Methods.....	77
3.4	Results and Discussions.....	83
3.4.1	MEV Characterization	83
3.4.2	MEV-mediated Phenotypic Reprogramming of M2-BMDMs.....	88
3.4.3	Role of MEV-anchored Endogenous Ligands on M2 to M1 Macrophage	
	Modulation.....	91
3.4.4	Programming Nanovesicles with Endogenous Ligands for Enhanced	
	Macrophage Repolarization	98
3.4.5	Programming MEVs with Exogenous Ligands for Enhanced Macrophage	
	Modulation.....	110
3.5	Conclusions.....	114
CHAPTER 4. CELL-DERIVED VESICLES FOR IN VITRO AND IN VIVO		
TARGETED THERAPEUTIC DELIVERY		115

4.1 Chapter Summary	115
4.2 Background.....	116
4.3 Methods.....	118
4.4 Results and Discussions.....	123
4.4.1 Characterization of Cell-Engineered vesicles.....	123
4.4.2 Targeting Specificity of CEVs Across Various Cell Types.....	128
4.4.3 In Vitro Delivery of Hydrophilic Cargo	131
4.4.4 Immunomodulatory Properties of A549 cell generated CEVs	133
4.4.5 CEV-mediated Chemotherapeutic Delivery to Cancer Cells.....	135
4.4.6 In Vivo Targeting and Delivery of Vesicles	141
4.5 Conclusion	144
CHAPTER 5. CONCLUSIONS AND FUTURE DIRECTIONS.....	146
REFERENCE.....	153
VITA.....	179

LIST OF TABLES

Table 3.1 Cytokine quantification in vesicles.....	93
--	----

LIST OF FIGURES

Figure 1.1 Tumor microenvironment.....	9
Figure 1.2 Macrophage phenotype modulation in the tumor microenvironment.	13
Figure 1.3 Tumor supportive role of M2 TAMs in the tumor microenvironment.....	17
Figure 1.4 Reprogramming TAMs for cancer immunotherapy.	21
Figure 1.5 Liposome for therapeutic delivery.....	23
Figure 1.6 Exosome for drug delivery.	26
Figure 1.7 Possible mechanism of exosome release by eukaryotic cells.....	27
Figure 1.8 Use of cell-engineered vesicles for macrophage reprogramming. This image was created with biorender.com.	35
Figure 1.9 Generation of cell-derived nanovesicles by extrusion.....	38
Figure 1.10 Nitrogen cavitation system for generating vesicles from mammalian cells..	42
Figure 2.1 Schematic illustrating the approach of generating vesicles.....	45
Figure 2.2 Macrophage-engineered vesicle (MEV) characterization.	58
Figure 2.3 Macrophage targeting specificity.	60
Figure 2.4 Reprogramming macrophage polarization with MEVs.....	63
Figure 2.5 Quantification of cytokine released by microglia.	67
Figure 2.6 Macrophage mediated neurotoxicity.	69
Figure 2.7 Targeting of MEVs onto A549 cells.	71
Figure 2.8 MEVs as biological nanocarriers.....	73
Figure 3.1 Macrophage Engineered Vesicles (MEVs) Characterization.....	85

Figure 3.2 Series of images showing DiI-labeled MEVs uptake by M2 BMDMs.	87
Figure 3.3 Reprogramming macrophage polarization by MEVs.	90
Figure 3.4 Cytokine content of MEVs.	94
Figure 3.5 Proteolytic digestion of membrane proteins present on MEVs eliminates the reprogramming capability.	97
Figure 3.6 TNF- α programmed nanovesicles cause M2 macrophages to repolarize more towards the M1 phenotype.	101
Figure 3.7 Western blot analysis of M1 and M2 macrophages compared to MEV treated M2 macrophages for p65 translocation.	102
Figure 3.8 CCL5-programmed CEVs for M2 to M1 macrophage reprogramming.	105
Figure 3.9 ICAM-1 programmed nanovesicles mediated M2 to M1 macrophage reprogramming.	108
Figure 3.10 Dose response studies.	109
Figure 3.11 Programming MEVs with TLR-ligands for enhanced M2 macrophage reprogramming towards an M1 phenotype.	112
Figure 4.1 Schematic illustrating our approach of cell-engineered vesicle generation, loading, and isolation.	125
Figure 4.2 Cell-engineered vesicle characterization.	127
Figure 4.3 Cell targeting specificity of cell-engineered vesicles.	130
Figure 4.4 Confocal image of HEK cells showing vesicle mediated cargo delivery.	132
Figure 4.5 Polarization of M0, M1 and M2 macrophages in vitro by A549EVs.	134
Figure 4.6 Efficacy of cisplatin loaded vesicles.	137

Figure 4.7 Programming BMDMs and MEVs with folate ligands.....	139
Figure 4.8 Programming MEVs with folate ligands for A549 cell targeting.	140
Figure 4.9 CEVs can reach the tumor xenograft in ice.....	143

CHAPTER 1. INTRODUCTION

1.1 Cancer

Cancer is one of the leading causes of death globally, accounting for one out of every six deaths¹. Cancer kills by rapidly disseminating aberrant cells throughout the surrounding tissue, including neurons and blood vessels, and interfering with their normal function. The American Cancer Society estimates that the United States will have an estimated 1.9 million new cancer cases and 600,000 cancer-related deaths in 2022. It is anticipated that by 2040, due to population growth and aging, there will be 27.5 million new cancer diagnoses and 16.3 million cancer deaths worldwide. The increasing prevalence of risk factors, such as smoking, poor diet, physical inactivity, and fewer births, will undoubtedly increase the future burden in economically transitioning nations. While significant progress has been made in treating cancer with existing therapeutic techniques, they are still unable to completely cure cancer. Therefore, there is an urgent necessity for the development of unique therapeutic strategies to treat this deadly disease. Surgery, radiotherapy, and chemotherapy are the most widely practiced forms of treatment for cancer, however, they themselves have limitations². Tumor resection therapy, a technique involving the surgical excision of the tumor and surrounding tissues³, is often recommended cancer treatment strategy for the treatment of primary tumors in their early stages, however, the overall success rate is still very low. A brief description of the benefits and drawbacks of existing cancer therapies is as follows.

1.2 Therapeutic Approaches for Treating Cancer

1.2.1 Radiation Therapy

Radiation therapy continues to be an important part of cancer treatment, with nearly half of all cancer patients getting radiation therapy over the course of their disease⁴. In

radiotherapy, highly energetic ionizing radiation are administered into the body in order to damage cells' genetic material (deoxyribonucleic acid, DNA), preventing future cell division and proliferation⁵. The drawback is radiation not only kills tumor cells, but also harms healthy tissue in the body. While normal cells are more capable than malignant cells in repairing DNA damage, some cells experience apoptosis as a consequence of the DNA damage, whereas others die during the cell division process because of the improperly repaired genetic damage^{6,7}. Irradiation also triggers many cell signaling pathways, which causes the release of too many immunostimulatory cytokines, thrombosis cascades, and damage to the blood vessels⁸. These changes cause swelling, ischemia, redness of the skin, high intracranial pressure in the central nervous system, and scarring of the lungs⁹⁻¹². Beside multiple complications stemming from irradiation, radiation is also responsible for the development of secondary cancers^{13, 14}.

1.2.2 Chemotherapy

Chemotherapy began to acquire importance when evidence of micro metastases and cancer recurrence after surgery and radiation treatment emerged¹⁵. Chemotherapy involves the systemic administration of high doses of anti-cancer drugs into the human body, aiming to kill quickly growing cancer cells. The commonly used chemotherapeutics kill cancer cells either by causing DNA damage or by affecting the cellular processes¹⁶. When a drug damages the DNA, several types of DNA repair mechanisms may become active depending on the nature of the damage¹⁷. Unfortunately, cells are unable to repair genetic damage in an effective manner due to the presence of high doses of cytostatic agents¹⁶. Other classes of therapeutics impede cellular activities that are involved in replication. This prevents further growth, which eventually results in the death of the cell¹⁷. While chemotherapy has

somehow boosted the survival rates of cancer patients in both children and adults, systemic administration of chemo-drugs into the human body has its inherent limitations: drugs administered have poor selectivity leading to a greater incidence of relapse in tumors and high drug-doses causing adverse effects to normal cells^{18, 19}. The adverse side effects of chemotherapeutic drugs are a direct reflection of how they work. Because these drugs nonspecifically target DNA and cellular proteins in rapidly dividing cells, they elicit adverse effects on cells present in the bone marrow, gastrointestinal (GI) tract, and hair follicles. This can cause immunosuppression, GI-related problems, infertility, liver and kidney damage, cardiac failure, neurotoxicity, tumor relapse, and metastasis^{16, 20-23}. In addition to inflicting the aforementioned side effects, the chemotherapy-based approach for treating cancer is undermined by the inherent drug-resisting properties of cancer cells. Tumor cells that were originally inhibited by an anticancer therapeutics acquire resistance throughout the course of treatment due to drug efflux, inactivation of drugs, drug target modification, damaged DNA repair, and cell death suppression^{1, 24, 25}.

1.2.3 Immunotherapy

Both radiotherapy and chemotherapy are found to weaken the immune system of the body as evidenced from the side effects of harmful radiation and high doses of chemo-drugs. In recent years a new approach of treating cancer is emerging called immunotherapy in which cells of the innate and adaptive immune system are activated to eliminate tumors from the body as well as prevent tumor relapse²⁶. Various categories of oncologic immunotherapy approaches include the use of cancer vaccines, cell-derived monoclonal antibodies (mAbs), chimeric antigen receptor (CAR) T-cell based therapies, cell signaling proteins, oncolytic viral therapies, and immune checkpoint inhibitors^{27, 28}.

One of the fundamental cancer characteristics is the ability to evade immune response²⁹. The immune system's capacity to recognize antigens on cancer cells is stimulated or restored by cancer vaccines³⁰. An example of a therapeutic dendritic cell-based vaccine with FDA clearance for the treatment of prostate cancer is sipuleucel-T³¹. The sipuleucel-T vaccine is made by using patients' own cells and, when administered in the body, makes the immune system attack prostatic acid phosphatase, an enzyme that is only found in prostate adenocarcinomas³². Sipuleucel-T vaccine is generally well tolerated, however patients taking part in clinical trials often report several adverse effects including chills, headaches, flu-like symptoms, hypertension, strokes, and cardiac arrests^{32, 33}.

A monoclonal antibody-based immunotherapeutic strategy uses antibodies made in the lab from cells that specifically target antigens on tumors and stops tumor growth by impeding tumor cell survival cascades, stopping blood vessels from growing around tumor tissue, and letting cancer cells avoid programmed cell death (PD) and circumvent immune checkpoints^{27, 34, 35}. Some monoclonal antibodies, like bevacizumab, blinatumomab, and brentuximab, have been approved by the FDA to treat cancer²⁷. However, monoclonal antibodies can cause a wide range of side effects, from mild headaches, diarrhea, temporary itching, and dermatitis to potentially fatal side effects like anaphylaxis and heart problems^{36, 37}.

Chimeric antigen receptor (CAR) T-cell based immunotherapy involves the administration of T-cells that have been genetically programmed to express CARs on the T-cell membrane^{34, 38}. Once these cells have been introduced into the patient, tumor-specific identification will take place. Following this, T-cell memory will allow the T-cells to multiply, destroying tumor cells while also conducting surveillance³⁹. The CAR T-cell based therapies, including tisagenlecleucel and axicabtagene, have been given the green light by the FDA⁴⁰. However, after being treated with CAR T-cell therapy, some patients

develop mild symptoms such as fevers, fatigue, vomiting, headaches, arthralgias, rigors, and myalgias^{41, 42}. But some patients can experience deadly symptoms like low blood pressure, fast heart rate, capillary leak syndrome, and multiple organ failure⁴³.

Therapies based on immune checkpoint inhibitors (ICI) target immunoregulatory mechanisms that certain malignancies use as a means of escaping immune surveillance⁴⁴. Immunologic checkpoints are a group of inhibitory mechanisms that are crucial in avoiding an autoimmune response. However, a wide variety of tumor forms may use immune checkpoint pathways to boost resistance against immune cells²⁷. In order for T cells to get activated, there must first be an interaction between the receptor in the T-cell and the MHC molecule on the macrophage, and then there must be a second signal generated by an additional ligand-receptor interaction. The interaction of CD80 or CD86 on macrophages or dendritic cells with CD28 molecules on T cells is one example of this kind of interaction. Alternately, CD80 or CD86 is capable of binding to an inhibitory receptor, such as cytotoxic lymphocyte antigen 4 (CTLA-4), expressed on immune cells or tumor cells⁴⁴. When this interaction takes place, the T-cell is prevented from being activated. Another major immune checkpoint pathway is mediated by the programmed death protein-1 (PD-1) expressed on T-cells and the programmed death ligand (PD-L1), mostly expressed on antigen-presenting cells and also on many tumors, where it serves to dampen the T-cell mediated immune response⁴⁵. The FDA has approved a number of checkpoint inhibitor-based immunotherapies for treating cancer. For example, atezolizumab, which targets PD-L1, is used to treat metastatic non-small cell lung cancer and advanced urothelial carcinoma; PD-L1 targeting avelumab is used to treat metastatic Merkel cell cancer; CTLA-4 targeting ipilimumab is used to treat advanced renal cell cancer; and mismatch repair deficient metastatic colorectal cancer^{27, 46, 47}. While checkpoint inhibitor-based immunotherapy approaches have been used to treat a variety of cancers, patients often experience multiple side effects after being administered with activated T-cells. Infusion reaction fatigue, diarrhea, fever, myalgias, colitis, hepatitis, pruritus, pneumonia,

dermatitis, thyroidism, hyperglycemia, nephritis, hepatitis, and nephritis are some of the most common side effects⁴⁸⁻⁵⁰.

Even though immunotherapy-based approaches seem like good ways to get rid of tumors in the body, there are still many problems with this technology that keeps cancer from being completely cured. The difficulty in predicting therapeutic efficacy and patient response to the treatment is one of the issues associated with cancer immunotherapy^{51, 52}. Other difficulties include the requirement for unique biomarkers, the emergence of resistance to existing therapies, the absence of clinical research designs that are streamlined to assess efficacy, as well as the increased costs and side effects associated with these treatments⁵¹⁻⁵⁵. These challenges demand the urgent necessity for innovative developments in cancer immunotherapy that will help to fix a lot of these problems. Newer innovations may include the development of more targeted treatments; personalized biomarker profiles; combinatorial therapies to improve efficacy and get rid of side effects; immunotherapy techniques that will reduce the number of people who get cancer; stop cancer from coming back; and lower the cost of the drugs that treat cancer.

1.2.4 Innovative Cancer Therapies

In recent years, numerous research investigations have concentrated on discovering innovative medicines to lessen the adverse effects of conventional therapies. The most known innovative approaches for cancer treatment include the use of nanomedicine, targeted therapy, gene therapy, thermal ablation of tumors and magnetic hyperthermia, and radiomics and pathomics⁵⁶. Nanomedicine involves utilizing nanoparticles ranging from endogenously released extracellular vesicles (EEVs) to synthetic liposomes and provides a diverse platform of biocompatible drug delivery devices that can specifically administer traditional chemotherapeutics *in vivo*, thereby enhancing their abundance surrounding cancer tissues, and optimizing their controlled release⁵⁷. These nanomaterials can

specifically target the tumor site minimizing their effect to the normal cells and this approach of treating cancer often known as targeted therapy⁵⁸. Similarly, genetic approaches for treating cancer, including expression of apoptosis and tumor suppressing genes, siRNAs mediated targeted gene silencing, are currently being evaluated in several clinical trials throughout the world⁵⁹⁻⁶¹. In addition, aiming to discover an alternative to more intrusive methods such as tumor surgery, precision medicines, including thermal ablation and magnetic hyperthermia, that localize treatments to a specific tissue of interest, have shown potential as an effective therapeutic strategy for the treatment of cancer^{62, 63}. Furthermore, novel disciplines such as radiomics and pathomics are leading to the creation of new methods for gathering massive quantities of data, developing novel therapy techniques^{64, 65}, and predicting correct responses, clinical outcomes, and tumor relapse^{66, 67}. Overall, these novel methodologies suggest that integrating several disciplines could lead to the discovery of cancer treatments with the best clinical outcomes. Despite the fact that a number of these ways for treating cancer have shown promise as potential alternatives, recurrence and metastasis continue to pose obstacles for these methods. Numerous of these limitations call for the immediate development of cutting-edge therapeutic methods to treat cancer.

1.3 Tumor Microenvironment

The physiological make-up of the tumor plays a primary role in the response to treatment. The notion of tumor microenvironment (TME) goes back to 1863, when Virchow established the link between inflammation and cancer^{68, 69}. The tumor microenvironment (TME) not only consists of tumor cells but also endothelial cells, immune cells including microglia, macrophages, and lymphocytes, signaling molecules including cytokines and chemokines, and the extracellular matrix^{68, 70, 71}. The interaction between tumor cells and its microenvironment often promotes the initiation and

development of malignant tumors⁷². Cancer cells present in the TME release signaling proteins that enhance blood vessel formation as well as immune evasion, whereas immune cells present in the microenvironment can release signaling molecules that enhance tumor metastasis⁷³⁻⁷⁵ (Figure 1.1).

Tumor Microenvironment

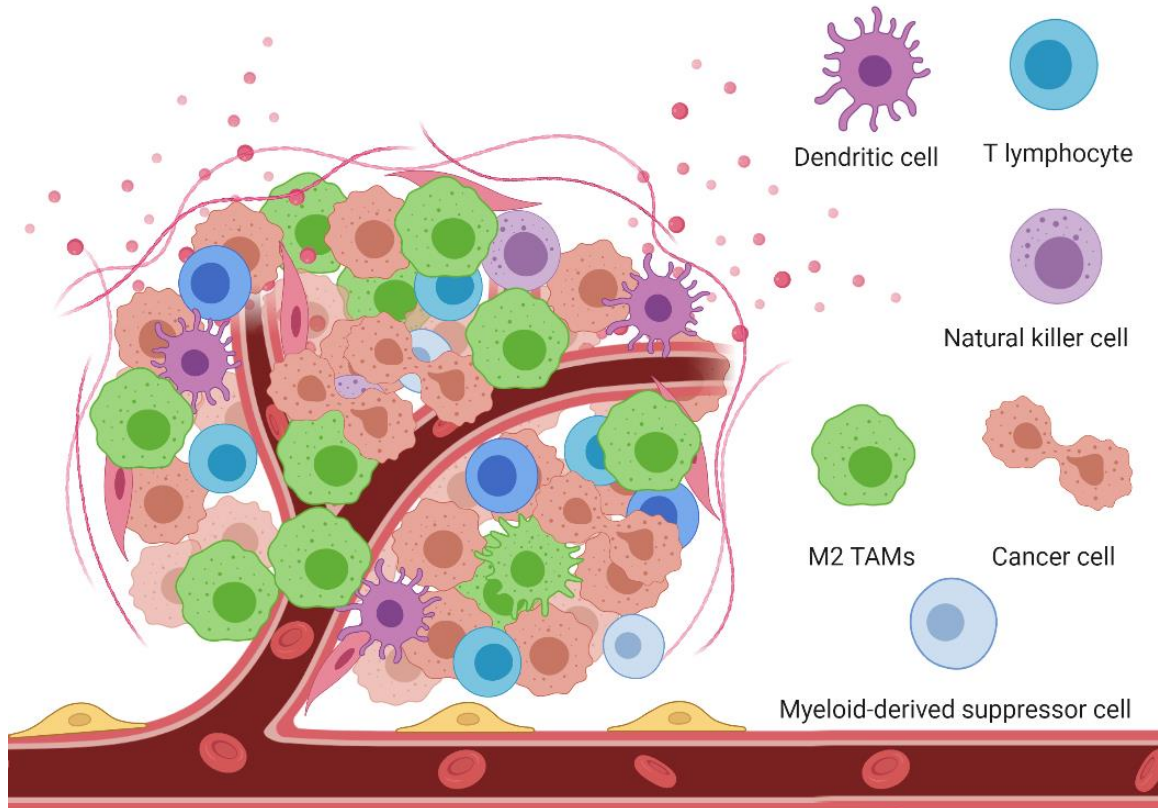


Figure 1.1 Tumor microenvironment.

The tumor microenvironment is composed of cellular and non-cellular portions. Cancer cells, endothelial cells, carcinoma-associated fibroblasts, and immune cells including tumor associated macrophages (TAMs), dendritic cells, B-cells, and T-cells, among others make up the cellular component. The extracellular matrix functions as a scaffold and reflects the non-cellular constituents of the tumor microenvironment. Multiple mechanisms, including the extracellular matrix, cell-cell interactions, and the secretion of cytokines, chemokines, and extracellular vesicles, contribute to the interplay between the various components of the tumor microenvironment. This image was created with [biorender.com](https://www.biorender.com).

1.3.1 Macrophage Polarization in the Tumor Microenvironment

Macrophages are the most common kind of immune cell seen in the tumor microenvironment, and they play both pro- and anti-tumorigenic roles as shown in Figure 1.2. Macrophages have an important function in the progression, maintenance, and clearance of cancer cells. Macrophages are able to adapt reversible physiological states in response to environmental cues, which allows them to play a variety of roles in the tumor microenvironment. In fact, they exhibit a continuum of functional states between a pro-inflammatory, entitled as M1 functional state, and an anti-inflammatory state, classified as M2. Macrophages that are either native to the tumor tissue or that have been attracted to the tumor microenvironment are often described as tumor-associated macrophages (TAMs)⁷⁶. Tumor-associated macrophages (TAMs) are known to originate from either circulating bone marrow-derived monocytes that change into TAMs after tissue infiltration or from tissue-resident macrophages that develop from embryonic progenitors that are implanted in resident tissues^{77, 78}. TAMs make up the majority of the cells in a tumor's microenvironment, and their functional states determine the progression or elimination of tumor cells⁷⁶. The process of polarization of TAMs is directly regulated by cancer cells that are located inside the tumor microenvironment, and the phenotypic ratio undergoes significant changes as the progression of cancer continues⁷⁹. In the beginning phases, the ratio is more advantageous for M1 macrophages; but, when cancer cells begin to hijack this process, the number of M2-like macrophages dramatically rises^{79, 80}.

M1 macrophages, also known as classically activated macrophages or pro-inflammatory macrophages, are characterized by the production of high levels of pro-inflammatory and immunostimulatory cytokines including interleukin (IL)-12, and tumor necrosis factor (TNF)- α . M1 macrophages exhibit antitumor activity and are able to

scavenge and kill the phagocytosed tumor cells. M1-like macrophages are a key kind of tumor-suppressing cell that first work inside the microenvironment of a tumor to inhibit the proliferation of tumor cells⁷⁹. M1-like macrophages execute anti-tumoral properties by attracting and activating CD8⁺ T and natural killer cells to the tumor microenvironment through antigen presentation and tumor associated release of chemokines including CXCL9, CXCL10, and CXCL11^{81, 82}. Upon activation, CD8⁺ T cells and natural killer cells release large amounts of pro-inflammatory cytokines like IFN- γ , GM-CSF, and TNF- α , as well as chemokines like CCL4, CCL5, and CCL23, which help bring in more immune cells and activate anti-tumorigenic pathways^{79, 83}. Phenotypically, M1 macrophages display elevated amounts of co-stimulatory markers CD80 and CD86, major histocompatibility complex class II (MHC II), and Th1 cell-attracting chemokines CXCL9 and CXCL10⁸⁴. M1 cells also secrete inducible nitric oxide synthase (iNOS), interleukin-12, and interleukin-1 that execute antitumoral functions^{85, 86}. The antitumor properties of the M1 phenotype are well known, and a higher M1/M2 TAM ratio has been linked to longer life durations and the best clinical outcomes in several solid tumors, including but not limited to breast, ovarian, lung, colorectal, gastric, liver, renal, and oral squamous cell carcinoma^{85, 87-91}.

As the tumor grows, cancerous cells may release M2-modulating cytokines and growth factors, such as IL-10, CCL2, CCL3, CCL4, CCL5, CCL7, CCL8, CXCL12, vascular endothelial growth factor (VEGF), and platelet-derived growth factor (PDGF), to draw more monocytes and M0 macrophages to the tumor microenvironment and turn them into M2 phenotype⁸⁵. M2 macrophages, also known as alternatively activated macrophages or anti-inflammatory macrophages, release high levels of immunosuppressive cytokines including IL-10, IL-13, and IL-4 and growth factors including vascular endothelial growth factors (VEGFs). Phenotypically, M2 macrophages express higher levels of distinct membrane markers including CD206, chemokine and chemokine receptors including CCL17, CCL22 and CCL24. Most macrophages present in the tumor exhibit M2-like

functional states, and a higher M2/M1 ratio is linked to an adverse clinical outcome in many types of cancer⁹². M2 TAMs present in the tumor microenvironment have been shown to have a direct connection to the development of tumors via the processes of angiogenesis, enhanced metastasis, and immune evasion and therapy resistance^{76,93}. While TAMs adopt tumor-supportive M2-phenotype, their phenotype is flexible. Therefore, given the relevant conditions, macrophages can be reprogrammed with immunosuppressive activity.

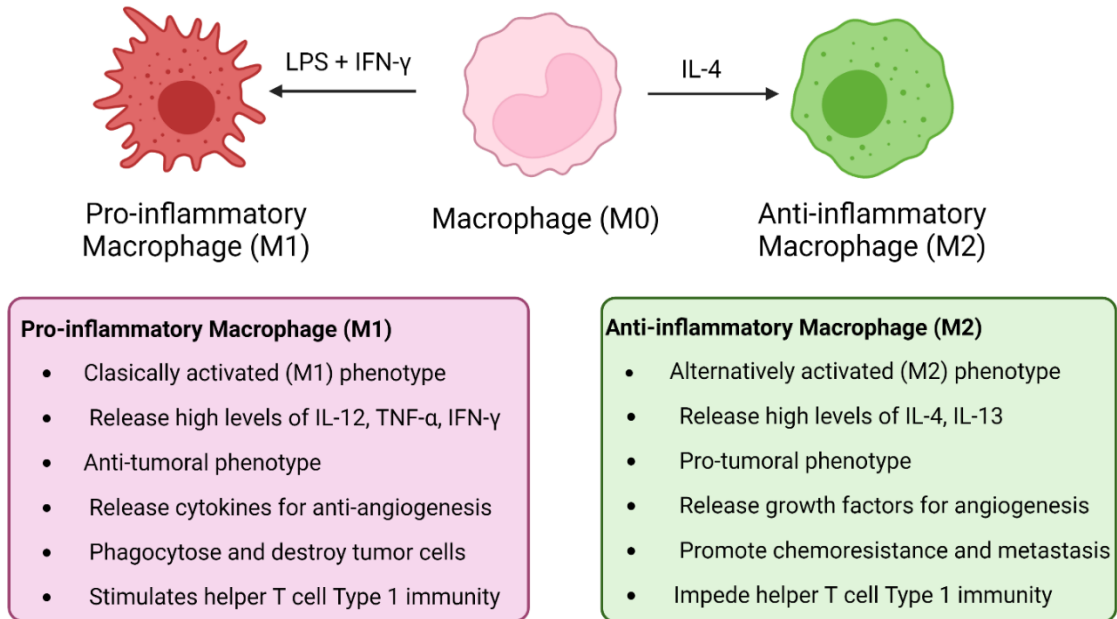


Figure 1.2 Macrophage phenotype modulation in the tumor microenvironment.

Various cell signaling molecules released by cells present in the tumor microenvironment can modulate macrophages towards either a pro- or anti-inflammatory phenotype. This image was created with biorender.com.

1.3.2 Role of M2 TAMs in Immune Suppression

M2-type macrophages dampen the immune response in the tumor microenvironment by secreting immunosuppressive factors including IL-10, IL-13, TGF- β , and human leukocyte antigen G (HLA-G)⁹⁴. In addition, M2-type macrophages can directly communicate with myeloid-derived suppressor cells (MDSC) and substantially dampen anti-tumor T-cell responses⁹⁵. M2 TAMs are also characterized by an increased expression of immune-suppressing ligands, including programmed cell death ligand 1 (PD-L1) and cytotoxic T-lymphocyte antigen 4 (CTLA4)⁸⁰. PD-L1 and CTLA4 are well-known immune checkpoints for cytotoxic T-cells and are characterized by their ability to impair the capacity of cytotoxic T-cells to kill cancerous cells present in the tumor microenvironment⁹⁶⁻⁹⁸. In investigations of individuals with hepatocellular carcinoma (HCC), higher levels of PD-L1 expression by tumor-associated macrophages (TAMs) were associated with worse clinical outcomes than those with lower PD-L1 expression⁹⁹. Recently, M2 TAMs were also found to express B7-H4, an immunosuppressive surface ligand, and it has been shown that B7-H4⁺ TAMs decrease CD4⁺ T-cell proliferation and IFN-production more than B7-H4⁻ TAMs, resulting in increased immunological evasion and suppression by TAMs⁹⁷.

1.3.3 Role of M2 TAMs in Cancer proliferation, Angiogenesis, and Metastasis

Cancer is characterized by a number of distinct features, one of which is uncontrolled growth. Tumor associated M2 macrophages are able to produce growth factors including transforming growth factor beta (TGF- β) and epidermal growth factor (EGF) that have the potential to have a direct impact on the proliferation of cancer cells^{100, 101}. These growth factors enhance tumor proliferation by activating signaling pathways that prevent apoptosis, promote proliferation and invasion, and promote metastasis¹⁰².

Similarly, tumor associated macrophages contribute significantly to angiogenesis⁷⁶. Angiogenesis is a vital process for the longevity of cancerous tissue since it provides nutrition and oxygen for its continued development. TAMs have been identified in animal models of ovarian, cervical, prostate, breast and cervical cancer as playing a crucial role in tumor angiogenesis¹⁰⁰. TAMs can detect hypoxia in tumors and stimulate matrix metalloproteinase 9 (MMP9) expression at greater levels. This increased MMP9 promotes the breakdown of extracellular matrix and the liberation of bioactive vascular endothelial growth factor A (VEGFA) in the tumor microenvironment¹⁰⁰. Tumor associated macrophage also contribute to the beginning of metastasis through the production of pro-angiogenic cytokines and growth factors^{103, 104}. Studies conducted *in vitro* have shown a relationship between the release of TNF- β by macrophages and an increase in the activity of the PI3K and AKT signaling pathways, which in turn promotes cell migration and invasion^{105, 106}. TGF- β is a tumor suppressing protein that impedes proliferation and promotes apoptosis in the early stages of tumor growth¹⁰⁷. However, as the tumor progresses, tumor cells eventually overcome the inhibitory effects of TGF- β . TGF- β then initiates the epithelial–mesenchymal transition (EMT), which promotes invasion and metastasis¹⁰⁷. TGF- β is overexpressed in several malignancies and M2 TAMs and this overexpression is linked to tumor growth, metastasis, angiogenesis, and a dismal prognosis¹⁰⁸.

1.3.4 Role of M2 TAMs in Resistance to Cancer Therapies

M2 tumor associated macrophages play an important role in inflicting resistance to multiple cancer therapies⁷⁶ (Figure 1.3). It has been found that tumor associated M2 macrophages are more resistant to radiation therapy than pro-inflammatory M1 macrophages making it challenging to treat cancer¹⁰⁹. TAMs that have an M2-phenotype also play a role in resistance to anti-angiogenic treatment by boosting the number of M2-

like macrophages in the tumor microenvironment (TME) following treatment with anti-angiogenic drugs¹¹⁰. TAMs are subject to phenotypic alterations as a result of chemotherapy⁷⁶. It was shown that the expression of genes associated with epithelial-to-mesenchymal transition was elevated in macrophages that had been treated with cisplatin and were cocultured with ovarian cancer cell lines¹¹¹. Treatment of tumors in mice with paclitaxel or carboplatin was negated by an enhanced secretion of IL-10 from tumor associated macrophages, leading to a downregulation of IL-12 expression by dendritic cells and a suppression of CD8⁺ T-cell mediated anti-tumor activity¹¹². TAMs are also a potential contributing factor in patients' resistance to immunotherapy that blocks immune checkpoints. M2 tumor associated macrophages express ligand molecules including PD-L1 or PD-L2 for check-point receptors, PD-L1/2 may hijack anti-checkpoint ligand monoclonal antibodies, making them ineffective cancer treatment¹¹³.

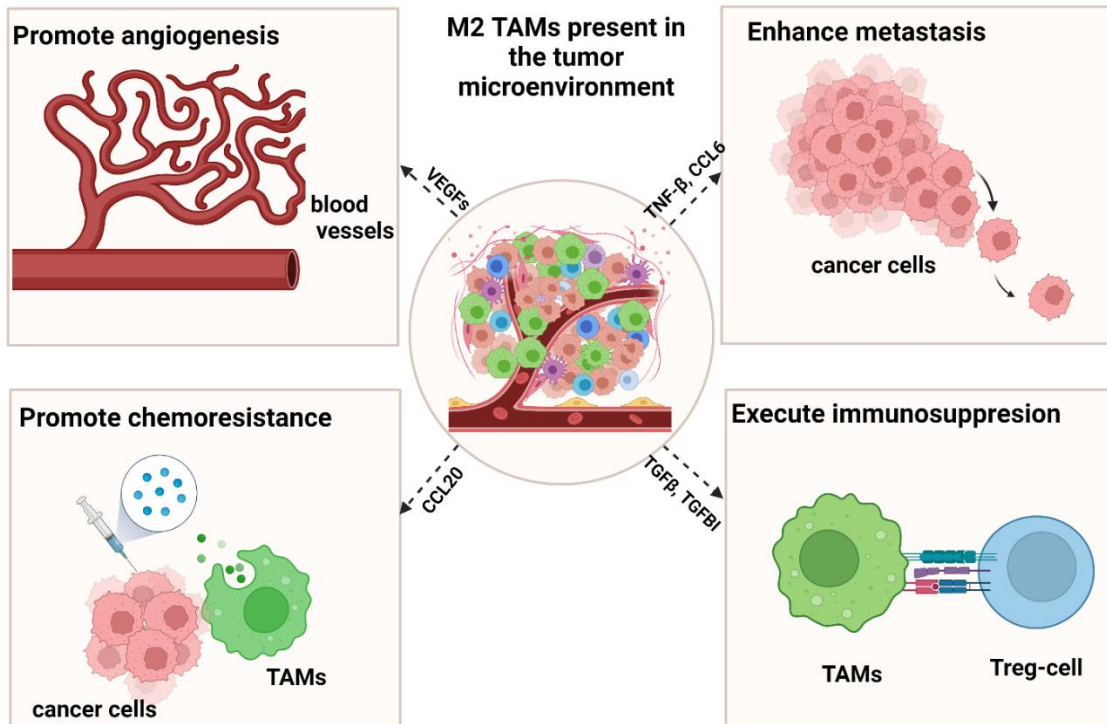


Figure 1.3 Tumor supportive role of M2 TAMs in the tumor microenvironment.

Different growth factors, cytokines, chemokines, or membrane proteins expressed by M2 TAMs in the tumor microenvironment help with angiogenesis, metastasis, chemoresistance, and shutting down the immune system. This image was created with biorender.com.

1.3.5 TAMs-based Cancer Therapy

Because TAMs are predominantly present in the tumor microenvironment and significantly contribute to immune suppression, tumor proliferation, angiogenesis, and metastasis, researchers are focusing on the development of newer therapeutics that target TAMs. Some of these treatments have been created with the intention of either inhibiting the recruitment of new TAMs, killing off existing TAMs, or reprogramming TAMs such that they have an M1 phenotype¹⁰⁷. Because colony-stimulating factor-1 (CSF-1) is one of the well-known tumor-derived factors that leads to monocyte recruitment via CCL2/CCR2 interaction, CCR2 blocking medications can inhibit TAM recruitment¹¹⁴. Some success has been seen with CCR2 inhibitors or anti-CCL2 monoclonal antibodies in pre-clinical murine breast cancer models^{115,116}. However, when anti-CCL2 therapy was stopped, mouse breast cancer models showed a resurgence effect, which led to more circulating monocytes getting into the tumor microenvironment and accelerated lung metastasis¹¹⁷.

Other sets of therapies aim to deplete TAMs present in the tumor microenvironment aiming to stop the activities of TAMs in tumor growth and therapy resistance. The colony-stimulating factor-1 (CSF-1) and colony-stimulating factor-1 receptor (CSF-1R) interaction is an intriguing target for lowering the quantity of TAMs since CSF-1 is essential for macrophage survival and proliferation¹⁰⁷. In a preclinical mouse model, the monoclonal antibody emactuzumab targets CSF-1R, lowering the number of TAMs and boosting the CD8⁺/CD4⁺ T-cell ratio in the TME¹¹⁸. The use of small molecules such as PLX3397 that block CSF-1R boosted CD8⁺ T-cell infiltration and enhanced therapeutic response in many mouse tumor models¹¹⁹. While targeting the CSF-1/CSF-1R route looks to be a promising strategy, studies have shown that long-term CSF-1R inhibition might lead to PI3K pathway activation and therapeutic resistance over time⁸⁰.

Another treatment paradigm that shows promise is a technique for reprogramming tumor-supportive M2 macrophages to a tumor-killing M1 phenotype¹²⁰. TAMs are the most numerous immune cell type in the tumor microenvironment. The repolarization of macrophages to an anticancer phenotype bears theoretical promise since a greater M1/M2 ratio in the tumor microenvironment corresponds with improved survival results in cancer patients¹²¹. Numerous approaches to repolarizing M2 TAMs have been investigated, all with the intention of improving precise targeting and reducing the number of unintended side effects.

1.3.6 Reprogramming TAMs for Cancer Immunotherapy

Accomplishing successful reprogramming of TAMs towards an M1 phenotype as shown in Figure 1.4 could be a clinically effective strategy to quench the pro-tumor activities and promote the anti-tumor immunity executed by macrophages present in the tumor microenvironment^{76, 122}. Existing strategies to selectively re-modulate macrophage physiology include the use of small molecules, including toll-like receptor (TLR) agonists¹²³ and tumor necrosis factor superfamily receptor (TNFSR) agonists. However, such molecules modulate multiple cell types, thereby inducing systemic toxicity¹²². Besides, the use of small molecules for therapeutic applications is compromised because of their rapid degeneration, inability to enhance anti-tumor functions in the recipient macrophages, and increased toxicity if used for prolonged periods. Other alternative approaches for macrophage reprogramming include the use of genetic materials, including in vitro transcribed mRNA, siRNA delivered using nanoparticles¹²². While such therapeutic approaches show modest ability to reprogram M2 like TAMs to M1 phenotypes, specificity remains challenge¹²². Liposomes loaded with therapeutics have been employed as nanocarriers as an alternative to small molecules and TLR-agonists; nevertheless, liposomes display non-specific targeting and are susceptible to clearance by

the immune system¹²⁴. Additionally, endogenous extracellular vesicles (also known as EEVs) that are produced by immune cells have been employed as an alternate method to convert TAMs into M1-like cells¹²⁵. Exosomes, which are generated by M1 macrophages as a result of normal physiological processes, have only recently been used in an effort to reprogram M2-TAMs in the direction of an M1 phenotype¹²⁵. Although exosomes have innate targeting specificity and the capacity to change macrophage phenotype in the microenvironment of a tumor, EEV-based treatments are restricted due to their poor manufacturing yield and the difficulty of separating the components¹²⁶. Nanovesicles formed from immune cells provide a number of benefits, including a high yield, the capability to target the cells from which they were created, and the capacity to reprogram the polarization of immune cells¹²⁷.

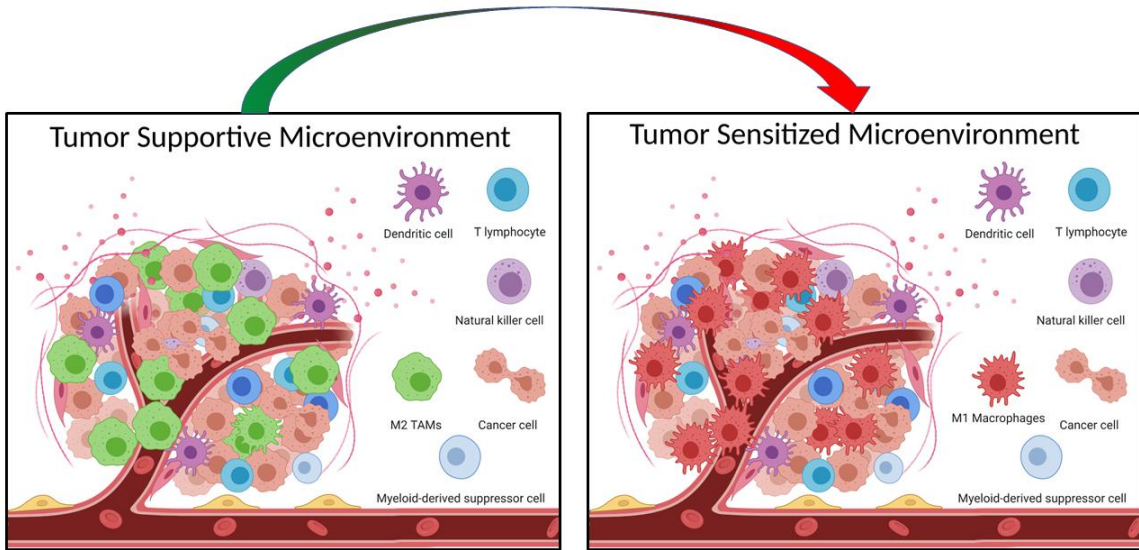


Figure 1.4 Reprogramming TAMs for cancer immunotherapy.

Modulating tumor-supportive M2 TAMs towards a tumor-killing M1 phenotype is one of the many immunotherapy approaches for treating cancer. This image was created with biorender.com.

1.4 Drug Delivery Systems

Treatment of cancer by conventional methods, including chemotherapy or immunotherapy, involves a systemic drug administration approach wherein drug molecules not only interact with the targeted tumor cells or immune cells but also with all other cells in the body. This strategy results in undesirable side effects, including the death of normal cells or an undesired immunological response. An alternative to this form of therapeutic administration is the delivery of therapeutic agents to the specific cells of interest. Researchers have recently become very interested in discovering an ideal drug delivery system that can be loaded with almost any type of drug molecule, is less immunogenic and biocompatible, can reach the targeted site selectively, and can release the drug continuously at the targeted site for a long time¹²⁸. Synthetic drug delivery systems like nanoformulations such as gold nanoparticles¹²⁹, carbon nanotubes¹³⁰, liposomes¹³¹, polymeric nanoparticles¹³² and dendrimers¹³³ are often used for targeted delivery to the specific tissue of interest. Similarly, endogenously released extracellular vesicles (EEVs) including exosomes, and microvesicles offer multiple advantages for their use as a drug delivery system. A brief description of the commonly used DDSs is as follows.

1.4.1 Liposomes

When it comes to targeted therapeutics delivery, liposomes are by far the most prevalent and extensively researched drug delivery systems. Liposomes are synthetic vesicles that have a spherical structure and can be manufactured using cholesterol and phospholipids¹³⁴. Liposomes may vary in size from 30 nm to several micrometers¹³⁴. Liposomes possess an aqueous center surrounded by one or more lipid bilayers as in Figure 1.5.

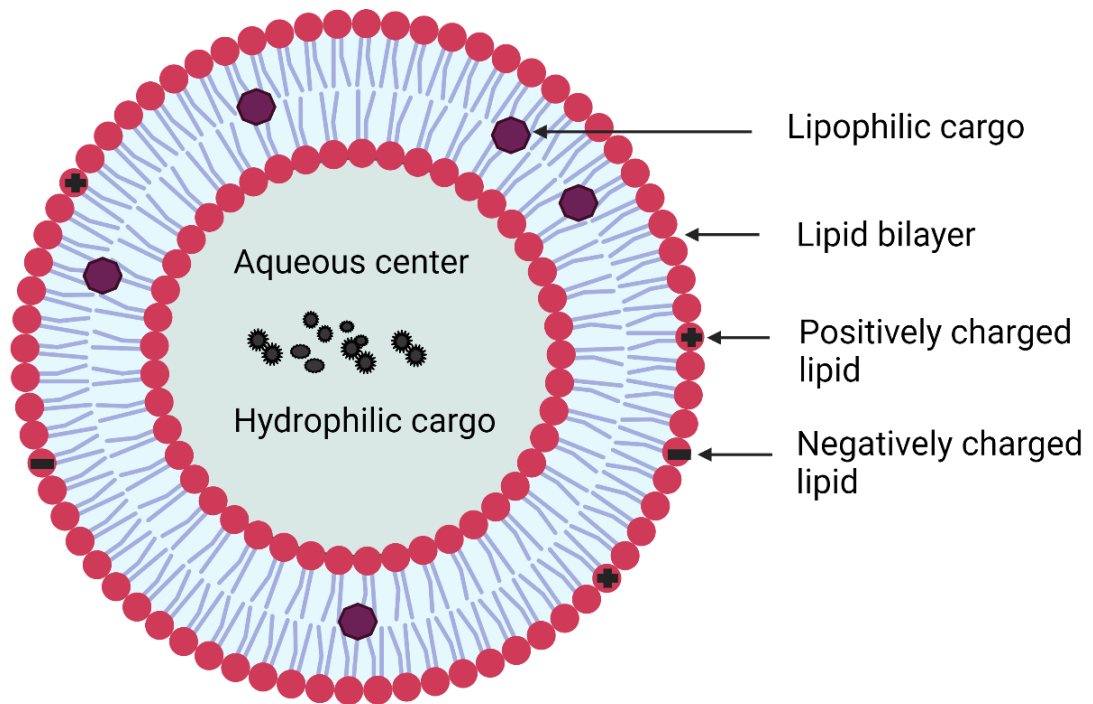


Figure 1.5 Liposome for therapeutic delivery.

Liposomes are spherical vesicles made up of at least one lipid bilayer surrounded by an aqueous core. Hydrophilic drug molecules can be trapped into the aqueous center, whereas lipophilic molecules can be loaded in the lipid bilayer. This image was created with biorender.com.

Hydrophilic drug molecules can be trapped inside of the vesicles whereas lipophilic cargo can be adsorbed onto the vesicle's phospholipid bilayer^{135, 136}. Liposomes have been utilized to encapsulate and securely transfer a wide array of therapeutics including antioxidants, cloned genes, recombinant proteins, and anticancer drugs, to the target tissue^{135, 137}. Liposomes-based cancer therapeutics recently created a lot of excitement after attaining FDA approval¹³⁸. While liposome-based therapeutics have been shown to be beneficial for a variety of biomedical applications, their efficacy is compromised by several biological obstacles, including clearance by immune cells present in the reticuloendothelial system (RES)¹³⁹.

1.4.2 Exosomes

To overcome the limitations of liposome-based drug delivery systems, recently scientists have developed exosomes, extracellular vesicles secreted endogenously by most eukaryotic cells involved in cell-cell communication, as therapeutic delivery systems. Exosomes are nanosized lipid bilayer membrane bound vesicles generated naturally by most eukaryotic cells¹⁴⁰. The size of the exosome ranges from 30-100 nm. Exosomes have many advantages as a drug delivery system. Firstly, they contain different types of membrane proteins, lipids, DNA, mRNA and miRNA specific to the cell from which they were originated which helps not only in intercellular communication, but also carrying biological information between such cells¹⁴¹⁻¹⁴³ (Figure 1.6). The smaller size of exosomes (50-100 nm) makes them stable in the blood for a prolonged period after administration into the body. Furthermore, exosomes are highly biocompatible and less immunogenic thus avoiding phagocytosis by macrophages^{140, 144}.

The process of exosome formation often begins when an endocytic vesicle is produced from the inward budding of the small region of the plasma membrane of the cell as shown in Figure 1.7. Next, during the process of maturation of the endocytic vesicle,

tiny vesicles are formed within the lumen. Intraluminal vesicles contain biological cargo associated with cells, such as proteins, membrane receptors, and genetic materials. The endosomes that have developed fully and include intraluminal vesicles are referred to as multivesicular bodies (MVBs). The MVBs either target the intraluminal vesicles to the lysosomes to begin the process of destruction, or the MVBs travel to the cell surface and fuse with the cell membrane, resulting in the release of these vesicles from the cell. The intraluminal vesicles released by this process are called extracellular vesicles. Extracellular vesicles whose diameter is below 100 nm are called exosomes.

Exosomes have many advantages as a drug delivery system. Due to significant clinical breakthroughs made in recent years, immunotherapy for cancer has garnered an unusual amount of interest. In the field of cancer immunotherapy, the use of endogenously released extracellular vesicles (EEVs) has helped to alleviate some of the difficulties posed by immunotherapy. Because of the multiple advantages they offer, EEVs have become one of the natural biomaterials that are highly favored for use in immunological engineering and therapeutic delivery. Herein , we provide a concise summary of the applications of the most commonly used EEVs for the treatment of cancer.

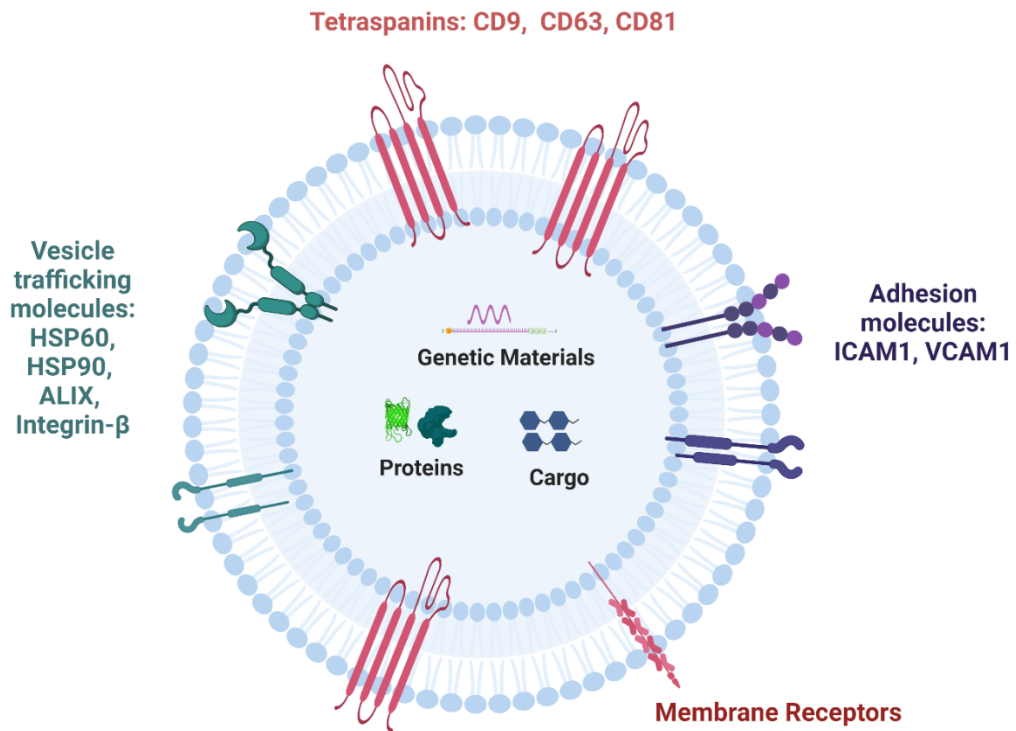


Figure 1.6 Exosome for drug delivery.

An exosome is an endogenously released extracellular vesicle that has a hydrophilic center surrounded by a lipid bilayer. In the aqueous center, there are biological molecules like proteins, mRNA, and miRNA. However, the outer lipid bilayer membrane expresses a large number of plasma membrane proteins. This image was created with biorender.com.

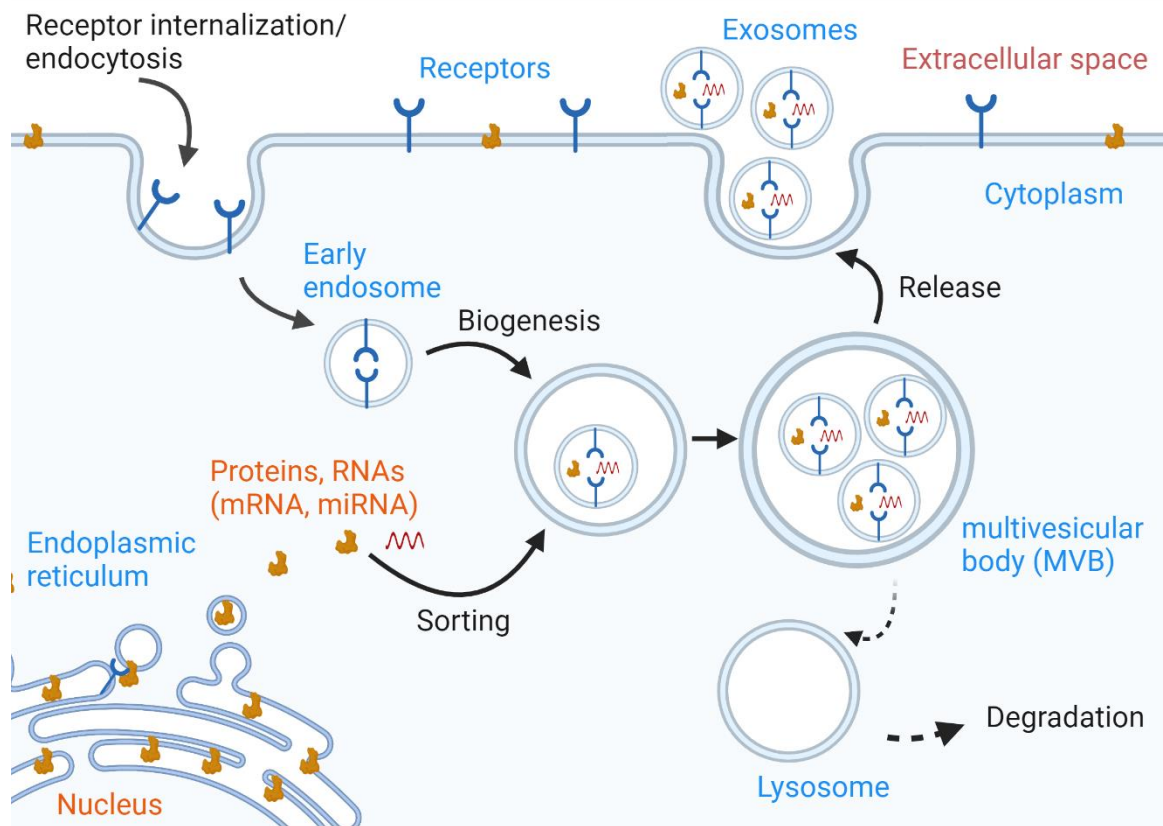


Figure 1.7 Possible mechanism of exosome release by eukaryotic cells.

The process of exosome formation starts at the cell membrane when cells internalize membrane receptors by inward budding of the plasma membrane to form an endosome. Early endosomes undergo maturation to form multivesicular bodies that contain intraluminal vesicles. Multivesicular bodies, when fused with the plasma membrane, release exosomes into the extracellular space. This image was created with biorender.com.

1.4.2.1 Cancer Cell Released Exosomes

EEVs produced by tumor cells offer several useful characteristics for cancer treatment, including prolonged circulation, targeting specificity, and antigen stimulation. Tumor cell derived EEVs express the innate immunological checkpoint CD47, a negative signal of phagocytosis¹⁴⁵, and therefore can avoid being consumed by macrophages. This helps them to persistently circulate in the body for a prolonged period of time¹⁴⁶. In addition, EEVs from tumor cells house surface adhesion molecules including N-cadherin and galectin-3, which allow these vesicles to specifically target the tumor tissue *in vivo*^{147, 148}. Furthermore, EEVs from tumor cells inherit tumor antigens and may therefore be endowed with immunological adjuvants for the production of cancer therapeutics¹⁴⁹⁻¹⁵¹. While use of EEVs offer several advantages, some of the tumor cell-expressed immunosuppressive proteins, including as PD-L1, Galectin-9, and Siglec-15, may be housed in these vesicles and limit the activity of tumor-infiltrating lymphocytes¹⁵²⁻¹⁵⁴.

1.4.2.2 Immune Cell Released Exosomes

Bone marrow stem cells differentiate into immune cells, including lymphocytes (B cells and T cells), antigen-presenting cells (macrophages and dendritic cells), neutrophils, and natural killer (NK) cells¹⁵⁵⁻¹⁵⁸. Extracellular vesicles, including exosomes released by these immune cells, are known for executing multiple functions ranging from the activation of innate as well as adaptive immunity to wound healing, cancer cell proliferation, and metastasis¹⁵⁹⁻¹⁶¹.

Mesenchymal stem cells (MSCs) are an important class of immune cells present in the tumor microenvironment. It has been shown that MSC-secreted EVs, when delivered *in vivo*, show immune tolerance, and could execute immunomodulatory functions by transporting factors from the parent cell to the targeted cell¹⁶². Fattore et al. recently

discovered that the EVs released from MSCs execute immunosuppressive functions on regulatory T cells¹⁶³. Lee et al. studied the role of MSC-derived EVs on breast cancer and found that exosomes from mesenchymal stem cells reduce the expression of vascular endothelial growth factor (VEGF) in breast cancer cells, which inhibits angiogenesis¹⁶⁴. Recently, it has been shown that through the activation of hepatocyte growth factor, microvesicles that are generated from human Wharton's jelly mesenchymal stem cells are able to increase the proliferation and aggressiveness of human renal carcinoma cells¹⁶⁵. While MSC-derived EVs are safe and low-immunogenic drug delivery systems, depending on the nature and stage of progression of the tumor, EVs from MSCs may either inhibit or enhance tumor growth¹⁶⁶.

Lymphocytes including T cells, and B cells execute the majority of adaptive immune responses. While T lymphocytes contribute to cellular immunity, B cells maintain humoral immunity¹⁶⁷. Recently, Tung et al. isolated extracellular vesicles from regulatory T-cells (Treg) and found that Treg-derived EVs modify the dendritic cell function by miRNA transfer¹⁶⁸. In another study, Lu et al. isolated CD4⁺ T cell-derived extracellular vesicles from activated CD4⁺ T cells and used those EVs for *in vivo* delivery in mice¹⁶⁹. They found that mice treated with Treg vaccine had a strong humoral immune response. In addition, they discovered that Treg EVs promote activation, proliferation, and antibody production by B cells. These results indicated that EVs isolated from CD4⁺ T cells could be used as an immunomodulatory therapeutic platform to enhance humoral immune responses¹⁶⁹. Zhang et al. found that CD19⁺ EVs isolated from B cells could inhibit CD8⁺ T cell-mediated immune responses, thereby reducing the efficacy of chemotherapy used for tumor treatment¹⁷⁰.

Recently, EVs isolated from antigen-presenting cells like dendritic cells and macrophages have attracted huge interest in the scientific community for their potential use in cancer immunotherapy. Dendritic cell (DC)-derived EVs were found to express major histocompatibility complexes (MHC) class I and class II molecules that could interact with

proteins on activated T cells, stimulate anti-tumor immunity, and promote Th1 cell secretion of interferon (IFN- γ)¹⁷¹⁻¹⁷³. The majority of EVs released by mature DCs contained IFN- γ , a proinflammatory cytokine that can elicit an anti-tumor immune response¹⁷⁴. EVs isolated from mouse bone marrow dendritic cells (BMDCs) have been shown to activate CD8⁺ T cells to inhibit tumor growth¹⁷⁵. EVs made from BMDCs caused B cells to develop strong antibody-specific immunity and provided long-term protection¹⁷⁵. Cheng et al. recently showed that when mice were injected subcutaneously with exosomes from pro-inflammatory (M1) macrophages, the exosomes had a strong affinity for lymph nodes and were mostly taken up by the neighboring antigen-presenting cells. This caused the release of multiple pro-inflammatory cytokines, indicating EVs from M1 macrophages could be used in cancer vaccines as an immunopotentiator¹⁷⁶. In another study Zhengtian Li and colleagues revealed that miRNA-16-5p housed in the EVs from M1 macrophages improved the T cell-mediated immune response by reducing the expression of PD-L1. This resulted in an inhibition of the development of gastric cancer both in vitro and in vivo¹⁷⁷.

During activation or apoptosis, platelets often release extracellular vesicles (EVs)¹⁷⁸. EVs from platelets are one of the most common types of EVs in the circulatory system¹⁷⁹. In recent years, researchers have shown interest in the development of therapeutics using platelet-derived extracellular vesicles for cancer immunotherapy. Recently, Wang et al. successfully delivered anti-PDL1 (programmed-death ligand 1 monoclonal antibody) engineered platelets to mice bearing partially removed primary melanomas (B16-F10) or triple-negative breast carcinomas (4T1)¹⁸⁰. Platelet-derived vesicles then release anti-PDL1, which targets circulating tumor cells and significantly increases the overall survival of mice after surgery by lowering the risk of cancer relapse and metastasis¹⁸⁰.

Using extracellular vesicles from immune cells as a way to deliver drugs has many benefits, such as a low risk of causing an immune response, the ability to present tumor

antigens, the ability to deliver endogenous cargo, and the ability to target tumor microenvironment *in vivo*, and ability to modulate the immune cells¹⁴⁶. However, challenges including high production costs, and cumbersome separation process demand other convenient alternatives for cancer immunotherapy. Although EVs have been proved to be an efficient drug delivery vehicles and are created in considerable quantities, the industrial translation of natural EEVs is limited by their poor yield and high manufacturing costs^{144, 181}.

1.4.3 Cell-Engineered Nanovesicles

While endogenously released extracellular vesicles (EVs) are widely used as therapeutic delivery systems because of their immunological tolerance and natural targeting capabilities, the heterogeneous composition, onerous purifying procedures, ineffective medication loading, limited yield, and uncertain scalability of EVs pose obstacles to their clinical translation^{182, 183}. But the problems with EV-based therapies could be overcome by using vesicles that are made by breaking up the cellular membranes¹⁸³. Artificially generated nanovesicles from cell membranes can overcome a variety of challenges seen *in vivo* because they retain the inherent features of the parent cells. These vesicles can be generated in high yields and retain the useful properties of endogenously released EVs. In addition, the nanovesicles made from cell membranes can be easily loaded with different cargo inside them or on the surfaces of therapeutically loaded nanovesicles. Here, we discuss the advantages as well as challenges of using various cell membrane-based drug delivery methods.

1.4.3.1 Cancer Cell-Engineered Nanovesicles

Cancer cells are characterized by the presence of membrane-bound tumor antigens, the ability to evade immune system clearance and the presence of homolytic cell adhesion properties^{29, 184}. Inspired by these unique properties, nanovesicles have been made by disrupting cancer cells so that these nanovesicles can be used as a therapeutic platform for cancer immunotherapy. In a recent study, Lin et al. generated curcumin-loaded nanovesicles by serially extruding B16F10 melanoma cells through filters with cut-off sizes of 10 μm and 5 μm ¹⁸². They demonstrated these nanovesicles not only inhibit cancer cell growth but also activate lymphocytes for anti-tumor immunity. Similarly, Kroll et al. employed B16F10 cancer cell membranes to generate CpG-PLGA encapsulated nanovesicles which when administered subcutaneously successfully activated DCs, which in turn stimulated antigen-specific T cells¹⁸⁵. The cancer cell membrane-bound tumor antigens MART1, TRP2, and GP100 were found to be present on the particles¹⁸⁵. Using cancer cell membrane-derived nanovesicles as a DDS has some benefits, like being able to target a tumor in an animal's body selectively. However, their therapeutic use is limited by the fact that when injected into the body, these vesicles may cause cancer cells to grow¹⁸⁶⁻¹⁸⁸. Recently, vesicles made from the membranes of immune cells have been used instead of vesicles made from cancer cells because they are safe, less likely to cause an immune response, and can be used to target specific cells.

1.4.3.2 Immune Cell-Engineered Nanovesicles

As a result of the expression of immune-related receptors and immune-modulating proteins that they contain, membranes generated nanovesicles from immune cells are becoming an increasingly popular topic of study. Neutrophils, T cells, macrophages,

dendritic cells (DC), and natural killer cells are among the immune cells that may be used as a source of membrane for generating nanovesicles for drug delivery.

In a recent study, Gao et al. developed a nanovesicle-based drug delivery system by employing nitrogen cavitation to quickly disrupt active neutrophils¹⁸⁹. Using intravital imaging on living mouse cremaster venules, researchers determined that these vesicles preferentially bind inflammatory vasculature because they contain intact integrin 2 targeting molecules. In addition, the administration of nanovesicles containing TPCA-1 (an NF- κ B inhibitor) significantly reduced acute pulmonary inflammation in mice¹⁸⁹. In another study, Cao et al. developed neutrophil membrane-derived nanoparticles loaded with celastrol¹⁹⁰, a natural anti-cancer drug. When given intravenously, the membrane-coated nanoparticles preferentially accumulated in the pancreatic tumor tissue and greatly reduced the development of the tumor. This finally resulted in treated animals having a survival rate that was almost three times higher than that of the control mice¹⁹⁰.

T-cell membrane-decorated nanoparticles are resistant to tumor-induced immune suppression and can neutralize PD-L1 expression on tumors and TGF- β 1 in the tumor microenvironment¹⁹¹. Kang et al. recently made nanoparticles using T-cells and showed that, unlike cytotoxic T-cells, these nanoparticles are resistant to the molecules that cancer cells make that stop the immune system from working, such as transforming growth factor-1 (TGF- β 1) and programmed death-ligand 1 (PD-L1)¹⁹¹. In addition, these nanoparticles exhibit enhanced immunotherapy efficacy by preferentially targeting the tumor site, releasing therapeutics, and initiating apoptosis through Fas ligands. In a recent study, chimeric antigen receptor-engineered T cells (CART-T cells) that make antibodies for glypican-3 expressed in hepatocellular carcinomas were used to make nanovesicles with the goal of improving nanovesicles' ability to target tumors¹⁹².

Nanovesicles generated from antigen-presenting cells (APCs), including macrophages and dendritic cells, have been found to mimic the properties of exosomes. Zang et al. recently generated cell-derived nanovesicles by extruding U937 and RAW 264.7 immortalized macrophages, and they discovered that the therapeutic-loaded nanovesicles travel specifically to tumor tissue and inhibit the development of tumors without causing the deleterious effects that are seen with equivalent amounts of free medication¹⁴⁴.

Cell-Engineered Nanovesicles for Cancer Immunotherapy

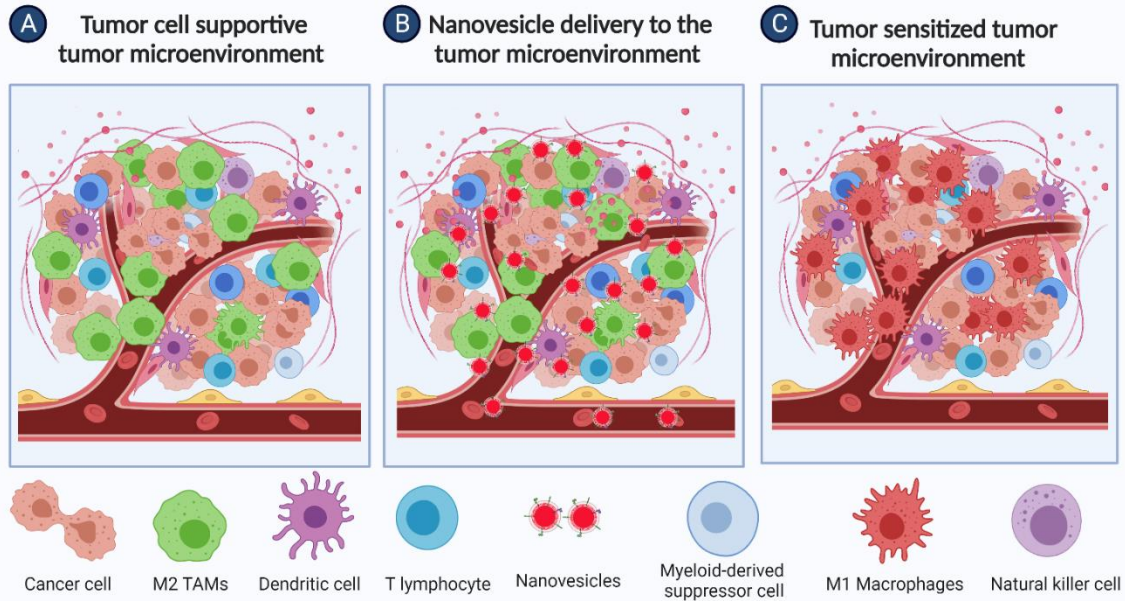


Figure 1.8 Use of cell-engineered vesicles for macrophage reprogramming. This image was created with biorender.com.

1.5 Novel Approaches for Generating Cell Engineered Nanovesicles

Recently, artificially generated cell membrane derived nanovesicles have shown potential for their use as drug delivery vehicles. These nanovesicles exhibit the positive features of exosomes, including low immunogenicity and the ability to specifically target the cell of origin. These vesicles can be generated with high yields; therefore they have the potential to be utilized in personalized medicine. Multiple innovative techniques that can load therapeutics more effectively, manufacture vesicles at high yields while maintaining low costs, and have the needed high yields for commercial manufacturing have been implemented for this purpose.

1.5.1 Extrusion

Extrusion is a technique often employed to generate artificial exosome-like nanovesicles with a regulated size distribution^{193, 194}. In this technique, cells are forced to pass across the pores of definitive sizes present in the polycarbonate membrane (Figure 1.9). By serially extruding cells over the filters with decreasing pore sizes, it is possible to transform cells into nanovesicles of uniform small size while preserving the distribution of cell membrane-anchored proteins¹⁴⁴. For extrusion-based methods, nanovesicles are typically manufactured utilizing a commercially available liposome extruder¹⁹⁵. Jang et al. originally generated exosome-mimetic nano-sized vesicles by passing human myeloid leukemia U937 cells and Raw 264.7 mouse macrophage cells across filters with decreasing pore sizes of 10, 5, and 1 micron, and then subjecting the mixture to density gradient ultracentrifugation (UC) at 100,000xg¹⁴⁴. Using this technique, they were able to obtain nanovesicles that maintained the features of endogenously released exosomes for their shape, size, protein markers, and anticancer activity after being loaded with

chemotherapeutics¹⁴⁴. In addition, the same protocol for extrusion has been extensively used to generate nanovesicles from a variety of cells for specific functions. For example, nanovesicles made from embryonic stem cells can speed up the growth of new cells¹⁹⁶. Nanovesicles made from NIH3T3 cells have been used to deliver siRNA effectively¹⁹⁷, and nanovesicles made from mesenchymal stem cells can be used as an effective drug delivery system to treat breast cancer or spinal cord injuries¹⁹⁸. In addition, Yang et al. found that nanovesicles generated from epithelial MCF10A cells can deliver siRNA to MCF-7 breast tumor cells and, therefore, execute anticancer functions and reduce the expression of CDK4 protein¹⁹⁹. Tao et al. produced nanovesicles loaded with a high concentration of LncRNA-H19 from human embryonic kidney (HEK) 293 cells and discovered that these nanovesicles had a stronger potential to counteract the impact of hyperglycemia on cell regeneration²⁰⁰.

For the production of nanovesicles, extrusion steps and the pore diameter of filters may be adjusted. Choo et al. lowered the pore size of the membrane filter to 1 μm , 400 nm, and 200 nm and generated M1 macrophage-generated nanovesicles from RAW264.7 cells that were treated with LPS201. Wu et al. recently used extrusion techniques to make nanovesicles from brain-derived endothelial cells in high yields. They did this by increasing the number of extrusion steps to 10 μm , 5 μm , 1 μm , 400 nm, and 200 nm²⁰². Even though the extruding method has been used a lot lately to make exosome-like vesicles, the yield of the nanovesicles is often lower because samples are lost during the process and the steps are less controlled because they are done by hand¹⁹³. In addition, with extrusion steps being carried out at room temperature, the stability of the biological cargo, including membrane proteins, can be of concern.

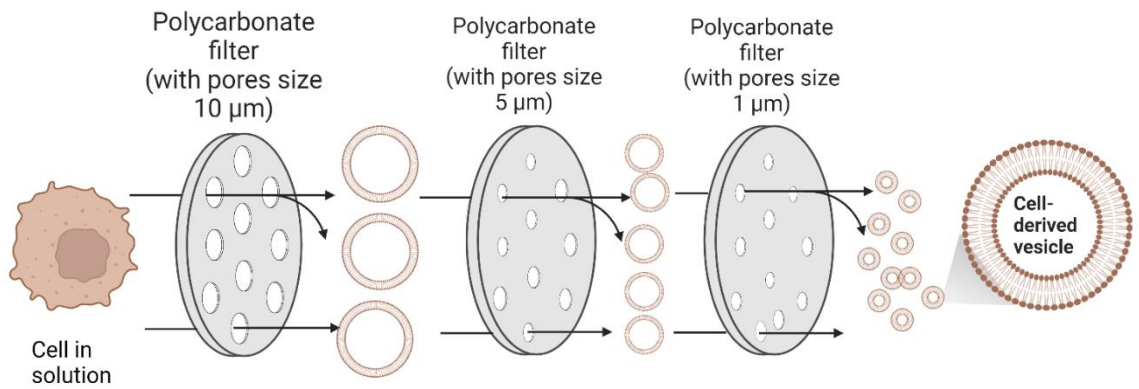


Figure 1.9 Generation of cell-derived nanovesicles by extrusion.

Cell-derived vesicles are generated when the cells in the solution are forced to move through a series of polycarbonate filters with decreasing pore size. This image was created with biorender.com.

1.5.2 Filtration-based Method

The filtration-based method, like extrusion, can be used to generate nanovesicles by using a series of membrane filters with varying pore sizes. Filtration-based approaches for generating exosome-like nanovesicles are more precise and demand less labor than those of the manual extrusion method¹⁹³. Jo et al. recently devised a mechanical system that eliminates the need for ultracentrifugation, which is usually carried out for the purification of nanovesicles²⁰³. Using this technique, large-scale production of nanoparticles can be achieved by the application of centrifugation forces to pass the cells through membrane pores (10 μm and 5 μm). Centrifugal force elongates cells, ruptures them, and assembles the cellular fragments into nano-sized vesicles. This technology yielded nanovesicles with an exosome-like morphology and a vesicle diameter²⁰³. Using this method, they also found that the nanovesicles made from mouse embryonic stem cells could carry RNA to target cells and trigger cell signaling pathways²⁰³. By employing spin cups equipped with two membrane filters (10 μm and 8 μm), Goh et al. streamlined the device and decreased the number of steps involved in vesicle production. Furthermore, they used U937 cells to generate nanovesicles with a size distribution comparable to exosomes¹²⁸. However, the yield of the nanovesicles obtained from this process is quite low.

1.5.3 Generating Vesicles with Sonication

Sonicators are often used to disrupt both bacterial as well as eukaryotic cells in solution into nano-sized fragments. The membrane fragments would then instantaneously rearrange to form nanospheres called nanovesicles. Nanovesicles thus generated maintain

the topology of the cellular membranes while excluding the luminal components and therefore mimic the properties of exosomes¹⁹³. Go et al. used sonication to make nanovesicles that were filled with dexamethasone²⁰⁴. They found that the nanovesicles were the same size and had the same physical properties as normal exosomes, but their yield was 200 times higher. In addition, these nanovesicles are capable of successfully delivering dexamethasone to endothelial cells to reduce the systemic inflammatory response caused by the outer membrane vesicles of gram-negative bacteria²⁰⁴. In another study, He et al. used sonication process to produce ibuprofen-loaded liposomes (IBU-Lip)²⁰⁵. Sonication methods have also been employed to load drugs in exosomes. Recently, Myung et al. generated paclitaxel encapsulated exosomes by sonicating exosomes in the solution containing paclitaxel²⁰⁶. The reformation of the membrane fragments resulting as a consequence of sonication led to a significant increase in therapeutic loading efficiency as well as sustained release of drug²⁰⁶. While sonication offers multiple advantages including ability to generate nanovesicles as well as load therapeutic cargo, sonication-based vesicle generation method is compromised by the excessive heat that results during the fragmenting process.

1.5.4 Generating Vesicles with Nitrogen Cavitation

While nitrogen cavitation was used initially to homogenize cells²⁰⁷ and to disrupt mammalian tissue²⁰⁸, in recent years this technique has been used for a plethora of applications, including membrane preparation^{209, 210}, organelle preparation²¹¹, and vesicle generation^{210, 212}. Nitrogen cavitation-based vesicle generation involves the uniform exposure of cells in solution to high-pressure N₂ in a prechilled nitrogen decompressor (Figure 1.10), followed by the fast release of pressure, which results in the development of gas bubbles that break the cellular membrane. These membrane fragments then rearrange to produce spheres, called vesicles¹⁸³. Through a series of centrifugation steps,

vesicles may be isolated from the cellular detritus²¹². Nitrogen cavitation based-vesicle generation technique offers multiple advantages over other mechanical disruption techniques. First, cellular samples are maintained at a lower temperature during the vesicle generation process as opposed to sonication or extrusion-based methods. This helps not only to maintain the chemical composition of the cell medium but also the biological integrity of the vesicles generated. Second, since nitrogen bubbles are created inside each individual cell during decompression, the nitrogen cavitation process is less restricted by cell size, sample size, and sample concentration²¹³. Nitrogen cavitation also provides more reliable findings since the force exerted by the N₂ gas at higher pressure is evenly delivered across the sample, which may be replicated with similar pressures^{213,214}. Third, the solution in which cells are suspended during cavitation is contained in the vesicles, which is one benefit of this technique. Thus, medicines or other cargos can be efficiently captured in vesicles during vesicle production²¹². Recently, Gao et al. used the nitrogen cavitation technique to efficiently produce extracellular vesicles (EVs)-like nanovesicles from neutrophils¹⁸³. A nitrogen cavitating vessel was filled with neutrophils in solution, which were then subjected to nitrogen cavitation twice at 400 – 500 psi and 0 °C. The nitrogen cavitation technique produces neutrophil derived nanovesicles that retain their targeting molecules and can specifically target the inflamed vasculature. Additionally, a thorough analysis of size, shape, and protein markers revealed that nitrogen cavitation-generated nanovesicles are comparable to naturally occurring endogenously released extracellular vesicles except that these nitrogen cavitation-based nanovesicles contain fewer genetic materials. Also, piceatannol-loaded nanovesicles were generated using nitrogen cavitation and showed that drug-filled nanovesicles could inhibit the NF-κB pathway activation in endothelium¹⁸³. Overall, nitrogen cavitation is a unique method for effectively producing exosome-like cell-derived nanovesicles for therapeutic applications, and this technique might be extended to a broad spectrum of cell types for tailored nanomedicine.

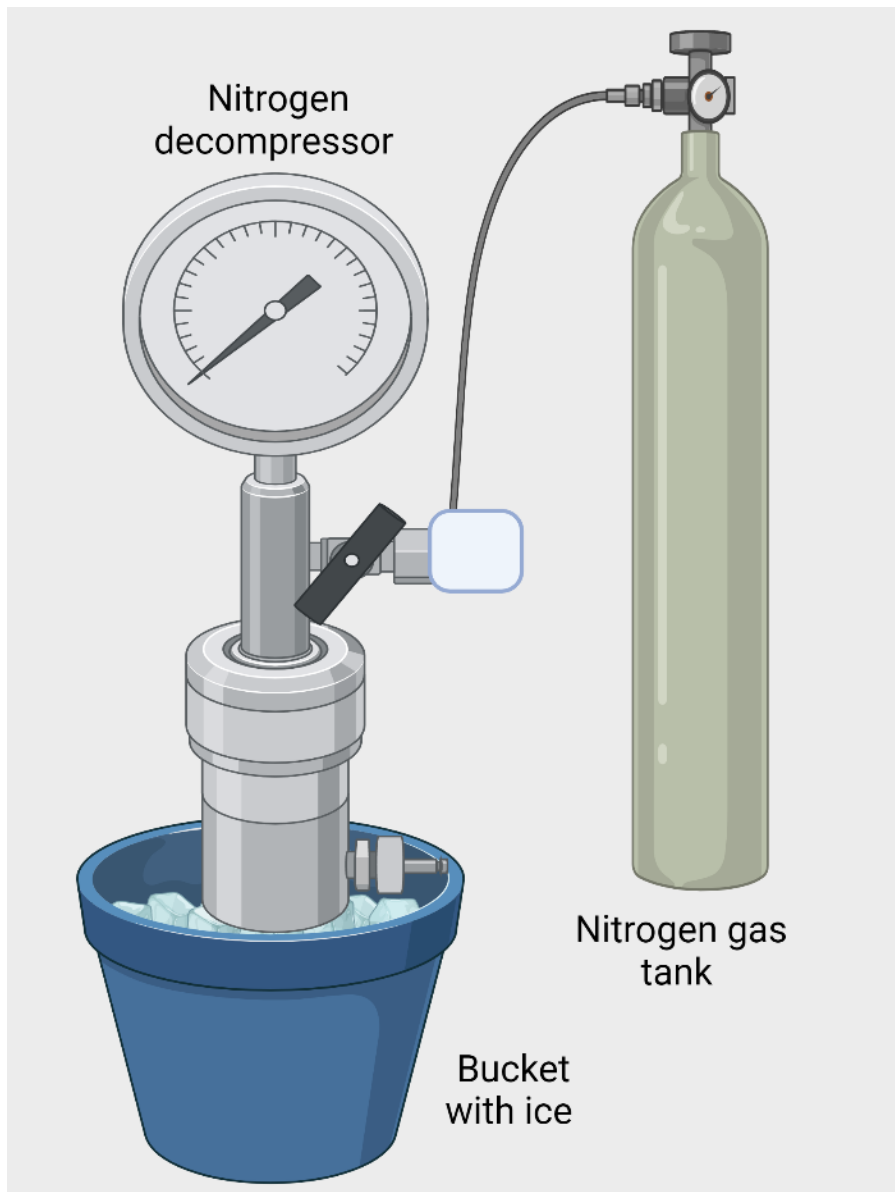


Figure 1.10 Nitrogen cavitation system for generating vesicles from mammalian cells.

Mammalian cells in solution were first kept in the nitrogen decompressor vessel and nitrogen gas was introduced. Cells get ruptured and form spherical vesicles when the valve is opened. This solution of vesicles was purified from the cell lysate by serial centrifugation. This image was created with biorender.com.

CHAPTER 2. MACROPHAGE-ENGINEERED VESICLES FOR THERAPEUTIC DELIVERY AND BIDIRECTIONAL REPROGRAMMING OF IMMUNE CELL POLARIZATION

Copyright information: Content of this chapter was published on <https://pubs.acs.org/doi/10.1021/acsomega.0c05632>. Reprinted with permission from: Neupane, K. R.; McCorkle, J. R.; Kooper, T.J.; Lakes, J.E.; Aryal, S.P.; Abdullah, M., Snell, A. A.; Gensel, J.C.; Kolesar, J.; Richards, C. I. “Macrophage-Engineered Vesicles for Therapeutic Delivery and Bidirectional Reprogramming of Immune Cell Polarization”. *ACS Omega* **2021**, 6, 3847–3857. Copyright © 2019 American Chemical Society

Note: Further permissions related to the material excerpted should be directed to the ACS.

2.1 Summary

Macrophages, one of the most important phagocytic cells of the immune system, are highly plastic and are known to exhibit diverse roles under different pathological conditions. The ability to re-polarize macrophages from pro-inflammatory (M1) to anti-inflammatory (M2) or vice versa offers a promising therapeutic approach for treating various diseases such as traumatic injury and cancer. Herein, it is demonstrated that macrophage engineered vesicles (MEVs) generated by disruption of macrophage cellular membranes can be used as nanocarriers capable of reprogramming macrophages and microglia towards either pro- or anti-inflammatory phenotypes. MEVs can be produced at high yields and easily loaded with diagnostic molecules or chemotherapeutics and delivered to both macrophages and cancer cells *in vitro* and *in vivo*. Overall, MEVs show promise as potential delivery vehicles for both therapeutics and their ability to controllably modulate macrophage/microglia inflammatory phenotypes.

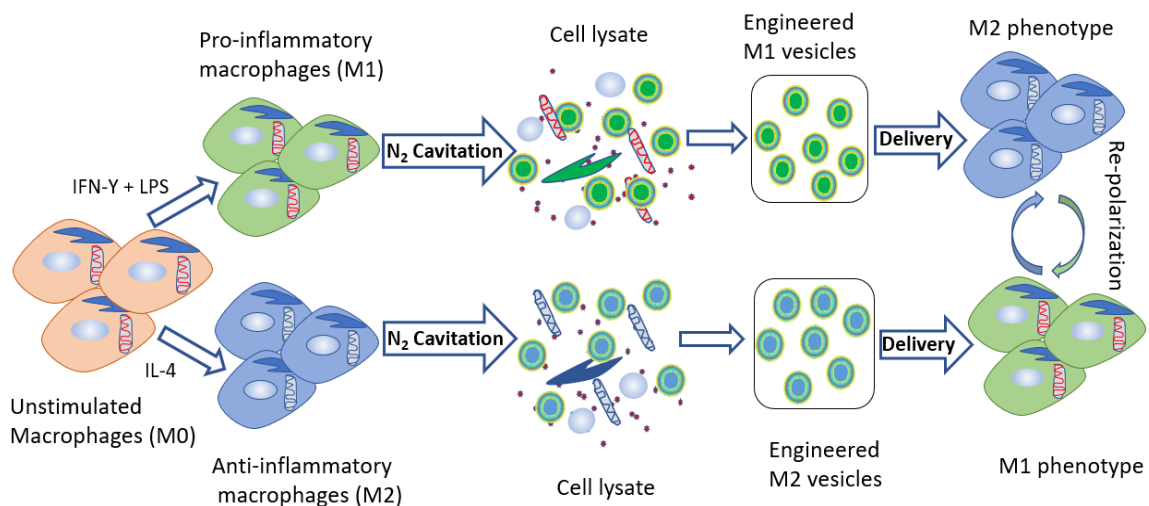


Figure 2.1 Schematic illustrating the approach of generating vesicles.

Fully differentiated unstimulated macrophages (M0) are polarized into either pro-inflammatory macrophages (M1) or anti-inflammatory macrophages (M2). Nitrogen cavitation is then used to fragment the cellular membranes of these cells generating M1-engineered vesicles (M1EVs) or M2-engineered vesicles (M2EVs). Vesicles are then separated from cellular fragments by serial centrifugation. These vesicles are then delivered to either unstimulated or polarized macrophage to shift the polarization toward the polarization type of the MEVs.

2.2 Background

Macrophages are an essential component of the innate immune system where they play a diverse role. Macrophage function includes clearing waste material such as cellular debris and participating in tissue repair and remodeling that occurs during wound healing.²¹⁵ They also serve as a defense against bacterial infections and other pathogens largely through phagocytosis.^{216, 217} Additionally, they are integral to the initiation of an adaptive immune response through their antigen presenting capabilities.²¹⁸ As a result of this versatile role, macrophages exhibit a range of functional activities which are often driven by stimuli in the surrounding environment.²¹⁹ Macrophages exist in a continuum of polarization states between a pro-inflammatory phenotype, classified as M1, and an anti-inflammatory phenotype, classified as M2.²²⁰ The polarization state is often mediated by environmental signals such as cytokines, fatty acids, and components from microorganisms such as lipopolysaccharides (LPS).^{221, 222} Pro-inflammatory macrophages are characterized by the production of nitric oxide and the release of high levels of inflammatory cytokines including IL-12, TNF- α , and IL-1 β .²¹⁵ Anti-inflammatory macrophages secrete cytokines which can dampen the immune response such as IL-10 and IL-4.²²³

The expression of specific macrophage cytokines is implicated in the progression of several disease states. For example, recent studies have shown that macrophages are involved in the progression of cancer, inflammatory diseases, and infectious diseases.²²⁴ In the tumor microenvironment, macrophages exhibit an anti-inflammatory phenotype and are known as alternatively activated or tumor-associated macrophages (TAMs).²²⁵ While IFN- γ and IL-12 release by pro-inflammatory macrophages have an anti-angiogenic effect and can block the formation of the new blood vessels in the tumor microenvironment, TAMs suppress production of these cytokines.²²⁶⁻²³⁰ Factors released by cancer cells in the

tumor microenvironment cause TAMs to become tumor supportive assisting in growth, tissue remodeling, angiogenesis, and metastasis.^{227, 231} Tumor progression is further supported by TAMs which produce reduced levels of the major histocompatibility complex (MHC)-II which suppresses the anti-tumor adaptive immune response.^{232, 233} Macrophages also play a critical role in the inflammatory response such as during spinal cord injury (SCI).²³⁴ As the blood-brain barrier is compromised following SCI, peripheral macrophages rapidly invade the spinal cord and contribute to both pathological and reparative processes.²³⁵ While pro-inflammatory macrophages contribute to neurodegeneration and tissue loss after SCI, anti-inflammatory macrophages contribute to tissue remodeling and axon regeneration.²³⁶⁻²³⁸ Control of macrophage phenotype through the ability to shift therapeutically between pro-inflammatory and anti-inflammatory polarizations has been proposed as a potential treatment for diseases such as some types of cancer and traumatic injury.^{239, 240} Under different pathological conditions, macrophages exhibit heterogeneity across a continuum of polarization states. The ability to repolarize macrophages from one phenotype to another is a promising technique which might enable alternative forms of treatment for several diseases. For example, repolarizing TAMs towards a pro-inflammatory phenotype is an attractive means to sensitize cancer to immunotherapy.^{241, 242} Similarly, repolarizing pro-inflammatory macrophages toward anti-inflammatory phenotypes thereby reducing the potential neurotoxic effects of M1 macrophages could be a promising approach for treating SCI and stroke.^{223, 238, 243}

The expression of specific macrophage cytokines is implicated in the progression. Studies have shown that endogenous extracellular vesicles (EEVs) such as exosomes obtained from immune cells like macrophages and dendritic cells possess the ability to repolarize TAMs to pro-inflammatory macrophages in the tumor microenvironment.^{26, 125, 244} Despite their promise in shifting macrophage phenotype as a therapeutic approach, EEV based therapies are still challenged by low production yields and difficulties in separating target vesicles from other similarly sized vesicles.¹⁴⁴ Vesicles

artificially generated from cellular membranes have been found to mimic many of the properties of EEVs.^{128, 144, 212, 242, 245-247} For example, recent studies demonstrated that vesicles derived from cellular membranes of RAW264.7 cells can stimulate anti-inflammatory macrophages toward a pro-inflammatory phenotype. Studies have also shown that cell derived vesicles from tumor cells exhibit targeted delivery back to the cell of origin.²¹²

In the present study, we generated vesicles from mouse bone marrow derived macrophages (BMDMs) and demonstrate that we can tune their capability to repolarize macrophages toward either pro- or anti-inflammatory phenotypes. We also characterized these macrophage engineered vesicles (MEVs) to show they are similar in size to EEVs and exhibit cell targeting capability for delivery of therapeutics to both cancer cells and macrophages.

2.3 Methods

Animals: We used 2-5 months old wild type C57BL/6 mice to extract bone marrow cells. Animals were properly accommodated in IVC cages by providing enough food and water. All experiments were performed following the guidelines of the National Institute of Health and were approved by the Institutional Animal care and use committee at the University of Kentucky.

Cell Culture: Bone marrow-derived macrophages (BMDMs) were isolated from both tibias and femurs of wild type mice at 2-5 months of age as previously reported.^{237, 248} Briefly, mice were first anesthetized and then killed by cervical dislocation. After removing femurs and tibias from the carcass, the bone marrow was extracted by a 10 mL syringe loaded with Roswell Park Institute (RPMI) Medium into a 50 mL centrifuge tube. The bone marrow in media was then triturated with 18-gauge needle until a single cell suspension was obtained followed by centrifugation at 1,200xg for 5 minutes. The

supernatant was carefully removed, and cells were resuspended in 4 mL of RBC lysis buffer (0.15 M NH₄Cl, 10 mM KHCO₃, and 0.1 mM Na₄EDTA) followed by swirling by hand for 3 minutes. 6 mL of RPMI media was then added followed by centrifugation at 1200xg for 5 minutes. The supernatant was aspirated off and the cells resuspended in differentiation media (RPMI supplemented with 10% Fetal Bovine Serum (FBS), 1% penicillin/streptomycin (PS), 1% HEPES, 0.001% β-mercaptoethanol, 1% Glutamine and 20% supernatant from sL929 cells) and plated in T-175 cell culture flasks in differentiation media. sL929 cell lines were maintained in RPMI media supplemented with 10% FBS, 1% PS and 1% glutamine. The supernatant from sL929 cells contains macrophage-colony stimulating factor (MCSF) which is essential for differentiating bone marrow cells into macrophages. Differentiation media was replaced on days 2, 4, and 6 and the cells were re-plated on day 7 at a cell density of 1×10⁶ cells/mL in re-plating media (Dulbecco's Modified Eagle's Medium (DMEM) supplemented with 10% FBS, 1% Glutamine and 1% PS). On day 8 cells were stimulated to M1 (LPS (20 ng/mL; Invivogen) + IFN-γ (20 ng/mL; eBioscience)) or M2 (IL-4 (20 ng/mL); eBioscience) macrophages, while the unstimulated macrophages from day 7 were termed M0 macrophages. For cytokine analysis, the supernatant from stimulated cells, macrophage conditioned media (MCM), was collected after 24 hours. Vesicles were added after 12 hours of stimulation and the supernatant was collected after 24 hours of vesicle addition to M1 or M2 macrophages. The MCM obtained was collected into eppendorf tubes and stored at -80 °C until the analysis was done.

Primary cultures of microglia were prepared from postnatal P2 to P4 pups from C57BL/6 mice. Briefly, pups were decapitated, and brains were kept in petri dishes filled with ice-cold Hank's Balanced Salt Solution (Ca²⁺, Mg²⁺, NaHCO₃, phenol red). Brains were dissected, and the hippocampal region was extracted for microglia isolation and culture. The tissues were then minced, and cell suspension was made. The cell suspension was treated with 2.5% trypsin (Quality Biological), incubated and finally resuspended in the astrocyte culture media containing DMEM with 10% FBS and 1 % PS. Cells were

incubated at a density of 2 million on a poly-L-lysine coated T75 flask containing astrocyte culture media. Cell culture media was changed every 3 days until the flask was confluent with cells. Microglia were detached from astrocytes and oligodendrocytes by shaking the flasks for 30 minutes at a speed of 180 rpm.

The mouse neuroblastoma cell line (also known as Neuro-2a or N2a) were maintained in N2a cell culture medium composed of 44% DMEM, 45% OPTI-MEM reduced-serum medium, 10% FBS and 1% PS. 40,000 N2a cells were plated in each well of a 96-well plate in N2a media supplemented with 20 μ M retinoic acid (Sigma-Aldrich) and allowed to differentiate for 24 hours. Retinoic acid helped N2a cells to differentiate into cells with neuron like properties.²⁴⁹ On day 1, the differentiation media was exchanged for 100 μ L of various macrophage conditioned media (MCM) in 20 μ M retinoic acid and two controls with and without 20 μ M retinoic acid. Cells were further incubated for 48 hours, and the neurotoxicity of MCMs was evaluated using an alamar blue cell proliferation assay.

Human lung cancer (A549) cells were maintained in A549 cell culture medium composed of 89% DMEM, 10% FBS and 1% PS. 40,000 A549 cells were plated in each well of a 96-well plate and left to incubate for 12 hours at 37 °C. After 12 hours, the old growth media was removed carefully being sure not to disturb the cells and was exchanged with A549 cell media containing cisplatin-loaded macrophage (M0, M1 and M2) engineered vesicles or empty (M0, M1 and M2) vesicles. After 24 hours of incubation at 37 °C, the media was aspirated off and 100 μ L of opti-mem was added followed by 20 μ L of alamar blue for the cell viability assay.

Cell Viability Assay: For cytotoxicity assays, the cell media from each well of a 96-well plate was exchanged for 100 μ L of Opti-mem (Invitrogen) followed by the addition of 20 μ L of alamar blue. Cells were then incubated for 35-45 minutes until a uniform purple coloration was developed. The resulting fluorescence was measured using Tecan 96-well plate reader equipped with an excitation filter set to 535 nm and the emission filter set to

595 nm. All measurements were done in quintuplicates (5 different wells) and at least three independent experiments were carried out.

MEVs Isolation: Completely differentiated macrophages from day 8 were used to generate macrophage engineered vesicles. The macrophage cell media was aspirated off from the flask containing macrophages and the cells were first washed with PBS. 3 mL of PBS were further added to each flask, and cells were detached by scraping them followed by resuspension in PBS. The cell suspension from all flasks was first collected into a 50 mL tube, and the total number of cells were counted using a hemacytometer. The cell slurry collected in the previous step was then centrifuged at 1200 rpm at 4 °C for 5 minutes and the obtained pellets resuspended in 10 mL PBS supplemented with protease inhibitor. To fragment the cellular membrane and generate the vesicles, cells were then subjected to a pressure of 300 psi for 5 minutes in a prechilled nitrogen gas decompressor (Parr Instruments Company, IL, USA) on ice. The pressure was rapidly released to generate fragmentation resulting in vesicles. The fragmented cell mixture including vesicles was centrifuged at 4000xg for 10 minutes at 4 °C. The pellet obtained was discarded but the supernatant centrifuged at 10,000xg for 20 minutes at 4 °C. The supernatant was again subjected to ultracentrifugation at 100,000xg for 60 minutes at 4 °C to pellet the remaining nanovesicles. The pellet was washed 5 times with PBS before being resuspended in 500 µL PBS buffer.

MEV Characterization: MEVs were generated by nitrogen cavitation followed by series of centrifugation steps as discussed above. Mean diameter, concentration, and zeta potential of MEVs were determined via nanoparticle tracking analysis (NTA) using a Nanosight 300 and a ZetaView PMX-120. Similarly, MEV stability was determined using dynamic light scattering (DLS). A ZetaPALS potential Analyzer (Brookhaven Instruments) was used to collect the DLS measurements.

MEV Labeling: Cells were detached from the flask and counted and resuspended in 9.9 mL of PBS. 100 µL of 100 mM fluorescein was added to the cell suspension so that

the final concentration of fluorescein becomes 1 mM in the cell suspension. The cell solution was fragmented using nitrogen cavitation and the vesicle pellet was obtained. The pellet was then washed with PBS to remove any unincorporated fluorescein inside the vesicle. Vesicles were then resuspended in 1 mL of PBS and transferred to a clean ultracentrifuge (UCF) tube where the vesicle suspension was diluted to 4 mL in PBS. For the complete removal of free dye, the diluted vesicle suspension was re-centrifuged at 100,000xg for 60 minutes at 4 °C. The supernatant from centrifugation was discarded and the pellet was washed with 1 mL PBS buffer. 500 µL of PBS was added to the UCF tube and the pellet was resuspended by pipetting several times. DiI was then added to the vesicle resuspension such that the final concentration of the dye becomes 2 µM and left to incubate for 30 minutes at 37 °C. DiI is a lipophilic dye which gets incorporated into the lipid bilayer of the vesicle. The free dye molecules were separated from the fluorescently labeled vesicles using a size exclusion spin column (PD MidiTrap column). The column was equilibrated first by running 15 mL of PBS through the column and the column centrifuged at 1000g for 2 minutes to remove any remaining PBS from the column. Then, 500 µL of vesicle solution was added carefully onto the center of the column from the top and centrifuged at 1000g for 2 minutes to obtain DiI labelled vesicles loaded with fluorescein.

MEVs Imaging: DiI or fluorescein-labeled vesicles were generated as discussed previously and deposited onto a glass bottom dish before imaging them using fluorescence microscopy. DiI-labeled vesicles were imaged using a 532 nm laser of 1.9 mW power with a gain of 990 and an exposure time of 200 ms. Similarly, fluorescein-loaded vesicles were imaged using a 488 nm laser of 0.8 mW power with a gain of 990 and an exposure time of 200 ms.

Confocal Imaging: A Nikon A1R laser scanning confocal microscope equipped with a 60X oil objective was used for confocal imaging of macrophages that had taken up dye labelled vesicles. Thus obtained images were analyzed with Nikon image processing software²⁵⁰.

MEVs Uptake: 100 million M1 and 110 million M2 macrophages were used to prepare M1EVs and M2EVs respectively for the study of MEVs uptake by M1 or M2 macrophages. MEVs were generated and labelled with DiI as mentioned previously. From total 500 μ L of each vesicle suspension, 50 μ L of DiI-labelled vesicles were then added separately to each glass bottom dish containing 90,000 M1 or M2 macrophages. Imaging was done at 0.5, 1, 1.5 and 2 hours using a fluorescence microscope equipped with a 20X objective with an exposure time of 32 milliseconds. The macrophage media with fluorescently labeled vesicles was first removed and the cells were washed twice with 1 mL L-15 prior to the addition of 1 mL L-15 to the cells for imaging.

Cisplatin-loaded MEVs: 100 million M0, M1 or M2 cells were used to generate macrophage-derived, cisplatin-loaded vesicles and deliver them to A549 cells. Macrophage media was first aspirated off and 3 mL of PBS was added to each flask prior to scraping them. The cell solution was collected into a 50 mL centrifuge tube and the number of cells was determined using a hemacytometer. The cell solution was pelleted at 2000xg for 2 minutes at 4 °C. The supernatant was discarded, and cells were resuspended in 8 mL of 8.33 mM cisplatin solution made in PBS with 1 tablet of protease inhibitor. The cell solution was nitrogen cavitated using a pre-chilled nitrogen decompressor on ice at 300 psi for 5 minutes. The cell lysate obtained was centrifuged at 4000xg for 10 minutes at 4 °C. The pellet thus obtained was discarded and the obtained supernatant was centrifuged at 10,000xg for 20 minutes at 4 °C. The supernatant obtained was again subjected to ultracentrifugation at 100,000xg for 60 minutes at 4 °C to collect the pellet containing cisplatin-loaded nanovesicles. This final pellet was first washed with 1 ml of PBS twice and resuspended in 750 μ L of PBS. Empty vesicles were generated using the same procedure discussed above but in the absence of cisplatin.

Cisplatin Concentration in MEVs: The concentration of cisplatin loaded in vesicles was determined using ICP-OES.²¹² Cisplatin loaded MEVs were first treated with 1% Triton X-100 to dissolve the lipid bilayer followed by 70% nitric acid treatment to release

platinum from cisplatin. The resulting solution was further incubated on a heat block at 60 °C for 2 hours followed by dilution to 5 mL such that final nitric acid concentration was 10% for analysis using ICP-OES. A standard curve using platinum standards in 10% nitric acid solution was used to determine the concentration. Ytterbium was used as an internal standard to compensate for the internal drift of the instrument. We have previously shown that vesicles generated by nitrogen cavitation are stable with no apparent cisplatin leakage for 72 hours.²¹²

Cytokine Analysis: MEVs were generated as described before. M1EVs were generated from 100 million M1 macrophages and resuspended in 500 µL of PBS. The number of vesicles present in the resuspension was determined using nanoparticle tracking analysis. 5.49×10^9 M1EVs were added into each well of a 24-well plate containing 1 million M0 and M2 macrophages in 950 µL of re-plating media. The plate was left to incubate at 37 °C for 24 hours. After 24 hours of incubation, MCM was collected in an Eppendorf tube (1mL) and later used for pro-inflammatory cytokine analysis. M2EVs were generated as before using M2 macrophages. 7.6×10^9 M2EVs were added to each well containing M0 and M1 macrophages. The plate was left to incubate at 37 °C for 24 hours before collecting the media for cytokine analysis. We performed a mouse pro-inflammatory seven-plex assay following the manufacturers protocol. Briefly, 25 µL of calibrators and MCM were added to each wells of a capture antibodies precoated MSD well plate. The plate was then allowed to incubate for an hour and detection antibody was added into each well of the MSD. After vigorously shaking the plate for an hour it was then washed with 0.5% tween PBS. Read buffer was finally added to each well and analyzed on the MESO SECTOR imager from Meso Scale Discovery. Standard curves were obtained by fitting the electrochemiluminescence signal from calibrators using Meso Scale Delivery Workbench analysis software.

In vivo Delivery: A549 cells (1×10^6) were injected subcutaneously into the interscapular region of 6 week old athymic nude mice. The mice were monitored until

palpable xenograft tumors developed greater than 200 mm³. M1EVs were generated using 100 million M1 macrophages by the procedure mentioned above. A NanoSight 300 multiple particle tracking system was used to determine the mean diameter and the concentration of MEVs. M1EVs were then labelled with DiR near-infrared fluorescent dye. Briefly, 1 µL of 1 mM DiR was added to the 199 µL of vesicle resuspension so that the final concentration of the DiR in the vesicle resuspension was 5 µM. DiR labeled vesicles were separated from free DiR using a size exclusion PD MidiTrap column equilibrated with PBS. 100 µL of DiR labelled M1EVs were then injected into the lateral tail vein of tumor-bearing mice. Isoflurane gas was used to anesthetize mice for imaging 72 hours post-injection using an IVIS Spectrum In Vivo Imaging System (PerkinElmer) controlled with LivingImage software (PerkinElmer). Epifluorescence images were acquired using 710 nm excitation and 760 nm emission filters, f/stop number 4 and binning factor 4, with a 35 second exposure.

Statistical Analysis: Statistical analyses were performed using Origin 2018. All data were expressed as mean ± SEM. At least three independent biological replicate experiments were performed for each condition (n ≥ 3). Two sample t-test or ANOVA with Post Hoc Tukey's HSD test were done when appropriate and results were considered statistically significant at p-value less than or equal to 0.01.

2.4 Results and Discussions

2.4.1 Characterization of Macrophage Engineered Vesicles (MEVs)

Macrophage engineered vesicles (MEVs) are generated through mechanical disruption of the cell membrane into nanosized fragments which reform into vesicles. Here we used a prechilled nitrogen decompressor and maintained bone marrow derived macrophages at a pressure of 300 psi for at least 5 minutes. The sudden release of pressure causes the cell membrane to fragment, and because the phospholipids composing the

membrane are amphipathic, the hydrophobic effect drives these fragments to spontaneously form vesicles in aqueous solutions. These vesicles are separated from cellular debris by a series of centrifugation and ultracentrifugation steps as depicted in Figure 2.1. Vesicles are generated in the presence of the solution in which the cells were initially suspended leading to the encapsulation of any hydrophilic therapeutic or other cargo present in the aqueous solution during vesicle generation. Figure 2.2A shows a fluorescence image of MEVs generated by nitrogen cavitation in the presence of a fluorescein containing solution. Fluorescein is a fluorescent dye that is soluble in an aqueous medium and is entrapped within the vesicles during their formation. Green punctate regions in the fluorescence image indicate the presence of fluorescein inside the vesicles and the successful loading of cargo during vesicles generation. Similarly, MEVs can be labeled with a lipophilic dye such as DiI. The fluorescence image in Figure 2.2B shows red punctate regions corresponding to DiI incorporation into the vesicle membrane.

To determine the yield of MEVs during nitrogen cavitation, we performed multiple particle tracking to extract both the size distribution of vesicles and their concentration. Particle tracking (NanoSight 300) determines particle size based on diffusion rates and the concentration by counting the number of particles in a defined volume. Vesicles generated from approximately 100 million M1 bone marrow-derived macrophages in culture using nitrogen cavitation yielded 5.5×10^{10} vesicles (M1EVs). Similarly, 100 million M2 macrophages yielded 6.9×10^{10} vesicles (M2EVs). The size distribution of MEVs generated by nitrogen cavitation at 300 psi is primarily between 100-200 nm which is similar to that of exosomes.^{251, 252} The mean diameter of M1EVs was found to be 144.6 nm (Figure 2.2C) and that of M2EVs was found to be 137.8 nm. (Figure 2.2D). We further measured the zeta potential of MEVs suspended in PBS buffer and found that M1EVs had a zeta potential value of -104 ± 2 mV and M2EVs had a zeta potential of -84 ± 2 mV. A large negative value for the zeta potential indicates the stability of MEVs in aqueous solution.^{144, 253-255} These initial characterization studies show that vesicles from BMDMs can be generated with

similar size as exosomes. Additionally, we were able to produce a large number of vesicles from a relatively small volume of tissue culture without the need to wait for long periods of time for the production of EEVs through normal physiological processes.

We next tested the stability of MEVs over time to determine their potential suitability as a drug delivery vehicle where they would be required to circulate within the human body for a period of time before delivery of cargo to a specific site. We tested the stability of MEVs generated by nitrogen cavitation by incubating them in solution for three consecutive days. We monitored vesicle size over time to determine the extent of aggregation. The size of MEVs remained relatively constant for the first two days signifying the stability of MEVs over that interval. After 48 hours, the stability gradually decreased as shown by the increase in the size of the vesicles (Figure 2.2E). Thus, in addition to their high yields, MEVs are also stable for times compatible with the likely circulation time needed for therapeutic delivery.

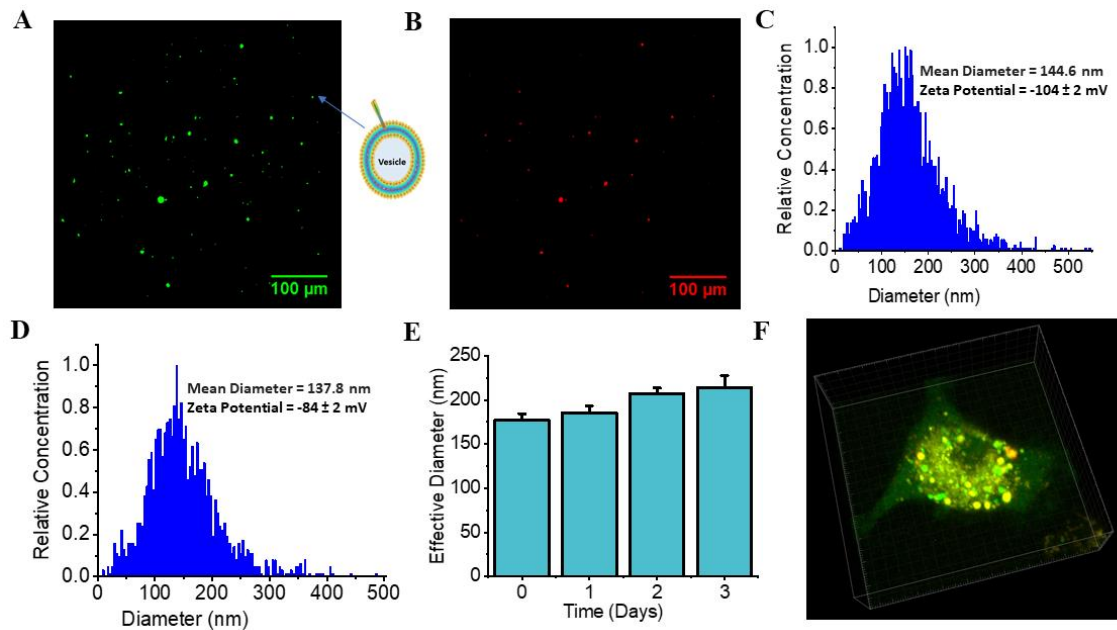


Figure 2.2 Macrophage-engineered vesicle (MEV) characterization.

(A) Fluorescence image of macrophage engineered vesicles (MEVs) loaded with a fluorescent dye (fluorescein) during vesicle generation illustrating the principle of encapsulation of cargo by MEVs. (B) Fluorescence image of MEVs labeled with lipophilic dye, DiI. (C) Size distribution of pro-inflammatory macrophage-engineered vesicles (M1EVs) measured by nanoparticle tracking analysis. (D) Size distribution of anti-inflammatory macrophage-engineered vesicles (M2EVs). The effective diameter of the vesicles generated by nitrogen cavitation was between 100-200 nm. (E) The effective diameter of M1 vesicles in PBS for 3 days measured using dynamic light scattering. (F) A 3D confocal image of an M2 macrophage after delivery of fluorescein (interior)-loaded M1EVs labeled with DiI (lipid bilayer) showing clear uptake of vesicles on the surface and inside by macrophages.

2.4.2 MEV Delivery to Macrophages.

Previous studies have shown that vesicles generated from cellular membranes can be used as efficient therapeutic delivery vehicles to deliver cargo to the interior of the cell.²¹² In order to investigate the ability of MEVs to deliver cargo into the interior of macrophages, we first generated MEVs from BMDMs stimulated to be M1 (INF- γ + LPS) and loaded with fluorescein. The M1EVs were labeled concomitantly with the lipophilic dialkylcarbocyanine fluorescent dye, DiI, which embeds into the lipid bilayer of the vesicles. Both fluorescent labels were separated from unloaded dye using a size exclusion column. We then incubated BMDMs stimulated with IL-4, to generate M2 cells, with the M1EVs. After incubation with these M2 macrophages, we observed bright fluorescence after 2 hours when imaged with confocal microscopy both under 488 nm (Fluorescein) and 532 nm (DiI) excitation. M1EVs were evident inside of M2 macrophages as shown from the fluorescence puncta both inside and on the membrane of macrophages (Figure 2.2F). At two hours after incubation, most vesicles remain intact and isolated on the membrane as well as inside of the cell.

After confirming the delivery of M1EVs onto M2 macrophages, we next performed a set of experiments to determine if vesicles generated from M1 and M2 BMDMs possess different macrophage targeting capabilities. We generated DiI-labeled vesicles from an equal number of M1 or M2 macrophages. We then determined the efficiency of delivery to M1 and M2 macrophages by measuring the fluorescence signal at various time points over 2 hours. We added M1EVs and M2EVs separately to M1 or M2-stimulated BMDMs.

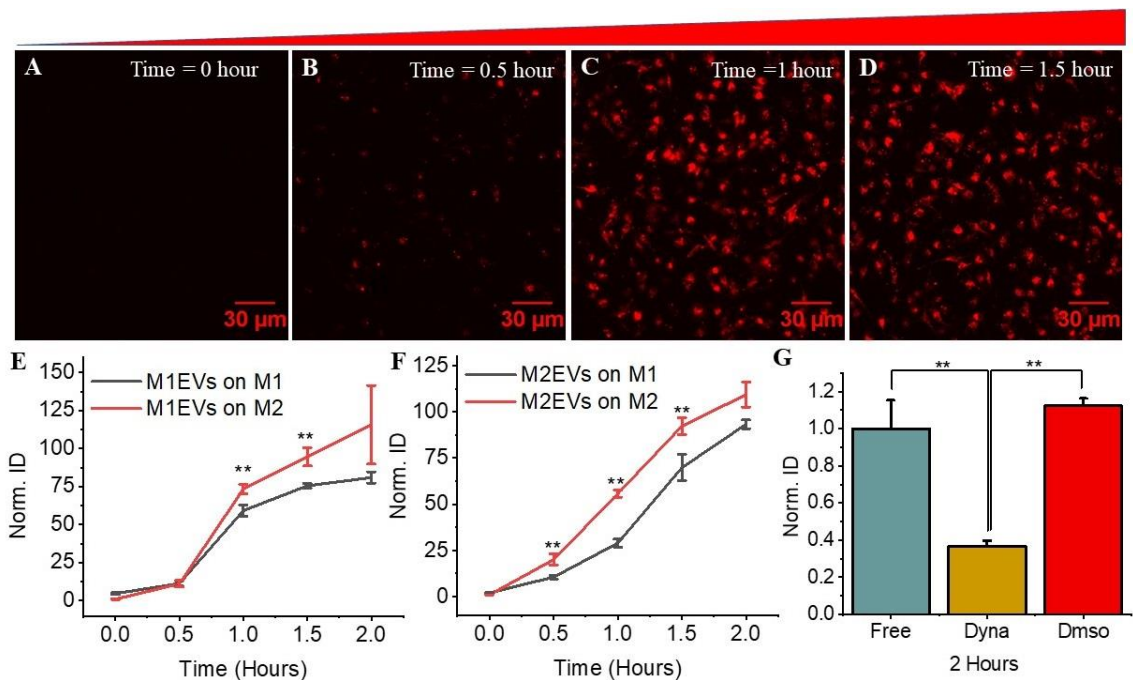


Figure 2.3 Macrophage targeting specificity.

(A-D) Widefield fluorescence images of M2 Macrophages showing the time dependent uptake of DiI-labeled M1EVs by M2 macrophages, scale bar = 30 μm . (E) Comparison of M1EVs delivered to M1 macrophages (black) versus M1EVs delivered to M2 macrophages (red). (F) Comparison of M2EVs delivered to M1 macrophages (black) versus M2EVs delivered to M2 macrophages (red). (G) Comparison of M2 Macrophages with M1EV delivery (green), M2 macrophages incubated with dynasore (80 μM) for 30 minutes prior to M1EVs addition (gold), and M2 macrophages with M1EV delivery in the presence of DMSO (delivery vehicle) (red). Each datapoint is the average of five independent replicates ($n = 5$). Norm. ID is the mean integrated density of the image normalized to the mean integrated density value of M2 Macrophages before adding vesicles. The data are presented as the mean \pm standard error of mean (SEM). ** $p < 0.01$ indicates a significant difference in the vesicle uptake by macrophages at respective time points.

Vesicles were then rinsed from the cells, and the cells were subsequently imaged using wide-field microscopy. We found time dependent uptake of MEVs by macrophages (Figure 2.3A-D). While both M1EVs and M2EVs were efficiently delivered to M1 and M2 macrophages, M2 macrophages showed a higher uptake of both M1EVs and M2EVs compared to M1 macrophages (Figure 2.3E-F).

Dynamin activity is an integral component of both endocytosis and phagocytosis.^{256, 257} Dynasore, a dynamin inhibitor, has been widely used to study the process of internalization of exosomes from the surface of macrophage.^{256, 258, 259} Recent studies showed that the knockdown of dynamin 2 almost completely inhibited the uptake of exosomes by RAW264.7 macrophage like cells.²⁶⁰ Since MEVs mimic exosomes, we next investigated whether they exhibited a similar mechanism of vesicle internalization by macrophages. We compared the uptake of fluorescently labeled M1EVs by M2 BMDMs in the presence and absence of dynasore. Dynasore (80 μ M) was added to cultured macrophages 20 minutes prior to the addition of labeled vesicles. M2 macrophages were left to incubate with M1EVs for 2 hours and subsequently imaged by wide-field microscopy. We found that dynasore had no effect on the cell viability and macrophages looked morphologically similar with and without treatment. We calculated the integrated density of the fluorescence signal to compare the uptake of M1EVs by M2 macrophages. We found that the dynasore resulted in 64% reduction in uptake of vesicles relative to the control (Figure 2.3G). We performed similar vesicle uptake control experiments in the presence of the vehicle, DMSO, at equal concentration. We found that there was no significant effect of DMSO on the M1EV uptake process by M2 macrophages relative to the control with no DMSO or dynasore. Macrophages are well established phagocytotic cells. The loss of cellular uptake with dynamin inhibition coupled with the observation of intact vesicles inside macrophages indicates that macrophages are likely internalizing vesicles via phagocytosis. These results demonstrate that MEVs exhibit similar properties as exosomes and are able to target macrophages.

2.4.3 MEVs Reprogram Macrophage Phenotype.

Previous studies have shown that exosomes generated from M1 or M2 macrophages can be used to differentiate naive macrophages into corresponding pro- or anti-inflammatory phenotypes.^{125, 261} After confirming that MEVs can be delivered to macrophages, we tested their ability to differentiate naive (M0) macrophages. M1EVs were generated using nitrogen cavitation from cultured M1 macrophages and then delivered to M0 macrophages to compare cytokine production from M0 macrophages, M1 macrophages, and M0 macrophages incubated with M1EVs. Macrophage-conditioned media (MCM) was extracted from the cell culture of each sample. We performed a Meso-Scale Delivery Sevenplex ELISA assay that simultaneously tested for seven mouse pro-inflammatory cytokines (IFN- γ , IL-10, IL-12p70, IL-1 β , IL-6, KC/GRO and TNF- α) in the cell culture supernatant. We observed clear pro-inflammatory markers from M1 macrophages and virtually no measurable levels for most of the cytokines in the M0 culture (Figure 3A). We also found that M1EVs can reprogram M0 macrophages toward an M1 phenotype as evidenced by the increased production of each of the pro-inflammatory cytokines (n = 3/group) from undetectable to 6 \pm 6% (IFN- γ), 45 \pm 2% (IL-10), 29 \pm 1% (IL-12p70), 81 \pm 63% (IL-1 β), 12 \pm 5% (IL-6), 36 \pm 13% (KC/GRO) and 20 \pm 8% (TNF- α) of the average concentration seen for M1 macrophages (Figure 2.4A). These results verified that M1EVs can stimulate M0 BMDMs toward a pro-inflammatory phenotype. We did not observe a shift toward a pro-inflammatory phenotype when M2MEVs were added to M0 macrophages. Our results reinforce the claim that MEVs exhibit similar properties as exosomes and can be used to polarize naive macrophages.

We next performed a set of experiments to determine the effect of vesicle delivery on macrophages that have already been polarized toward a specific phenotype. We examined the ability of pro-inflammatory vesicles to influence anti-inflammatory macrophages as well as the ability of anti-inflammatory vesicles to influence pro-

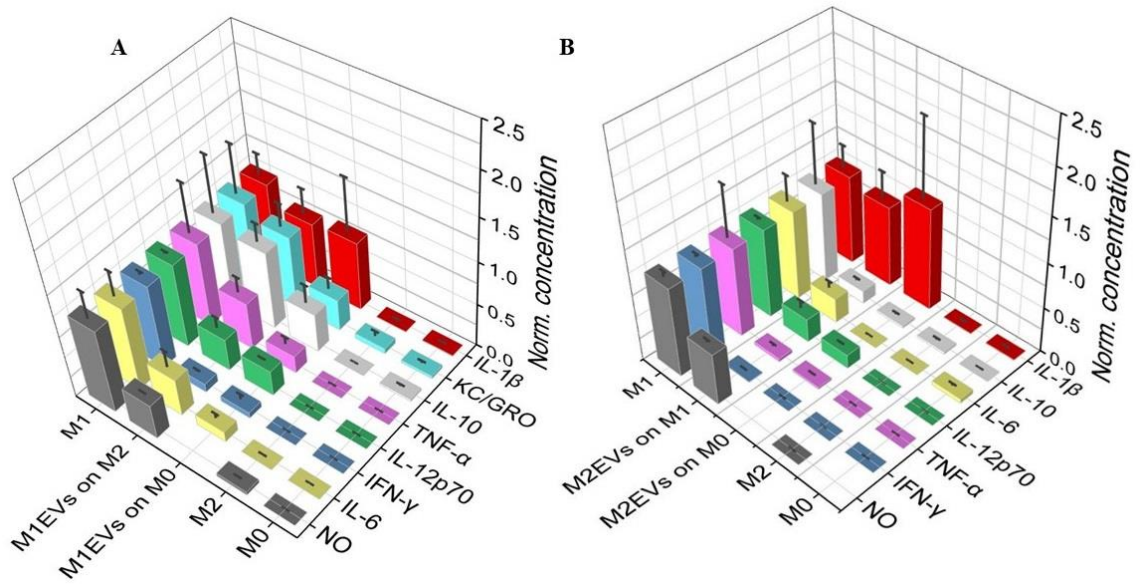


Figure 2.4 Reprogramming macrophage polarization with MEVs.

(A) Measurement of the proinflammatory cytokines and nitric oxide (NO) released by M0, M1, and M2 macrophages compared to the production of cytokines released after M1EV delivery to M2 and M0 macrophages. Both M0 and M2 macrophages are polarized towards an M1 phenotype upon interaction with M1EVs in vitro. (B) Quantification of pro-inflammatory cytokines and NO expression by M0 and M1 macrophages when incubated with M2EVs for 24 hours in vitro. Pro-inflammatory cytokines released by M1 macrophage are significantly reduced upon interaction with M2EVs which shows M2EVs are capable of re-programming M1 macrophage towards an M2 phenotype. Each data point is the average of at least 3 experiments (n=3). The data are presented as the mean \pm SEM.

inflammatory macrophages. To test the capability of MEVs to reprogram already polarized macrophages, we treated cultured M2 BMDMs with M1EVs and compared the cytokine production from M1 macrophages, M2 macrophages, and M2 macrophages exposed to M1EVs. For M2 macrophages that had been treated with M1EVs, we found significant increase in the production of cytokines ($n = 3/\text{group}$) from undetectable to $10 \pm 1\%$ (IFN- γ), $91 \pm 20\%$ (IL-10), $37 \pm 12\%$ (IL-12p70), $77 \pm 30\%$ (IL-1 β), $44 \pm 20\%$ (IL-6), $85 \pm 27\%$ (KC/GRO) and $55 \pm 18\%$ (TNF- α) of the average concentration seen for M1 macrophages (Figure 2.4A). We further performed a Griess assay to assess the nitric oxide (NO) presence in MCM collected from M1, M2 and M2 macrophages that were incubated with M1EVs. We found a significant increase in the production of nitric oxide from negligible initial amounts in M2 to $41 \pm 0.4\%$ of the average concentration seen for M1 macrophages when M2 macrophages were treated with M1EVs. Comparing M2 vs. M0 macrophages treated with M1EVs, M1EVs were able to induce a greater increase in pro-inflammatory indicators in M2 macrophages. Control studies showed that MEVs themselves only have marginal amounts of cytokines and that would not be responsible for the amounts seen after the shift (Table 3.1). These results indicate that M1EVs can repolarize M2 bone marrow-derived macrophages toward a pro-inflammatory M1 phenotype as evidenced by the increase in inflammatory cytokine production.

We also added M2 vesicles to cultured M0 macrophages and compared the cytokine production from M1 macrophages, M0 macrophages and M0 macrophages incubated with M2EVs (Figure 2.4B). We found that upon incubation of M0 macrophages with M2EVs, M0 macrophages did not produce most of the proinflammatory cytokines indicating M2EVs do not induce most of the proinflammatory properties in target M0 macrophages (Figure 3B). This indicates that the delivery of vesicles themselves are not simply generating a proinflammatory response that was seen only with M1EV delivery. We further compared the cytokine production from M1 macrophages, M2 macrophages and M1 macrophages incubated with M2EVs. We observed clear pro-inflammatory markers from

M1-macrophages but virtually no levels for most of the pro-inflammatory cytokines in the M2 culture. We further observed a clear decrease in the levels of all the pro-inflammatory markers for M1 macrophages that were incubated with M2EVs (Figure 2.4B). M2EVs significantly attenuated cytokine released by M1 macrophages by 99% (IFN- γ), 85% (IL-10), 74% (IL-12p70), 9% (IL-1 β), 72% (IL-6), 78% (KC/GRO) and 96% (TNF- α) of the average concentration seen for M1 macrophages (Figure 3B, S5). We also observed a significant reduction (49%) in NO production by M1 macrophages that were incubated with M2EVs compared to the average concentration seen for M1 macrophages. This indicates that M2EVs can reprogram M1 macrophages away from a proinflammatory phenotype. This has important implications on the use of MEVs to reprogram macrophage phenotype as part of a therapeutic approach. The phenotype used to generate MEVs appears to dictate their ability to reprogram both naive and already polarized macrophages toward a desired phenotype. The ability to alter macrophage inflammatory properties could be an important therapeutic tool to reprogram anti-inflammatory macrophages to a proinflammatory phenotype.

2.4.4 Repolarization of Microglia

Microglia are immune cells present in the central nervous system.²⁶² Like macrophages, microglia are also polarized to M1 and M2 phenotypes and play pro- and anti-inflammatory roles, respectively.²⁶³ To determine if macrophage derived vesicles are able to reprogram microglia phenotypes, we delivered vesicles derived from macrophages to primary microglia cells in culture. We induced M2 microglia polarization using IL-4. M1EVs generated from bone marrow derived M1 (LPS + INF- γ) macrophages were then added to cultured M2 microglia to compare the cytokine production from M1 microglia, M2 microglia, and M2 microglia incubated with M1EVs. We observed clear pro-inflammatory

markers from M1 microglia and virtually no measurable levels for most of the cytokines in the M2 microglia culture. We also observed an increase in the levels of all the pro-inflammatory markers for M2 microglia that were incubated with M1EVs (Figure 2.5). The ability of M1EVs to reprogram M2-polarized microglia toward a proinflammatory (M1) phenotype in a controlled fashion suggests that we can reprogram both macrophage and microglia inflammatory properties by the delivery of vesicles that are targeted to specific cell types. Furthermore, similar to macrophage exosomes, MEVs can deliver corresponding signals to unstimulated macrophages and differentiate them into specific phenotypes. This has implications for therapeutic approaches where the goal is to either initiate or suppress a proinflammatory response.

The ability of MEVs to reprogram immune cells is likely due to membrane bound proteins on the surface of the vesicle. As they are derived from parent immune cells, MEVs carry a wide range of transmembrane proteins, membrane bound cytokines, and other cell signaling endogenous ligands. These proteins can interact with membrane receptors on the target cell initiating signaling cascades that lead to repolarization.

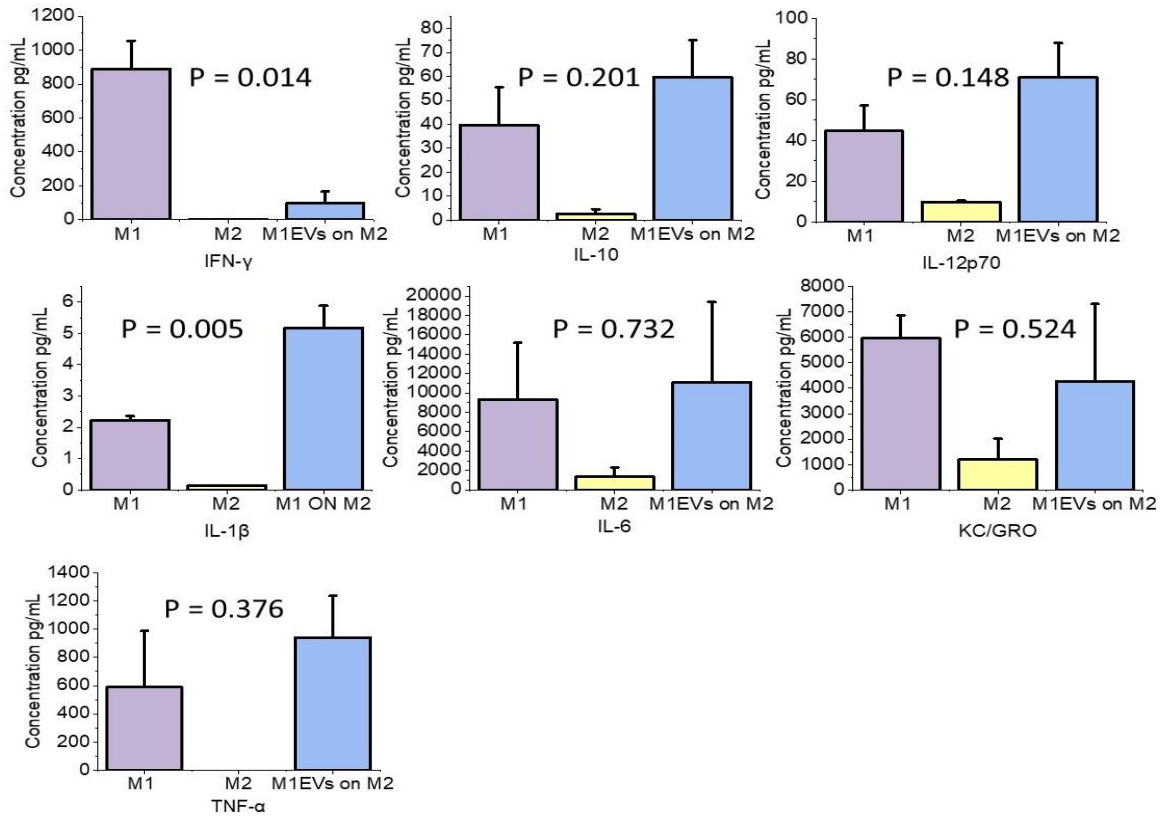


Figure 2.5 Quantification of cytokine released by microglia.

Cytokine released by M1 microglia, M2 microglia and M2 microglia that were incubated with M1EVs. Each data point is the average of at least 3 experiments. The data are presented as the mean \pm SEM. One-Way ANOVA was done to test the statistical significance of the result.

2.4.5 Macrophage Induced Neurotoxicity

Classically activated M1 macrophages, stimulated with LPS + IFN- γ , are neurotoxic and contribute to neuronal degeneration by releasing high levels of specific pro-inflammatory cytokines and oxidative metabolites such as nitric oxides.^{223, 264} Pro-inflammatory cytokines such as TNF- α , IFN- γ , IL-12 and IL-6 have been found to be involved in neuronal death.²⁶⁵⁻²⁶⁷ Alternatively activated, M2 macrophages do not induce cell death but rather help the repair process by releasing growth factors and anti-inflammatory cytokines.^{236, 237} Recent studies showed that azithromycin (AZM), a frequently used macrolide antibiotic, also possesses the ability to reduce macrophage-mediated neurotoxicity by altering macrophage phenotype from pro-inflammatory to anti-inflammatory.^{223, 268} We sought to determine if MEV induced reprogramming of M1 macrophages toward an M2 phenotype could moderate neurotoxicity in a similar fashion to AZM.²²³ We used LPS + IFN- γ to stimulate an M1 macrophage phenotype and IL-4 to stimulate an M2 phenotype. We generated vesicles from M2 macrophages and then exposed M1 macrophages to M2 MEVs which reduces the production of pro-inflammatory cytokines (Figure 2.6B). We collected supernatant from M1 macrophages and M1 macrophages that had been exposed to M2EVs for 24 hours. Media from both conditions were used to separately treat differentiated Neuro-2A (N2a) cells. N2a cells are a mouse neural crest-derived cell line which possess the ability to differentiate into cells with neuron like characteristics. We found that media from M1 macrophage resulted in a 40% reduction in neuron viability relative to the control media (Figure 2.6A) (n = 5/group). We further found that media collected from M1 macrophages that had been exposed to M2EVs for 24 hours resulted in no significant reduction in neuron viability relative to the control (Figure 2.6A). This is likely due to the significant reduction of proinflammatory cytokines by M1 macrophages upon incubation with M2EVs (comparable to AZM treated M1 cells, Figure 2.6B) and the corresponding increase in neuron viability suggest that proinflammatory

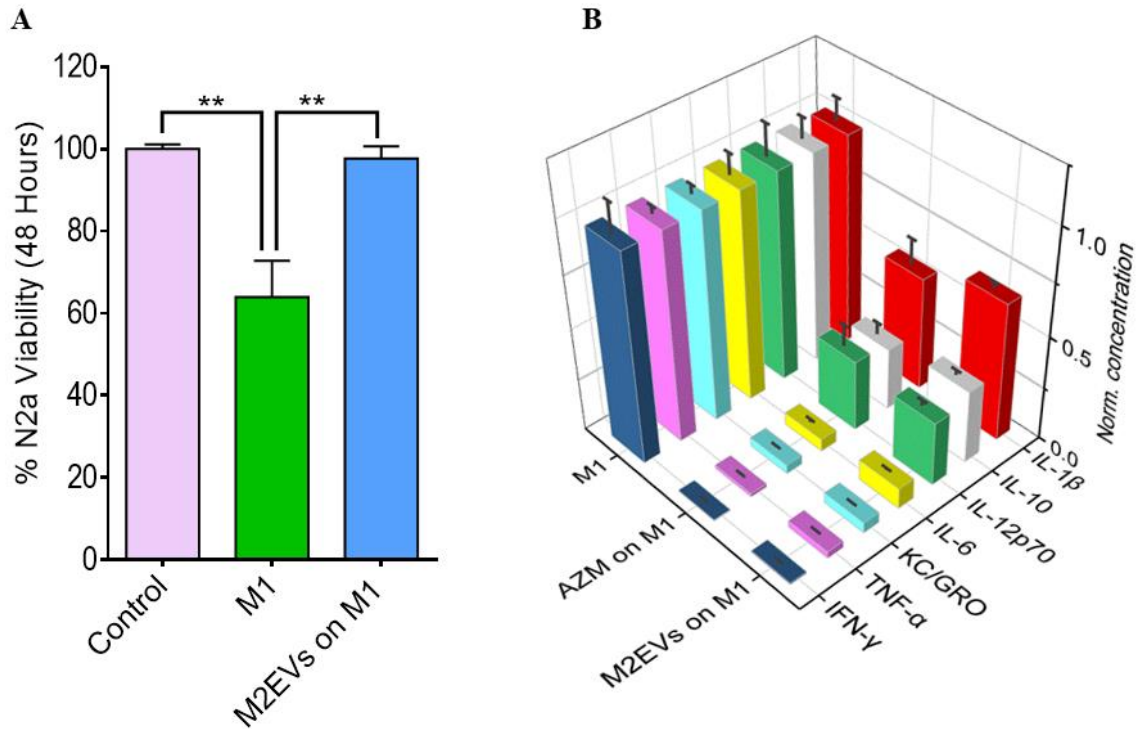


Figure 2.6 Macrophage mediated neurotoxicity.

(A) The effect of macrophage-conditioned media on the viability of differentiated N2a cells was determined using a cell viability assay for control cells with growth media (pink), for supernatant from M1 macrophage culture (green), and for supernatant from M1 macrophage culture after treatment with M2EVs (blue). (B) Comparative study of the ability of M2EVs and azithromycin (AZM) in solution (10 μ M) to reprogram M1 macrophages towards an M2 phenotype. Each data point is the average of five independent replicates ($n = 5$). $**p < 0.01$ indicates results are statistically significant. The data are presented as the mean \pm standard error of mean (SEM).

cytokines released by M1 macrophages play a major role on the cytotoxicity of N2a cells. These results also indicate that reprogramming M1 macrophages toward an anti-inflammatory phenotype using M2EVs is comparable to an immunomodulatory pharmacological agent and reduces the cytotoxicity normally observed with pro-inflammatory macrophages.

2.4.6 MEVs for Therapeutic Delivery

Previous studies have shown that vesicles generated from A549 (lung carcinoma) cells can target as well as deliver chemotherapeutics to the same cell type from which they were generated.²¹² There is some concern about the use of cancer cell derived vesicles for drug delivery because of the potential for these vesicles to be cleared by the body's immune system and that these vesicles might increase the metastatic potential. We tested MEVs to determine if they had similar targeting and therapeutic delivery features as was previously observed for cancer cell vesicles. MEVs lack any cancer characteristics and would not increase the metastatic potential. We first performed an experiment to determine the targeting ability of MEVs for A549 cells. We generated vesicles from macrophages and labeled them with DiI. We then determined the efficiency of delivery of MEVs by measuring the fluorescence signal at time points over 4 hours. We observed an increase in the fluorescence intensity over time resulting from an uptake of MEVs by the A549 cells. The uptake of MEVs by A549 cells suggests that MEVs can serve as a potential drug delivery vehicle in the delivery of chemotherapeutics (Figure 2.7A).

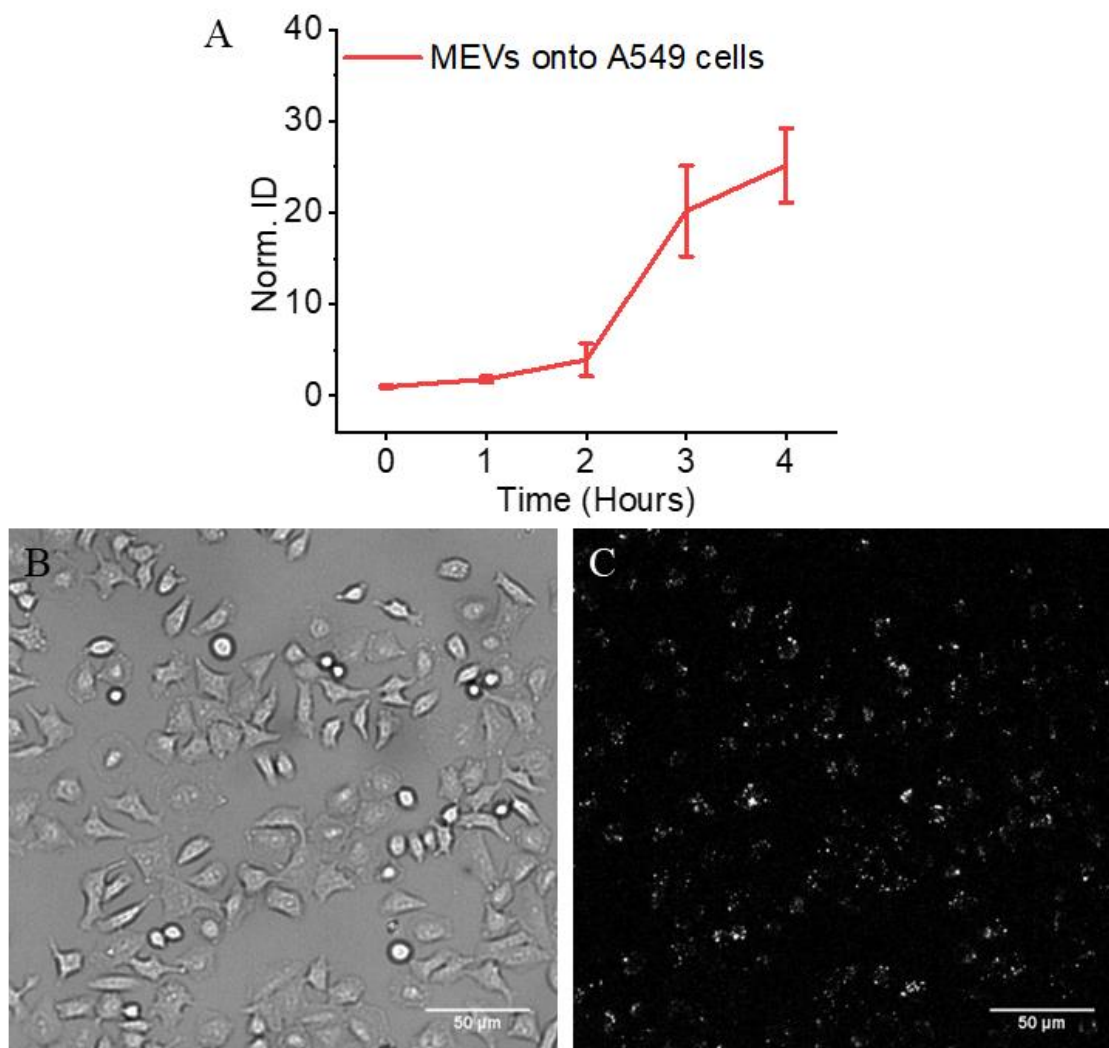


Figure 2.7 Targeting of MEVs onto A549 cells.

(A) Increasing fluorescence intensity of A549 cells over time due to the uptake of fluorescently labeled MEVs. (B) Bright field image of A549 cells. (C) Fluorescence image of A549 cells that had taken up DiI-labeled MEVs. Each datapoint is the average of five independent replicates. Norm. ID is the mean integrated density of the image normalized to the mean integrated density value of A549 cells prior to vesicles addition. The data are presented as the mean \pm SEM (n=5).

We next determined if MEVs could be loaded with cisplatin and delivered to cancer cells while maintaining the efficacy of the therapeutic. We also compared the specificity of cisplatin-delivery onto A549 cells using M0EVs, M1EVs and M2EVs (Figure 2.8A). We found that empty M0EVs and M2EVs had no significant effect on A549 cell proliferation. However, M1EVs resulted in 10% A549 cell death in 24 hours. We further generated cisplatin loaded-M0EVs (Cs-M0EVs), -M1EVs (Cs-M1EVs) and -M2EVs (Cs-M2EVs) from an equal number of M0, M1 and M2 macrophages. Previous studies have shown that vesicles generated using nitrogen cavitation can efficiently encapsulate chemotherapeutics and are stable for 2 days.²¹² Therapeutic loaded MEVs were then delivered to cancer cells to determine cytotoxicity. Cisplatin-loaded M0 and M2 vesicles resulted in 45% and 40% cell death, respectively, at 24 hours. However, cisplatin loaded M1 vesicles resulted in a 60% A549 cell death in 24 hours (Figure 2.8A). This is a clear indication that cisplatin loaded M1 MEVS are more efficient in killing cancer cells compared to cisplatin loaded M0 and cisplatin loaded M2 macrophages.

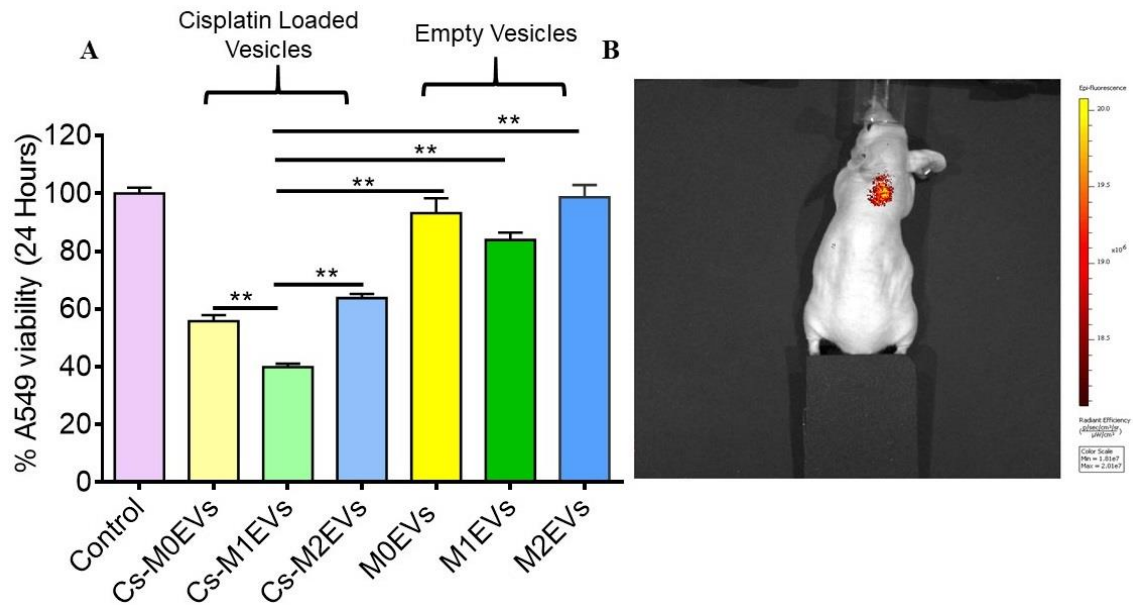


Figure 2.8 MEVs as biological nanocarriers.

(A) Comparison of targeting specificity of cisplatin-loaded M0, M1 and M2-engineered vesicles to A549 cells. Each data point is the average of five independent replicates ($n = 5$). Anova with Post Hoc Tukey's HSD was used to test the significance of the results. $**p < 0.01$ indicates results are statistically significant. The data are presented as the mean \pm SEM. (B) Mice bearing A549 xenografts were injected with DiR labelled M1EVs, demonstrating M1EVs can reach the tumor of the mice.

2.4.7 In vivo Delivery of MEVs to Tumor Xenografts

To determine if MEVs exhibited similar targeting features in vivo as we observed in cell culture, we generated vesicles from M1 macrophages and labeled them with a membrane dye, DiR. Free dye was separated from MEVs using PD Miniprep columns. We found that M1EVs targeted tumor xenografts (subcutaneous injection A549 cells) implanted in immune-compromised athymic nude (nu/nu) mice. After the tumor xenograft reached at least 100 mm³, we injected 2×10^{10} vesicles through the tail vein of each of the three different mice. We used an IVIS whole animal imager for in vivo imaging. Imaging was done at 48 hours and 72 hours post-injection of labeled vesicles. DiR alone when injected into the mice as a control showed nonspecific accumulation. We observed clear delivery of the labeled vesicles to the tumor xenograft at 72 hours post-injection of labeled vesicles (Figure 2.8B). These results verify that M1EVs can specifically target tumor tissue in vivo.

2.5 Conclusions

In conclusion, BMDMs can be used to engineer nanosized vesicles with high yield using nitrogen cavitation. These vesicles can be loaded with various cargo during their generation and can be used as drug delivery vehicles both in vitro as well as in vivo. In addition, MEVs when interacting with the macrophage itself, possess the ability to reprogram macrophages and microglia into specific inflammatory phenotypes that dictate macrophage function (e.g. neurotoxicity, tumor migration). This shows the potential for MEVs as a novel and versatile therapeutic to target and reprogram macrophages.

CHAPTER 3. PROGRAMMING CELL-ENGINEERED VESICLES FOR ENHANCED IMMUNOMODULATORY PROPERTIES

3.1 Summary

Tumor-associated macrophages are the predominant immune cells present in the tumor microenvironment, and mostly exhibit a pro-tumoral M2-like phenotype. However, macrophage biology is reversible, so they can also acquire an anti-tumoral M1-like phenotype. A promising therapeutic strategy for treating cancer may be achieved by modulating macrophages from an M2-to an M1-like phenotype. Here, we to generated programmed nanovesicles as an immunomodulatory therapeutic platform that has the greatest capability to re-polarize M2 macrophages to an M1-like phenotype. Programmed nanovesicles engineered from cellular membranes to have specific immunomodulatory properties including the capability to bidirectionally modulate immune cell polarization. These programmed nanovesicles decorated with specific membrane-bound ligands can be targeted toward specific cell types. Utilizing macrophage derived vesicles can be engineered to enhance immune cell reprogramming of proinflammatory and anti-inflammatory immune cells.

3.2 Background

Vesicle based nanoparticles including exosomes¹²⁵, microvesicles^{26, 269}, and liposomes¹³² have been leveraged as potential therapeutic tools for cancer treatment due to their ability to specifically target the tumor environment and their ability to elicit a tumor specific immune response. Exosomes are nano-sized (diameter 40-150 nm) extracellular vesicles (EVs) released by the cells though normal physiological process^{270, 271} and contain a wide range of biological cargo including proteins and RNA which can be used to communicate information to target cells.²⁷²⁻²⁷⁴ Exosome targeting specificity can be

harnessed to controllably deliver therapeutics *in vivo*. In addition, exosomes released by the antigen presenting cells (APCs) including dendritic cells and macrophages can also activate the immune system.^{26, 125} Despite these promising characteristics, low production yields and difficulty in separating exosomes from biological solutions still pose barriers for their use in clinical applications.^{144, 275} Liposomes, synthetically generated nano-sized vesicles, have been used as an alternative to exosomes in therapeutic delivery.²⁷⁶ While liposome can be produced in large quantities, they lack the inherent biocompatibility seen with endogenous exosomes and are prone to immune clearance when delivered *in vivo*.¹²⁴ Recently, cell-derived vesicles (CDVs) obtained by fragmenting cellular membranes have been found to mimic many of the positive attributes of exosomes and have shown promise as therapeutic delivery platforms because they can be produced in high yield, exhibit targeting specificity and low immunogenicity when delivered *in vivo*.^{144, 212, 247}

Vesicles derived from antigen presenting cells offer additional potential avenues for therapeutics because of their ability to serve as immunomodulatory platforms.^{125, 261} Macrophages are the most abundant immune effector cells present in the tumor microenvironment and exhibit a continuum of functional states between a pro-inflammatory (M1) and an anti-inflammatory state (M2).²⁷⁷ M1 macrophages are known to have anti-tumoral properties by engulfing and destroying the phagocytosed tumor cells and stimulating helper T-cell type 1 (Th1) response while M2 macrophages stimulate tumor angiogenesis and inhibit the anti-tumor immune response mediated by T-cells.^{224, 227} Along with small molecule immunomodulators¹²³ and extracellular vesicles¹²⁵, cell derived vesicles¹²⁷ from M1 macrophages have been shown to alter the polarization of tumor associated macrophages which play a role in the chemotherapy resistance and promote metastasis. While these therapeutic approaches show promise, they suffer from unique challenges. The efficacy of small molecules based therapeutics is limited by their rapid degradation and inability to preferentially target TAMs *in vivo*. While EVs are biostable, exhibit targeting specificity, and can modulate macrophage phenotype in the tumor

microenvironment, EV-based therapies are challenged by their low production yield. Cell-derived vesicles based therapies overcome several challenges that limit other nanoscale therapeutics, but CDVs would be more effective with more specific targeting and higher efficacy in repolarizing anti-inflammatory macrophages to a proinflammatory phenotype.

One approach for increasing the macrophage targeting or reprogramming capability of drug delivery systems, including cell derived vesicles, is to functionalize their surface with specific moieties that would endow them with enhanced immunomodulatory and macrophage targeting capabilities. A similar approach has been utilized for synthetic therapeutic-loaded lipid-polymer based nanoparticles which were engineered with DSPE-PEG-mannose and monophosphoryl lipid A (MPLA) to simultaneously improve their antigen presenting cell targeting and ability to execute enhanced immune responses²⁷⁸. Similarly, TLR7/8 agonists presenting nanoparticles have been generated using poly(ethylene glycol)-poly(lactic acid) (PEG-PLA) to enhance immunomodulatory properties of nanoparticles²⁷⁹. Here, we developed programmed cell derived nanovesicles generated from multiple cell types including macrophages through the targeted over-expression of specific ligands to achieve greater efficacy in reprogramming anti-inflammatory macrophages towards a proinflammatory phenotype. Overall, programmed nanovesicles based therapeutics show promise for enhanced ability to modulate immune cell inflammatory phenotype.

3.3 Methods

Animals: 2-5 month-old wild-type C57/BL6 mice were used to extract bone marrow cells. Animals were properly housed in IVC by providing sufficient food and water. We performed all experiments following the guidelines from National Institute of Health that were approved by the Institutional Animal Care and Use Committee at the University of Kentucky

Cell Culture: Bone marrow-derived macrophages (BMDMs) were obtained from 2-5 month old mice according to previously published method¹²⁷ with minor modifications. In brief, femurs and tibias were flushed with (Dulbecco's Modified Eagle's Medium (DMEM). Thus obtained solution was then centrifuged to collect the cell pellet which was resuspended in RBC-lysis buffer (0.15 M NH₄Cl, 10 mM KHCO₃, and 0.1 mM Na₄EDTA) to lyse the erythrocytes present in the cell pellet. Cells were resuspended in the standard medium (RPMI1640 supplemented with 10% fetal bovine serum (FBS), 5% penicillin/streptomycin (PS), 1% glutamine, 1% HEPES(4-(2-hydroxyethyl)-1-piperazineethanesulfonic acid), 0.001% β-mercaptoethanol and 20% supernatant from sL929 cells), transferred into 75-cm² culture flasks, and allowed to grow for 2 days. Standard medium was then replaced every two days until day 7. Cells were re-plated on day 7 at a cell density of 1×10⁶ cells/mL in re-plating media (Dulbecco's Modified Eagle's Medium (DMEM) supplemented with 10% FBS, 1% Glutamine and 1% PS) and on day 8 cells were stimulated to M1 (LPS (20 ng/mL; Invivogen) + IFN-γ (20 ng/mL; eBioscience)) or M2 (IL-4 (20 ng/mL); eBioscience) macrophages.

Vesicles Isolation: Mouse bone marrow derived pro-inflammatory macrophage engineered vesicles (MEVs) were generated according to the previously published method^{127, 212}. Briefly, fully differentiated pro-inflammatory (M1) macrophages were used to generate MEVs. Cells were first washed with PBS and resuspended in a PBS solution supplemented with one protease inhibitor tablet per 10 ml of buffer. The cell slurry was then transferred into a pre-chilled nitrogen cavitation vessel (Parr Instruments Company, IL, USA) on ice and subjected to a nitrogen gas pressure of 300 psi for 5 minutes. The pressure was rapidly released, resulting in the fragmentation of the cells and the subsequent generation of vesicles. The cell lysate obtained from nitrogen cavitation was centrifuged at 4000xg for 10 minutes at 4 °C. The pellet thus obtained was discarded and the supernatant was again centrifuged at 10,000xg for 20 minutes at 4 °C. The supernatant obtained was again ultracentrifuged at 100,000xg for 60 minutes at 4 °C to collect the pellet containing

nanovesicles. The pellets obtained after ultracentrifugation were washed with PBS before resuspending them in PBS.

Nanoparticle tracking analysis: MEVs size and concentration of the samples were obtained via nanoparticle tracking analysis (NTA) using NanoSight NS300 equipped with NTA analytical software and a 488 nm laser. Briefly, MEVs samples were diluted 1000 times in ultrapure water and five 30 seconds videos were recorded for analysis. Software settings for analysis were kept constant for every measurement for any specific sample.

Western blotting: Vesicle pellets and cells were first lysed separately in the RIPA buffer (150-mM NaCl; 1% Triton X-100; 0.5% sodium deoxycholate; 0.1% SDS; 50-mM Tris pH 8.0; 1× protease inhibitor cocktail (Roche)). Protein concentration was measured using UV/VIS Spectrophotometer. 30 ug of the respective protein samples were resolved on 12% lab-made polyacrylamide gels, then transferred onto a nitrocellulose membrane. Equal amount of protein from various samples was loaded per lane for comparison studies. The membrane was then blocked for 1 hour and then incubated for 2 hours with primary antibodies in non-reducing environment at room temperature with constant shaking. After washing and removal of the primary antibody, HRP-conjugated secondary antibody was added and incubated for 1 hour at room temperature with constant shaking. Then, the membranes were washed again, and bands were visualized by chemiluminescent detection (Clarity, Bio-Rad) using Chemi-Doc system (Bio-Rad).

Cytokine Quantification: Macrophages were cultured at a density of 50,000 in 96 well plates and then stimulated to M1 or M2 phenotypes with LPS (20 ng/mL; Invivogen) + IFN- (20 ng/mL; eBioscience) and (IL-4 (20 ng/mL; eBioscience), respectively. For cytokine analysis, the supernatant from stimulated cells or the cells treated with MEVs, macrophage conditioned media (MCM), was collected after 24 hours. Vesicles were added after 24 hours of stimulation and the supernatant was collected after 24 hours of vesicle addition. MCM was collected and kept at -80 °C until it was analyzed. We performed a mouse seven-plex pro-inflammatory cytokine assay from Meso Scale Discovery (MSD)

following the manufacturer's protocol. We used this assay to measure the presence of seven mouse pro-inflammatory cytokines (IFN- γ , IL-10, IL-12p70, IL-1 β , IL-6, KC/GRO, and TNF- α) at the same time. Briefly, 50 μ L of calibrators and MCM were dispensed into each well of a pro-inflammatory cytokine capture antibody-precoated MSD well plate and left to incubate for 2 hours with continuous shaking (10,000 rpm) at room temperature. The plate was then washed three times with wash buffer and 25 μ L of detection antibody solution was added into each well. After 2 hours of incubation, the plate was washed again and 150 μ L of the read buffer was added to each well. The MSD plate was finally analyzed for the pro-inflammatory cytokines on the MESO SECTOR imager from Meso Scale Delivery. A standard curve was obtained using Meso Scale Discovery Workbench analysis software. All samples were run in triplicates using a mouse seven-spot well plate to measure the pro-inflammatory cytokines present in the cell culture supernatant. We used vesicle suspensions in PBS to measure the proinflammatory cytokines present in the vesicle suspension. In some experiments, the same protocol as previously discussed was used to measure the concentration of TNF- α in the MCM using a single spot well plate.

Chemokine Quantification: Chemokines present on the MEVs were detected using Mouse Chemokine Array C1 (Ray Biotech, Code AAM-CHE-1-2) and semi-quantified following the manufacturer's protocol. Briefly, chemokines were first extracted from MEVs and M2 macrophages, a control, using cell lysis buffer as provided by the manufacturer. The protein concentration in M1EVs and M2 samples was measured using a UV/VIS Spectrophotometer(Thermo Scientific). For proteomic analysis, first the antibody arrays were incubated in 2 mL of blocking buffer for half an hour with constant shaking at room temperature. After half an hour, the blocking buffer was aspirated off and about 500 μ g of the protein samples were loaded into each well of an incubation array and left to incubate for 3 hours at room temperature. Following several washes, a biotinylated antibody cocktail was added to each well and incubated for 2 hours at room temperature. The biotinylated antibody cocktail was then aspirated off, followed by multiple washings.

After this, 1x HRP-Streptavidin was added to each well and incubated for 2 hours at room temperature. After multiple washings, 500 μ L of detection buffer mixture was added onto each membrane and visualized by chemiluminescent detection (Clarity, Bio-Rad) using the Chemi-Doc system (Bio-Rad). The immunoblot images were analyzed using ImageJ software.

Ligand Incorporation into MEVs: MEVs were generated from 150 million M1 macrophages and resuspended in a 500 μ L solution containing ligands (Pam3CSK4, rhodamine-labeled Pam3CSK4 or CpG-ODN) at 1 mg/mL. The ligand-MEV solution was then sonicated using a Model Qsonica Q125 sonicator with a 0.125" tip with the following settings: 20% amplitude, 20 cycles of 30 seconds on/off for 10 minutes. The MEV-ligand solution was allowed to cool down on ice for two minutes between each cycle. After completion of the sonication cycle, the ligand-MEV solution was left to incubate on ice for 60 minutes to allow the recovery of the MEV-membrane. Thus obtained ligand-decorated MEVs containing solution was diluted to 4 mL in PBS and subjected to ultracentrifugation at 100,000xg for 60 minutes at 4 °C to collect the pellet containing ligand-decorated MEVs. This final pellet was first washed with 1 mL of PBS twice and resuspended in 500 μ L of regular macrophage media. The number of MEVs present in the resuspension was determined using NTA. 1×10^{11} MEVs were then added into each well of a 96-well plate containing 50,000 M2 macrophages in 100 μ L of replating media. The plate was left to incubate at 37 °C for 24 hours. After 24 hours, MCMs were collected and used for pro-inflammatory cytokine analysis.

RelA translocation assay: We used a nuclear translocation assay to determine MEV-mediated NF- κ B pathway activation by comparing the amount of p65 subunit (RelA) translocated into the nucleus. M1 macrophages, M2 macrophages and MEV-treated M2 macrophages were counted and fractionated into nuclear and the cytoplasmic fractions using the NF- κ B Assay Kit (FIVEphoton Biochemicals, San Diego, CA) following the

manufacturers protocol. Supernatants containing the nuclear and the cytoplasmic fractions were collected, and p65 was quantified in each by western blot.

Confocal Imaging: A Nikon A1R laser scanning confocal microscope equipped with 10X, 20X, and 60X objectives were used for confocal imaging of the cells that had been programmed to overexpress specific ligands on their surface. The obtained images were analyzed with Nikon image processing software.

Transfection: HEK cells were transfected using Lipofectamine 2000 reagent (Invitrogen) using the manufacturers protocol. We used 2-5 month old wild-type C57BL/6 mice to isolate bone marrow monocytes. Monocytes were then differentiated into macrophages. On day five, macrophages were transfected with a plasmid. Macrophages were transfected using the jetPEI-Macrophage *in vitro* DNA transfection reagent following manufacturers protocol. Transfection efficiency was compared by confocal imaging and western blotting. Thus programmed M1 macrophages were used to generate programmed nanovesicles.

Statistical Analysis: Statistical analyses were carried out using Origin. Data was reported as the mean \pm standard deviation of the mean (SEM). At least three separate experiments were conducted for each condition ($n = 3$). A one-way ANOVA was done to determine statistical significance. The results are considered statistically significant if the p-value is less than or equal to 0.01.

3.4 Results and Discussions

3.4.1 MEV Characterization

We utilized pro-inflammatory (M1) bone marrow derived macrophages (BMDMs) to generate macrophage engineered vesicles (MEVs) through the disruption of the cell membrane with nitrogen cavitation. In this technique cells suspended in solution are kept in a prechilled nitrogen decompressor with a pressure of 300 psi for five minutes. When the pressure is rapidly released, nitrogen gas bubbles are formed that disrupt the macrophage membrane into nano-sized fragments. These fragments now have their hydrophobic ends exposed in the aqueous solution resulting in them rearranging to form vesicles²⁸⁰. To characterize MEVs concentration and the size distribution, we used nanoparticle tracking analysis (NTA) which allows us to measure both the size distribution and the concentration of the vesicles in solution. We found that 100 million M1 BMDMs generated approximately 2×10^{12} MEVs. The size distribution of the MEVs obtained from nanoparticle tracking analysis is primarily between 50-200 nm (Figure 3.1a), which is similar to the range reported for exosomes. The mean diameter of MEVs obtained from NTA was 127 nm. To determine the stability of MEVs, we next measured the surface charge of the MEVs using a Malvern Zetasizer. The zeta potential of MEVs was -5.2 mV. This is similar to values seen for endogenously released vesicles such as exosomes which have been reported to have a zeta potential between -5 mV to -20 mV. We next utilized SDS-PAGE gel electrophoresis to determine the proteins present on the surface of MEVs in comparison to the parent M1 macrophage. We observed similar protein bands from MEVs and M1 macrophages indicating that vesicle formation retains most of the same proteins present on the cell surface (Figure 3.1b). Exosomal marker proteins such as tetraspanins (CD9 and CD63), integrins (CD81, CD82), chaperones (HSP60, HSP70), immunoglobulins (ICAM-1, VCAM1) and major histocompatibility complex class I (MHC-I) and II (MHC-II) have been shown to be present on M1 exosomes and have been

implicated in adhesion, signaling and activation when exosomes are delivered to target macrophages. We performed western blotting for several of these exosomal marker proteins including CD9, CD54, CD63, CD81, CD106 and found that the majority of these proteins including CD54 (ICAM-1), CD63, MHCII, CD11b, CD81 are present in MEVs (Figure 3.1c). However, we found that other exosomal marker proteins including CD9, CD106 were absent in MEVs. Similar to protein extracts taken from MEVs, western blotting analysis demonstrated that CD9 and CD106 were absent in protein samples taken from M1 BMDMs. Tetraspanins including CD9, and CD63 are integral membrane proteins, embedded within the cellular membranes and have been shown to play a vital role in the fusion of exosomes with target cells. Similarly, intercellular cell adhesion molecule-1 (ICAM-1) is a transmembrane glycoprotein which has been shown to mediate cell-cell interaction and outside-in cell signaling during an immune response. The presence of a majority of the same surface markers in MEVs indicates that vesicles engineered through nitrogen cavitation likely have similar properties to exosomes.

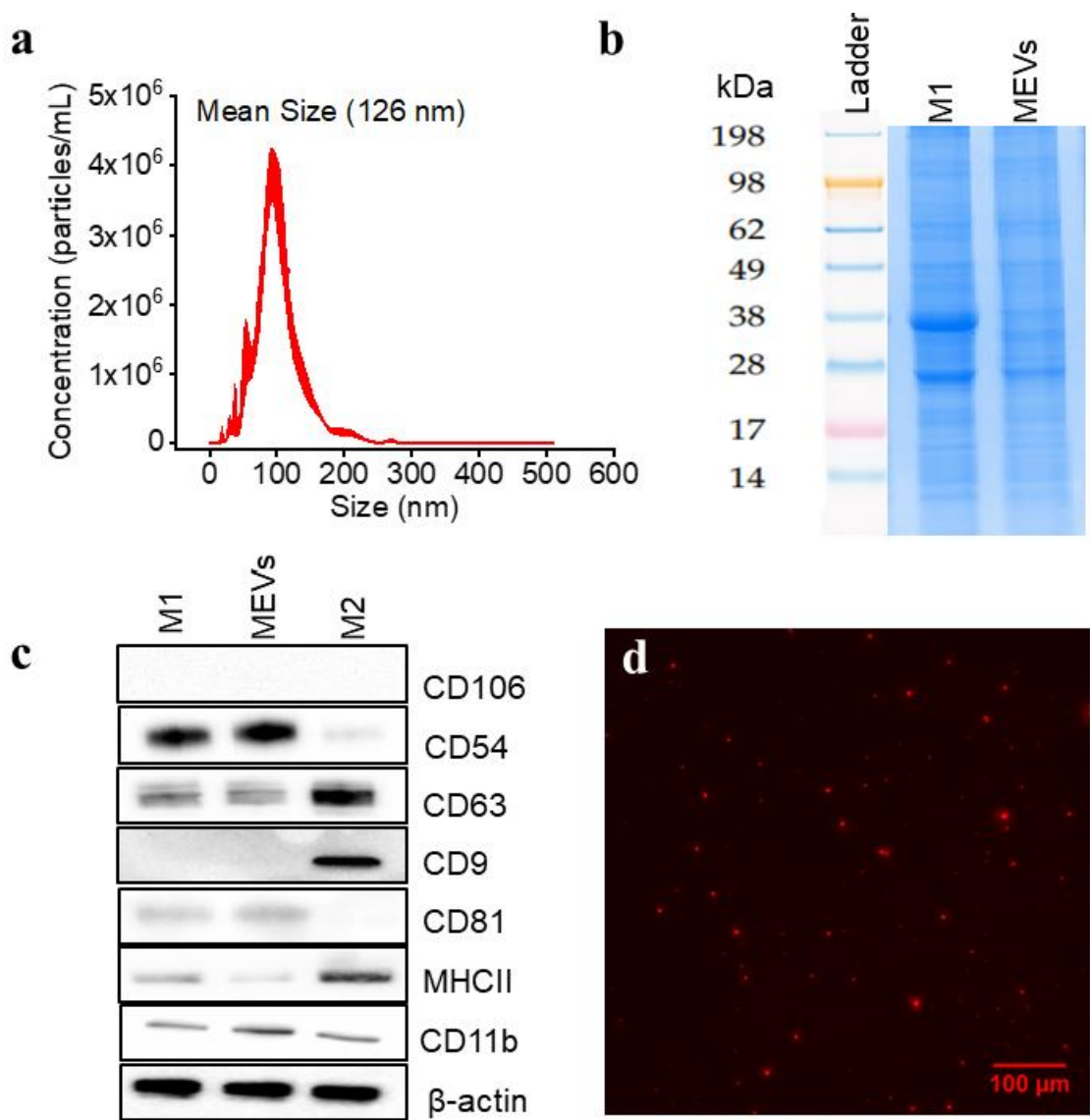


Figure 3.1 Macrophage Engineered Vesicles (MEVs) Characterization.

(a) Size distribution of MEVs obtained from Nanoparticle Tracking Analysis (NTA). (b) Sodium dodecyl sulfate polyacrylamide gel electrophoresis (SDS-PAGE) analysis of the protein content of MEVs compared to M1 macrophages. (c) Validation of exosome marker proteins in MEVs. Equal amounts of total proteins extracted from MEVs, M1 macrophages and M2 macrophages were immunoblotted for CD106, CD54, CD63, CD9, CD81, MHCII and CD11b. (d) Wide-field fluorescence image of MEVs labelled with a lipophilic dye DiI.

We next performed a set of experiment to see if MEVs could successfully be delivered to M2 BMDMs similar to what has been shown for exosomes^{125, 261}. We first labeled MEVs with DiI, a lipophilic, non-toxic, fluorescent label that embeds into the membrane of the vesicles. We confirmed the labeling of these vesicles by exposing the labeled vesicles to green excitation light and observing them with fluorescence microscopy. The red punctuates regions as seen in the Figure 3.1d indicates the successful labeling of vesicles with DiI. We used these labeled vesicles in time lapse imaging experiments at recording vesicle delivery at multiple time points for 2 hours by incubating 1×10^9 labeled vesicles with 30,000 M2 BMDMs. MEV uptake was tracked through the measurement of the fluorescence intensity of the labeled vesicles in the otherwise unlabeled cells. Images were taken at 10-minute time intervals for 2 hours. We observed a gradual uptake of MEVs by M2 BMDMs (Figure 3.2) over time as indicated by the increase in fluorescence intensity. These preliminary characterization results suggest that nitrogen cavitation generated MEVs have similar size, zeta potential, surface markers as exosomes and these vesicles are efficiently taken up by M2 BMDMs.

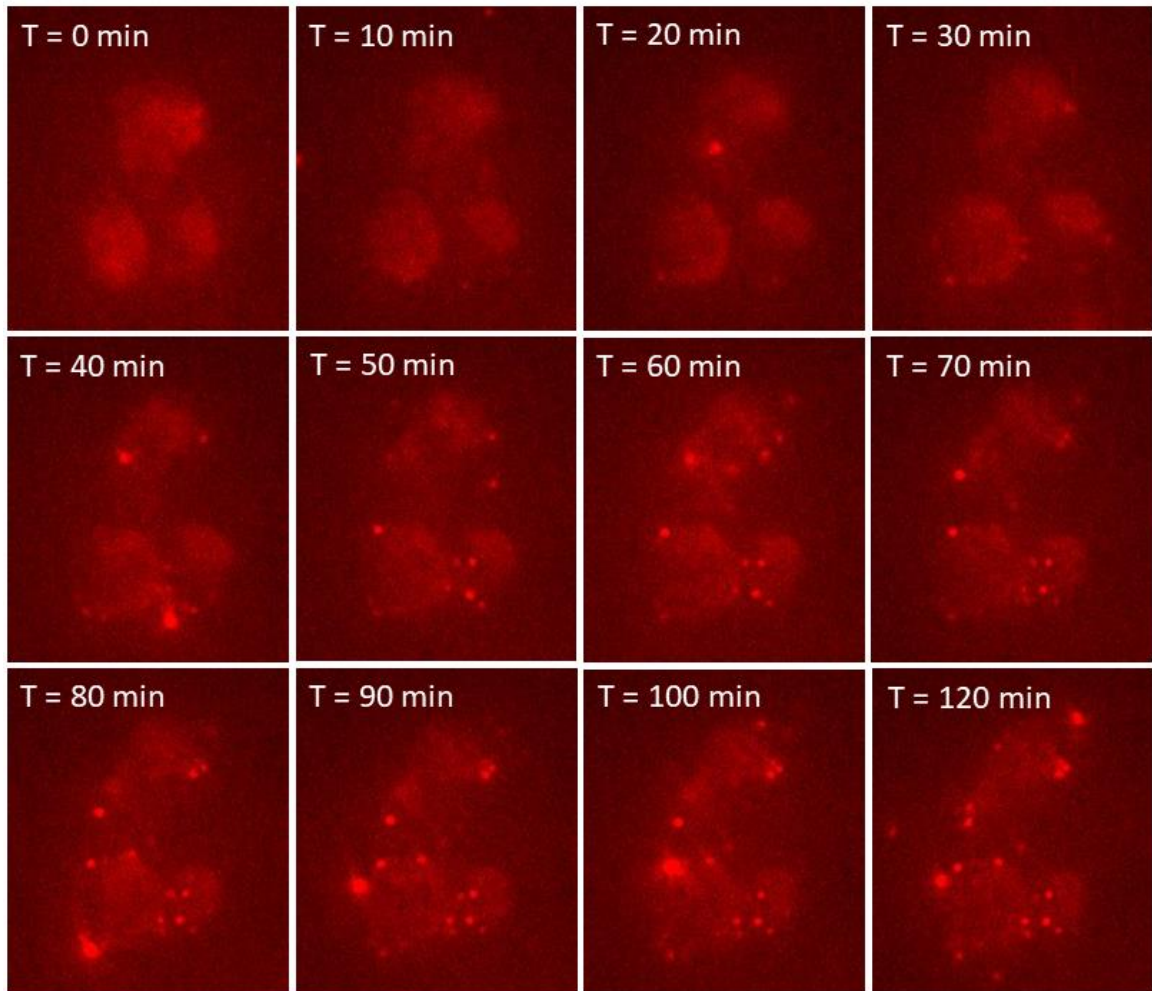


Figure 3.2 Series of images showing DiI-labeled MEVs uptake by M2 BMDMs.

Vesicles were added after first time point in real time and images were taken for 2 hours in every 10 minutes. 40x air objective was used with 561 laser. Vesicles were labelled by DiI dye.

3.4.2 MEV-mediated Phenotypic Reprogramming of M2-BMDMs

We next confirmed the ability of pro-inflammatory (M1) macrophage engineered vesicles (MEVs) to reprogram anti-inflammatory (M2) bone marrow derived macrophages (BMDMs) towards a proinflammatory phenotype using a series of cell membrane modifications. We first validated a shift in macrophage phenotype using immunocytochemistry analysis to measure the expression of iNOS, a pro-inflammatory macrophage marker, in M2 BMDMs while they were incubated with different concentrations of MEVs. We incubated 50,000 M2 BMDMs with an increasing concentration of MEVs ranging from 10^7 to 10^{11} for 12 hours at 37 °C . We observed a clear increase in iNOS for M2 BMDMs upon incubation with increasing concentration of MEVs (Figure 3.3a-e). At a concentration of 10^{11} vesicles, we observed a robust expression of iNOS (Figure 3.3e). These results demonstrate that M2 BMDMs can be reprogrammed through MEV exposure shifting polarization toward a pro-inflammatory phenotype as evidenced by the expression of M1 macrophage markers. We performed additional immunocytochemistry analysis to understand the effect of MEV-driven M2 to M1-like polarization on CD206, a M2 macrophage marker, expression. We observed a gradual decrease in CD206 expression (Figure 3.3a-f). Overall, these results indicate that at a suitable concentration, MEVs can reprogram M2 BMDMs toward an M1-like phenotype as evidenced by the expression of pro-inflammatory macrophage markers with the simultaneous decrease in M2 macrophage markers.

We also performed a time dependent repolarization assay for M2 macrophages incubated with MEVs and simultaneously assessed seven different pro-inflammatory cytokines (IFN- γ , IL-10, IL-12p70, IL-1 β , IL-6, KC/GRO, and TNF- α) released by MEV-treated M2 BMDMs. We added 1×10^{11} vesicles to 50,000 macrophages in culture and

analyzed cytokine release by MEV-treated M2 macrophages after 0.5, 1, 1.5, 2, 3, 6, 12, 24 hours of incubation. Compared to the low level of pro-inflammatory cytokines released by unmodified M2 BMDMs, we observed an increase in cytokine levels as early as 2 hours of incubation. As the incubation time progresses, we observe an increase in cytokine release by MEV-treated M2 BMDMs. Pro-inflammatory cytokine release into the supernatant plateaued after 12 hours of incubation of M2 BMDMs with MEVs (Figure 3.3g-h). We did not see differences in the cytokine release by MEV-treated M2 BMDMs between 12 hours and 24 hours of incubation time. These results indicate that MEV-mediated M2 to M1 repolarization depends both on the concentration of MEVs and the incubation period.

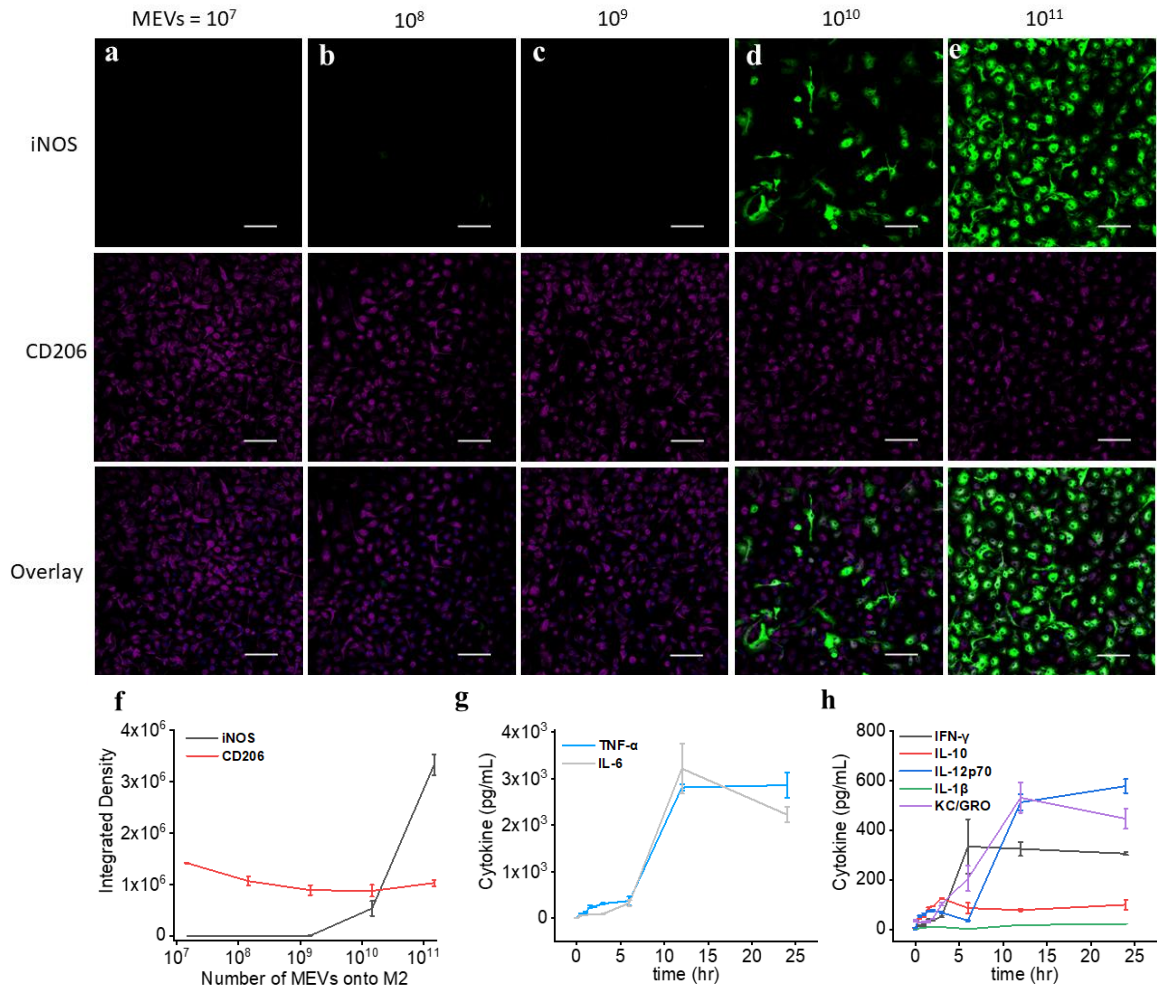


Figure 3.3 Reprogramming macrophage polarization by MEVs.

(a-f) Immunostaining of iNOS (M1 macrophage marker) and CD206 (M2 macrophage marker) in M2 macrophages after incubation with 10^8 , 10^9 , 10^{10} and 10^{11} MEVs for 24 hours. Each data point is the average of at least 5 experiments ($n=5$). The data are presented as the mean \pm SEM. (g, h) Measurement of the proinflammatory cytokines including IFN- γ , IL-10, IL-12p60, IL-1 β , IL-6, KC/GRO, and TNF- α released by M2 macrophages after incubating them with 1×10^{11} MEVs in a time dependent manner. Each data point is the average of at least 3 experiments ($n=3$). The data are presented as the mean \pm SEM.

3.4.3 Role of MEV-anchored Endogenous Ligands on M2 to M1 Macrophage Modulation.

We hypothesized that proteins anchored within the membrane of MEVs control targeting, cellular uptake, and drive changes in macrophage phenotype. Because MEVs are generated from parent pro-inflammatory macrophages and maintain proteins resident on the surface of M1 macrophages (Figure 3.1b), MEVs may carry a wide range of membrane bound cytokines, chemokines, transmembrane proteins, and other cell signaling endogenous ligands that belong to the parent macrophage. These proteins present may interact with the surface proteins on the recipient anti-inflammatory (M2) macrophages initiating signaling cascades that lead to their repolarization towards M1 phenotype. We first performed a set of studies to validate that membrane proteins played a role in MEV induced macrophage repolarization. It is possible that cytokines, cell associated signaling proteins, anchored in the plasma membrane of the cell could be responsible for macrophage reprogramming. For example, pro-inflammatory cytokines including TNF- α , IFN- γ , IL-12 produced by classically activated macrophages can stimulate macrophage polarization towards an M1 phenotype. We examined vesicle solutions for seven pro-inflammatory cytokines including IFN- γ , IL-10, IL-12p70, IL-1 β , IL-6, KC/GRO, and TNF- α to determine if residual cytokines contributed to mechanism of MEVs-mediated M2 to M1 repolarization. To analyze the cytokines entrapped in the interior of MEVs, we freeze-fractured MEVs to rupture them and released the entrapped cargo from inside of the vesicles. Cytokine assays showed that MEVs contain low levels of pro-inflammatory cytokines in the interior of the vesicles and virtually no cytokines in the vesicle solution (Table 3.1). We further investigated if the amount of cytokines present in the vesicle suspension is sufficient to reprogram M2 towards M1 macrophages. We performed an IFN- γ dose response with M2 macrophage and assessed TNF- α released by M2 macrophages

into the supernatant after treatment (Figure 3.4a). Results showed that the small amount of cytokines present in MEVs (~40 pg/mL) was not capable of altering M2 macrophage phenotype and had a negligible contribution to mediating M2 to M1 repolarization (Figure 3.4b).

Table 3.1 Cytokine quantification in vesicles.

MEV were freeze-ruptured (FR-MEV) in liquid nitrogen to assess cytokines present inside of the MEVs.

Cytokines	MEV (pg/mL)	FR-MEV (pg/mL)
IFN- γ	3 \pm 0.5	4 \pm 0.2
IL-10	16 \pm 1	17 \pm 4
IL-12p70	12 \pm 1	11 \pm 3
IL-1 β	4 \pm 1	4 \pm 1
IL-6	28 \pm 6	23 \pm 6
KC/GRO	3 \pm 0.2	3 \pm 0.2
TNF- α	13 \pm 1.6	13 \pm 2.9

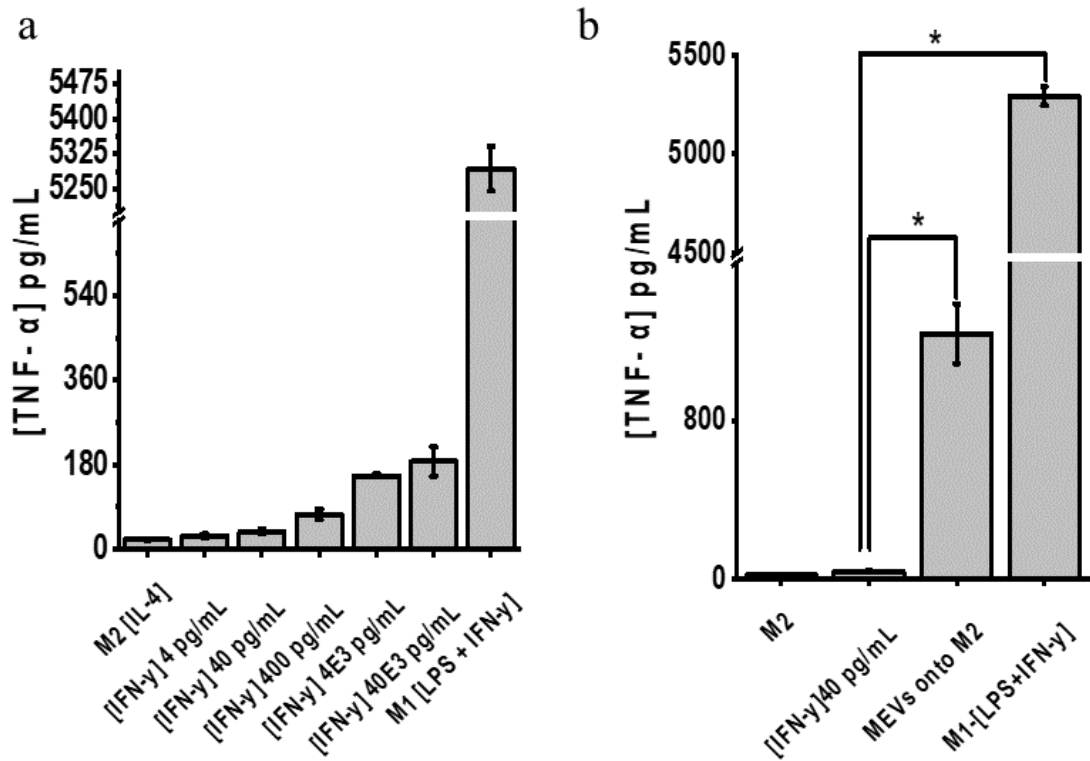


Figure 3.4 Cytokine content of MEVs.

(a) A dose response study showing the pro-inflammatory cytokine-TNF- α released by M2 macrophages after incubation with different concentration of IFN- γ for 24 hours. (b) Quantification of pro-inflammatory cytokine-TNF- α released by M2 macrophages after incubation with 40 pg/mL IFN- γ which is representative of the cytokine present on 1×10^{11} MEVs, 1×10^{11} MEVs and M1 polarizing stimulants (LPS (20 ng/mL) + IFN- γ (20 ng/mL)) for 24 hours. Supernatants were assayed in triplicate using a mouse TNF- α V-PLEX cytokine assay kit from Meso Scale Discovery.

We next investigated the importance of ligand-receptor interactions on the uptake of MEVs by M2 macrophages and MEV-mediated M2 to M1 macrophage repolarization. For this, we carried out proteolytic digestion of the membrane proteins embedded in the membrane of MEVs using proteinase-K (0.5 mg/mL). Proteinase-K is a broad-spectrum proteolytic enzyme which is commonly used to digest proteins present in the biological sample. We performed western blotting analysis to confirm the elimination of membrane anchored proteins present in the MEVs after proteinase-k digestion. We compared the expression of Na⁺K⁺ ATPase (a plasma membrane marker), calnexin (an endoplasmic reticulum marker), CD54 (a transmembrane glycoprotein), and CD63 (a transmembrane protein) in M1 macrophages (control), MEVs, and proteinase-K-treated MEVs. We found that proteinase-K treatment of MEVs resulted in nearly the complete digestion of most of the membrane proteins that we analyzed (Figure 3.5a). We performed a set of experiments to compare the delivery of purified proteinase-K treated MEVs (pkt-MEVs) and regular untreated MEVs to target M2 macrophages. MEVs were labeled with the lipophilic fluorescent dye, DiI, and further purified from free dye before incubation with M2 macrophages. Equal numbers of DiI-labeled pkt-MEVs and DiI labeled MEVs were left to incubate with separate M2 macrophage cultures for 0.5, 1, 1.5 and 2 hours. We used wide-field microscopy to compare the uptake of fluorescently labeled pkt-MEVs by M2 BMDMs. We found that the proteinase-K treatment of MEVs resulted in a 20% reduction in uptake of MEVs by M2 macrophages (Figure 3.5b-d). Even after the digestion of membrane proteins present on MEVs, the limited loss of cellular uptake of pkt-MEVs compared to untreated MEVs indicates that the uptake of MEVs by M2 macrophages is not limited to ligand receptor interaction but likely driven by the inherent phagocytosis ability of M2 BMDMs.

We next tested the ability of proteinase K treated MEVs (pkt-MEVs) to reprogram M2 macrophages towards an M1 phenotype. We incubated M2 macrophages with different concentration of pkt-MEVs and assessed the release of the pro-inflammatory cytokine

TNF- α secreted by M2 macrophages compared to TNF- α secreted by M2 macrophages that had been incubated with the corresponding concentration of regular MEVs. We found that eliminating the proteins on the surface of MEVs using proteinase-K (pkt-MEVs) resulted in a near complete loss in the ability of MEVs to re-polarize M2 BMDMs towards an M1 phenotype. This suggests that interactions between the membrane proteins present on MEVs, and the surface proteins present on M2 macrophages is the primary driver of MEV induced macrophage repolarization.

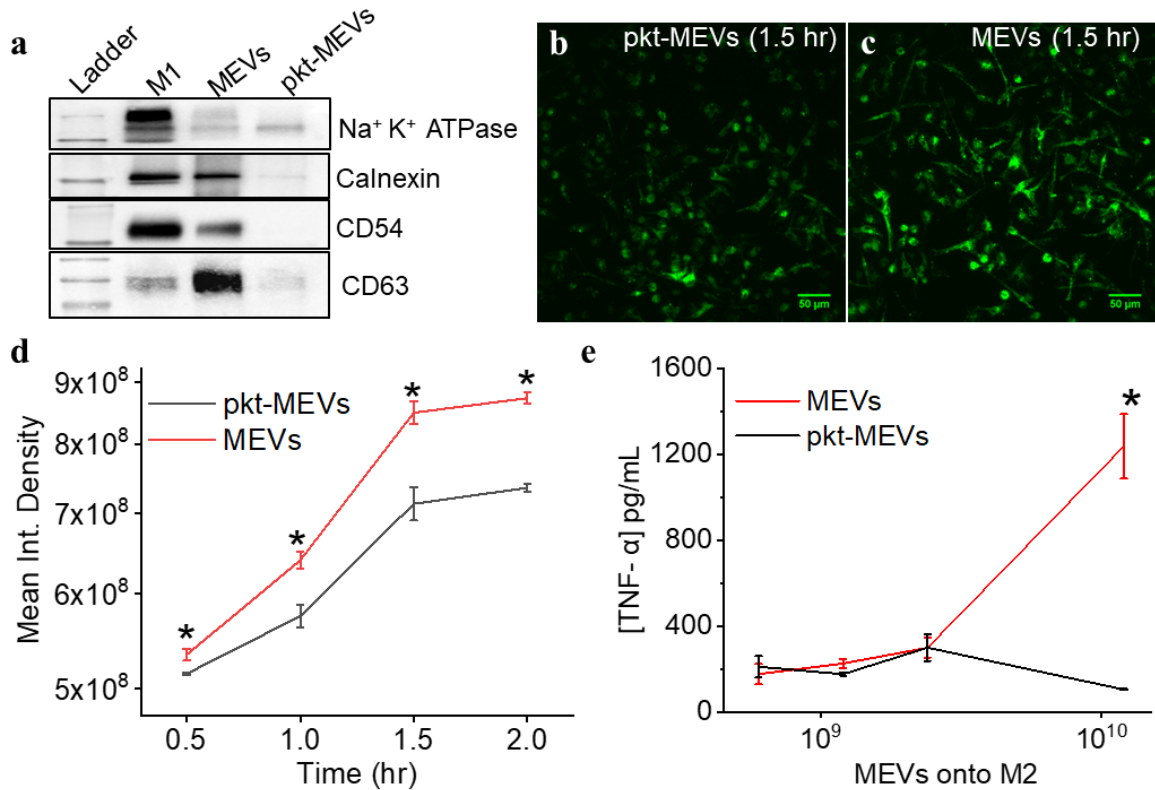


Figure 3.5 Proteolytic digestion of membrane proteins present on MEVs eliminates the reprogramming capability.

(a) Western blotting to compare the presence of membrane-anchored proteins in MEVs treated with and without proteinase-K. (b) Widefield fluorescence images of DiI labeled proteinase-K treated MEVs (pkt-MEVs) and untreated MEVs delivered to M2 macrophages after 1.5 hours show the reduction in uptake of proteinase-K treated MEVs. (c, d) Comparison of delivery of fluorescent labeled MEVs (red) and fluorescent labeled pkt-MEVs (black) to M2 macrophages. (e) TNF- α is released by M2 macrophages in a dose-dependent manner after 24 hours of interaction with increasing concentrations of MEV or pkt-MEVs. The data is presented as the mean \pm SEM. *P < 0.01 indicates that the results are statistically significant.

3.4.4 Programming Nanovesicles with Endogenous Ligands for Enhanced Macrophage Repolarization

A large number of protein classes have been shown to modulate immune cell polarization. We tested MEVs for the presence of four classes of proteins, including ligands for TNF superfamily receptors, chemokines, tetraspanins, and heat shock proteins known to modulate immune cell polarization, and then used representative proteins from these groups to engineer MEVS to determine if they improved reprogramming capability.

The interaction of endogenous ligands for TNF receptor superfamilies (TNFRSF) and the corresponding receptor in macrophages is known to activate the NF- κ B pathway and initiate the immune cell's pro-inflammatory response²⁸¹. Herein, we first performed western blotting to identify several ligands, including TNF- α , CD40L, CD137L, CD178L, OX40L, and CD254 that could be expressed in MEVs. Western blotting results indicated the expression of some of these ligands, including CD137L, OX40L, and CD254 on MEVs (Figure 3.6a). Since TNF- α is a pro-inflammatory cytokine that is anchored in the plasma membrane and is well known for its robust ability to activate immune cells upon interaction with its corresponding receptors TNFR1 and TNFR2 present on the immune cells²⁸², we then overexpressed TNF- α on the cell membrane and developed TNF- α overexpressing programmed nanovesicles aiming to improve the efficacy of nanovesicles to modulate macrophage polarization. In order to program cells by over-expressing TNF- α on their membrane, we first transfected HEK cells, then proceed to mouse bone marrow-derived macrophages. We used GFP tagged mouse TNF- α plasmid for transfection. TNF- α expressing HEK cells were used to generate programmed HEK cell derived nanovesicles P(TNF)-HNVs. We polarized TNF- α expressing BMDMs to M1 phenotype using LPS + IFN- γ and used those cells for generating programmed macrophage engineered vesicles (P(TNF)-MEVs). We confirmed TNF- α overexpression on the cells using confocal microscopy which showed clear GFP fluorescence on the surface of these programmed

cells (Figure 3.6b,d). We then compared the macrophage repolarization efficacy of programmed nanovesicles including P(TNF)-HNVs and P(TNF)-MEVs relative to their respective controls, using equal concentrations of vesicles in the experimental and control groups. The repolarization efficacy of the programmed nanovesicles was evaluated based on the cytokine production of nanovesicle-treated M2 BMDMs. We found that incubating M2 BMDMs with programmed HEK cell derived nanovesicles P(TNF)-HNVs resulted in significantly higher levels of pro-inflammatory cytokines such as IL-12p70, IL-6, IL-10, KC/GRO, and TNF- α (Figure 3.6c). However, unmodified HEK cell-derived vesicles do not elicit any proinflammatory cytokine production in M2 BMDMs. Similarly, we found that M2 macrophages treated with programmed MEVs P(TNF)-MEVs produce significantly higher levels of pro-inflammatory cytokines such as IL-12, IL-6, KC/GRO, and TNF- α when compared to M2 macrophages treated with unmodified MEVs (Figure 4e). We found that vesicle solution contained minimal levels of TNF- α (~20 pg/mL) indicating their negligible contribution to the cytokine concentration seen after macrophage reprogramming. These results indicate that, under similar conditions, programmed nanovesicles exhibit greater immunomodulatory properties compared to unmodified cell-derived vesicles illustrating the capability to program functionality into MEVs via protein expression. These studies suggest that NF- κ B may be one of the possible signaling pathways driving MEV-mediated M2 to M1 repolarization. Nuclear factor- κ B (NF- κ B) is one of the main transcription factors of M1 macrophages and regulates the expression of genes that control factors such as inflammation²⁸³. Activation of NF- κ B is characterized by the nuclear translocation of the p65 component of the NF- κ B complex²⁸⁴. To determine if MEV delivery to M2 BMDMs activated the NF- κ B signaling pathway, we incubated M2 Macrophages with MEVs for 6 hours, then fractionated the cells into cytoplasmic and nuclear fractions to study the effects of MEV delivery on the translocation of p65 subunits to the nucleus. We performed western blotting analysis to compare the p65 content in MEV-treated M2 BMDMs using untreated M1 and M2-BMDMs as controls. Western

blotting analysis indicated a significant translocation of p65 from the cytoplasm to the nucleus indicating the NF- κ B pathway is activated when MEVs interact with M2 BMDMs (Figure 3.7)

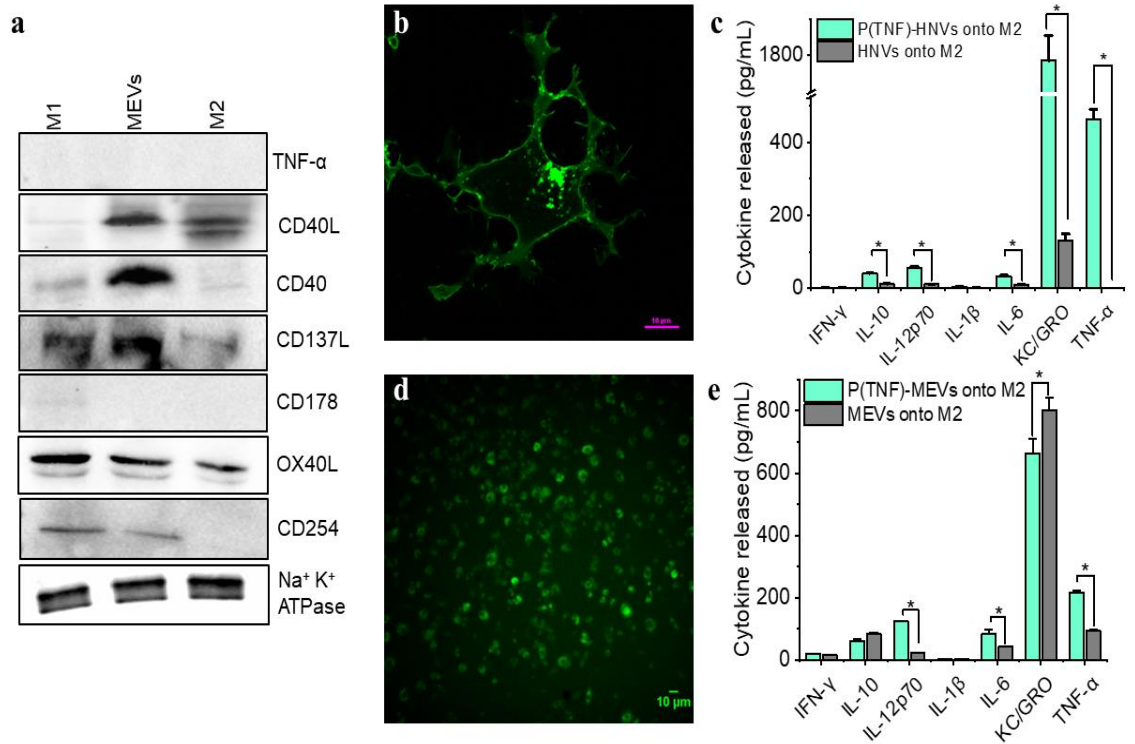


Figure 3.6 TNF- α programmed nanovesicles cause M2 macrophages to repolarize more towards the M1 phenotype.

(a) Western blot analysis showing differences in expression of TNF- α , CD40-L, CD40, CD137L, CD178, OX40L, and CD254 taking Na⁺K⁺ ATPase as a loading control. (b) Fluorescence image of HEK cells transfected with a mouse GFP-tagged TNF- α plasmid. (c) Cytokines released by M2 macrophages after incubation with TNF- α programmed HEK-cell derived nanovesicles (P(TNF)-HNVs) and HNVs. (d) A fluorescence image of macrophages transfected with a mouse GFP-tagged TNF- α plasmid. (e) Comparison of cytokines released by M2 macrophages incubated with P(TNF)-MEVs and regular M1 macrophage-derived vesicles (MEVs). (d) Programmed MEVs exhibit a higher repolarization efficiency compared to regular MEVs. The data is presented as the mean \pm SEM. * $p < 0.01$ indicates that the results are statistically significant.

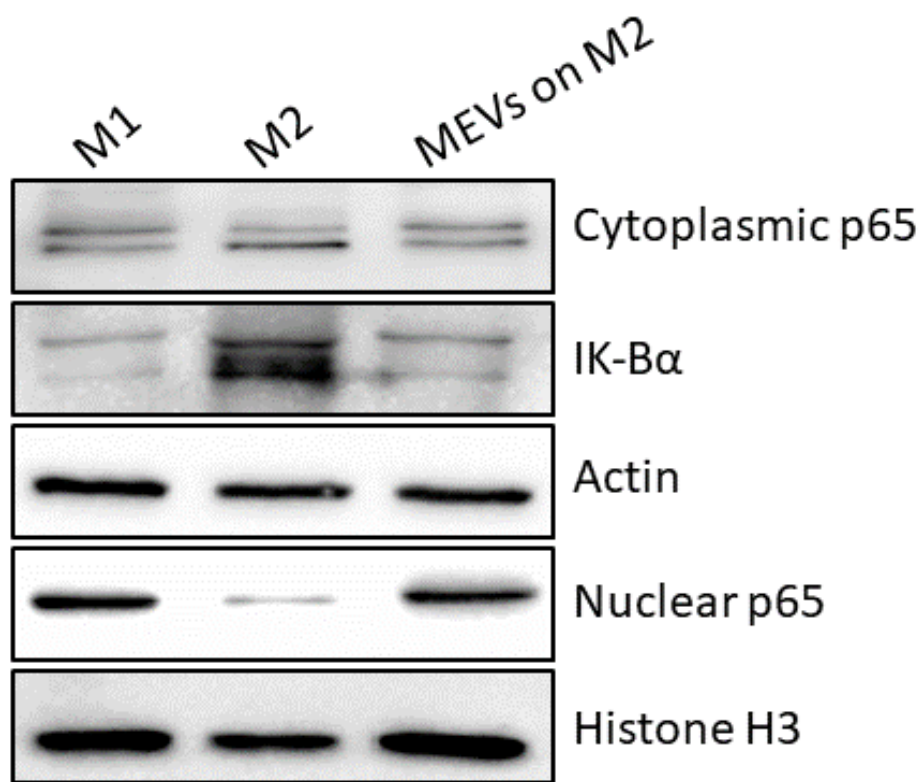


Figure 3.7 Western blot analysis of M1 and M2 macrophages compared to MEV treated M2 macrophages for p65 translocation.

We next sought to improve the capability of nanovesicles to modulate macrophage polarization by generating programmed nanovesicles that overexpress specific membrane-bound chemokines. Chemokines are chemotactic cytokines produced by various cells including macrophages^{285, 286}. While chemokines are mostly known for their role in monocyte recruitment/migration, they can promote macrophage differentiation as well as polarization^{261, 287, 288}. For example, C-C motif chemokine ligand 5 (CCL5) have been shown to activate M1 polarization and inhibit M2 polarization²⁸⁹. We first analyzed MEVs for the presence of 25 different macrophage-associated chemokines. Only nine chemokines including C-C motif chemokine ligand 5 (CCL5), C-X-C motif chemokine ligand 9 (CXCL9), macrophage inflammatory protein 1- γ (MIP1- γ), C-C motif chemokine ligand 1 (CCL1), macrophage inflammatory protein-2 (MIP-2), C-C motif chemokine ligand 27 (CCL27), C-X-C motif chemokine ligand 16 (CXCL16), C-C motif chemokine ligand 2 (CCL2), and monocyte chemotactic protein 5 (MCP-5) were found to be present on MEVs. We next compared the level of these observed chemokines for MEVs compared to M2 macrophages. We found that several M1-polarizing chemokines including CCL2^{288, 290}, CCL5²⁸⁹, and CXCL9²⁹¹ were present at significantly higher levels in MEVs compared to M2 macrophages (Figure 3.8a,b). Because CCL5 is known for polarizing macrophages to the M1 phenotype, we next generated programmed CCL-5 overexpressing HEK cell derived nanovesicles (P(CCL5)-HNVs) and compared the macrophage repolarization efficacy of (P(CCL5)-HNVs) with the regular HEK cell derived nanovesicles. HEK nanovesicles themselves do not polarize M2 macrophages. Therefore, by overexpressing CCL5 on HEK nanovesicles, we can determine the role of CCL5 present in macrophage modulation. We confirmed CCL5 expression in programmed HEK cells as well as programmed nanovesicles by western blotting (Figure 3.8c). While HEK cells did not express mouse CCL5 prior to transfection, programmed HEK cells and programmed nanovesicles showed a clear band for CCL5, confirming CCL5 expression in both programmed cells and programmed nanovesicles. In order to compare the repolarization

efficacy of programmed vesicles relative to regular HEK vesicles, we added 4×10^9 vesicles to 50,000 M2 macrophages in culture, incubated for 24 hours, and tested the cell culture supernatants for pro-inflammatory cytokines. We found that M2 macrophages that were left to incubate with CCL5-programmed HEK cell-derived nanovesicles (P(CCL5)-HNVs) produced roughly three times more KC/GRO compared to M2 macrophages that were incubated with regular HEK cell-derived nanovesicles (Figure 3.8d). However, we did not observe significant difference in the production of other cytokines by M2 macrophages. We found similar results when we incubated M2 BMDMs with CCL5-programmed nanovesicles generated using M1 macrophages. These results indicate that, under similar in vitro conditions, CCL-5 programmed nanovesicles can cause higher KC/GRO production by M2 macrophages. However, CCL5-programmed nanovesicles do not increase other pro-inflammatory cytokine production by M2 BMDMs.

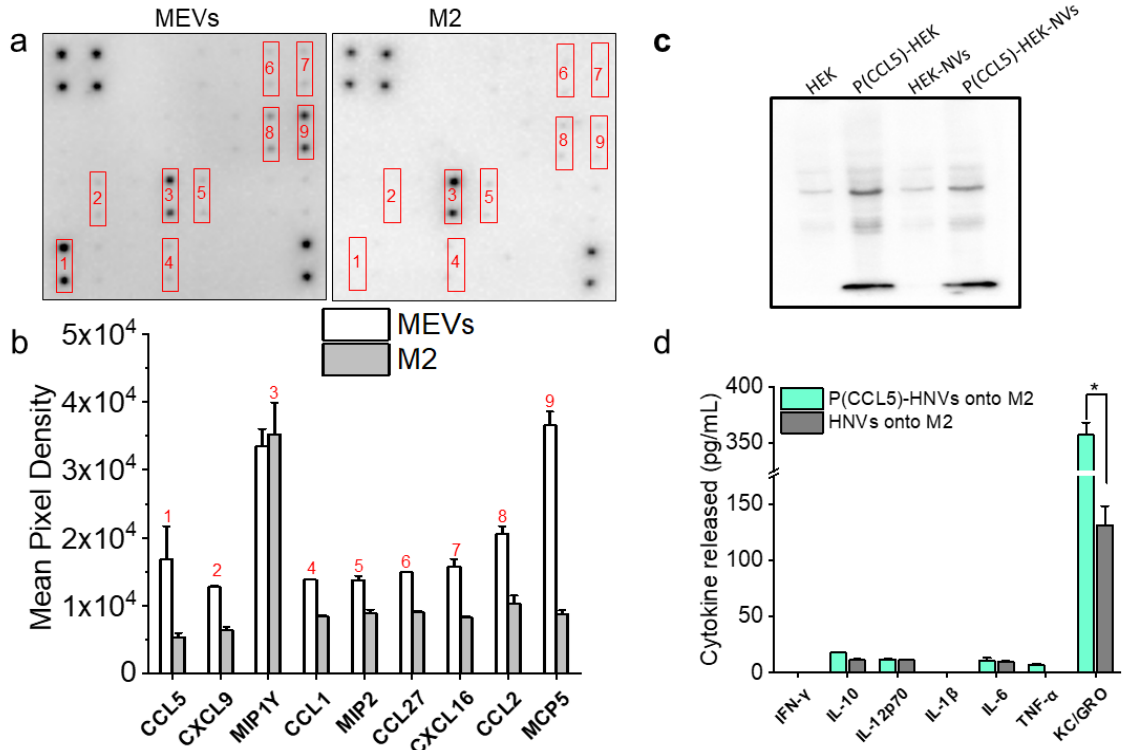


Figure 3.8 CCL5-programmed CEVs for M2 to M1 macrophage reprogramming.

(a) Chemokine expression image of the chemokine antibody array for MEVs and M2 macrophages. Dark spots in the images indicate the presence of the specific chemokine. (b) Comparison of mean pixel integrated density measurements between chemokines present on MEVs and M2 macrophages. (c) Western blotting shows that programmed HEK cells express more CCL5 than regular HEK cells. Accordingly, vesicles generated from programmed HEK cells express a greater CCL5 concentration. (d) CCL5-programmed vesicles derived from HEK stimulate M2 BMDMs to produce more KC/GRO. Each data point is the average of at least 3 experiments ($n = 3$). The data is presented as the mean \pm SEM. * $p < 0.01$ indicates that the results are statistically significant.

We have established that MEVs express various exosomal marker proteins, including CD54 (ICAM-1), CD63, MHCII, CD11b, and CD81 (Figure 3.1c). Recent studies have shown that ICAM-1 prevents M2 polarization and inhibits tumor metastasis²⁹². Therefore, we generated programmed nanovesicles that overexpress CD54 to assess their efficacy in macrophage phenotype modulation. For this, we first transfected M1 macrophages with a mammalian expressing mouse ICAM-1 plasmid, then polarized them to an M1 phenotype and used those macrophages to generate programmed macrophage engineered vesicles (P(CD54)-MEVs). We performed western blotting analysis to obtain the relative expression level of ICAM1 both in programmed macrophages as well as programmed MEVs relative to control. Western blotting analysis demonstrates that programmed cells and programmed nanovesicles express about 10 fold higher concentration of ICAM1 relative to their respective controls (Figure 3.9). We next compared the macrophage repolarization efficacy of (P(CD54)-MEVs) with regular MEVs by delivering an increasing concentration of each type of MEV onto M2 macrophages and quantifying the cytokine released by MEV-treated M2 BMDMs. We found that M2 BMDMs incubated with programmed MEVs (P(CD54)-MEVs) produced higher levels of pro-inflammatory cytokines compared to M2 BMDMs incubated with the same number of regular MEVs (Figure 3.10). When we analyzed the cytokine release by M2 BMDMs incubated with the specific concentration of MEVs (4×10^9), we found that M2 macrophages incubated with programmed MEVs produced roughly three times more KC/GRO, two times more IL-6 and IL-1 β , and 25% more IL-12p70 and TNF- α compared to M2 macrophages that were incubated with non-programmed MEVs (Figure 3.9c). As a control study, we generated CD54-overexpressing programmed nanovesicles using CD54-transfected HEK cells and then delivered these nanovesicles to M2 BMDMs in culture. We found similar results when we incubated M2 BMDMs with vesicles derived from HEK cells (Figure 3.9d). These results further support the idea that endogenous proteins can be

overexpressed in programmed nanovesicles to yield greater immunomodulatory properties compared to unmodified cell-derived vesicles.

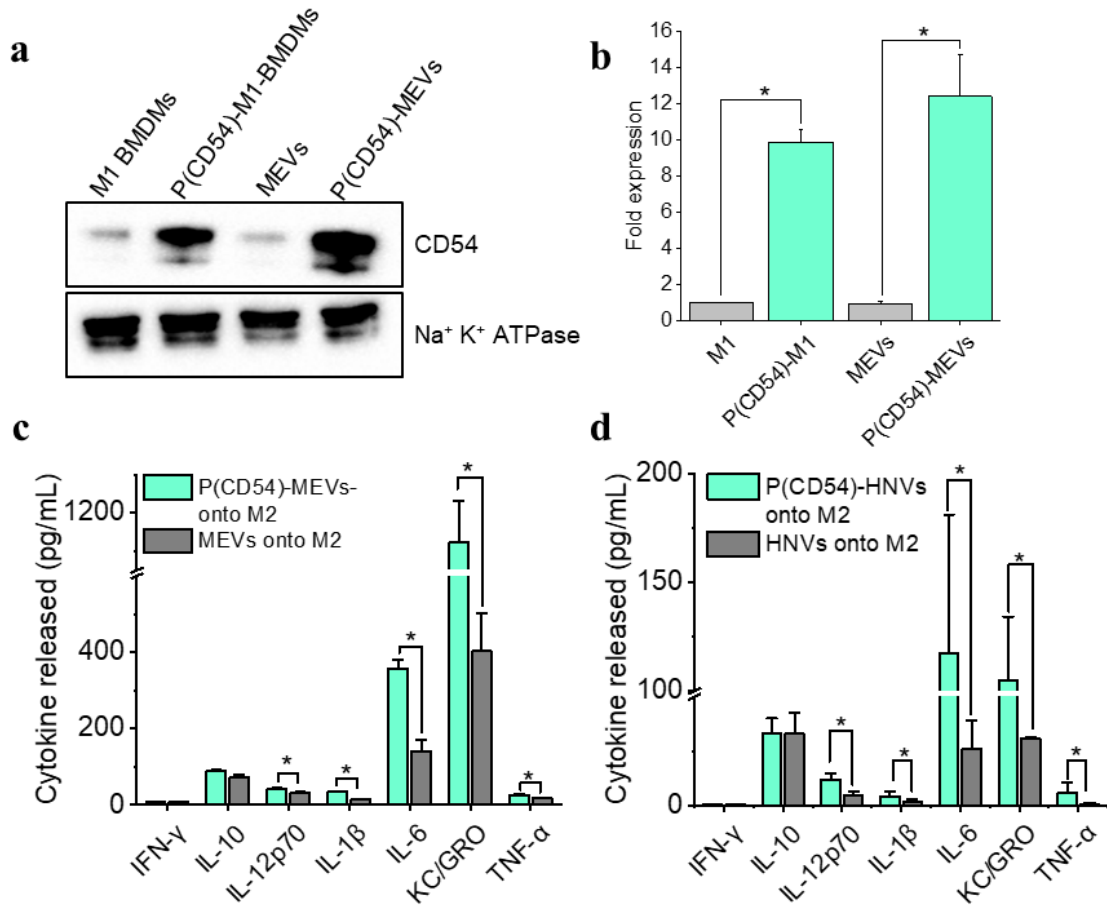


Figure 3.9 ICAM-1 programmed nanovesicles mediated M2 to M1 macrophage reprogramming.

(a) Western blotting showing CD54 transfected programmed M1 macrophages (P(CD54)-M1) express more CD54 than non-transfected M1 macrophages. Similarly, vesicles derived from programmed macrophages (P(CD54)-MEVs) have a higher concentration of ICAM-1. (b) Relative fold of CD54 expression in M1 macrophages, programmed M1 macrophages, MEVs, and P(CD54)-MEVs. CD54 expressions are normalized to Na⁺K⁺ ATPase, a plasma membrane marker. (c, d) CD54-programmed vesicles exhibit higher repolarization efficiency compared to regular nanovesicles. The data is presented as the mean \pm SEM. * $p < 0.01$ indicates that the results are statistically significant.

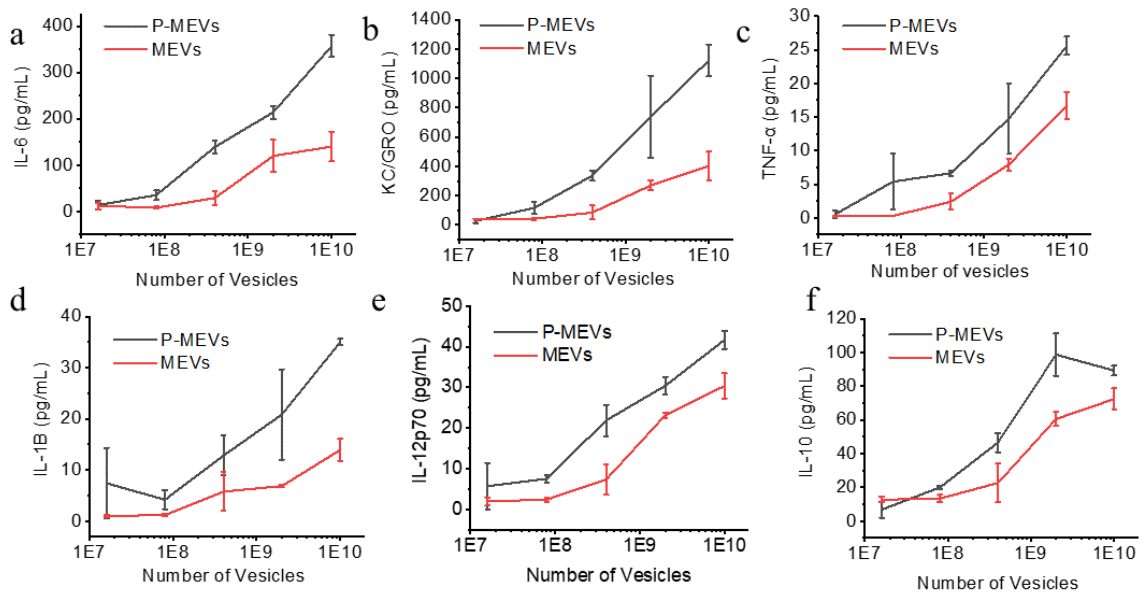


Figure 3.10 Dose response studies.

(a-f) Quantification of cytokine released by M2 macrophages that had been incubated with an increasing concentration of MEVs or CD54-programmed MEVs.

3.4.5 Programming MEVs with Exogenous Ligands for Enhanced Macrophage Modulation

The incorporation of specific non-endogenous ligands into MEVs could yield improved levels of M2 macrophage reprogramming capability as these ligands have the potential to directly interact with receptors present on M2 macrophages and initiate downstream signaling cascades. Here in, we demonstrate that decoration of TLR agonist on the surface of MEVs enhance their capability to modulate TAMs toward M1 phenotype. We first generated macrophage engineered vesicles from mouse pro-inflammatory M1 macrophages (MEVs) and then Pam3CSK4, a toll like receptor 2(TLR2)/TLR1 ligand, was grafted onto the lipid bilayer membrane of the vesicles by sonication. We used Rhodamine-labeled Pam3CSK4 to confirm the successful decoration of Pam3CSK4 on the surface of vesicles. Green punctate regions in figure 3.11b, a widefield fluorescence image of MEVs that had been programmed with Rhodamine-labeled Pam3CSK4, showed the successful decoration of Pam3CSK4 on the surface of MEVs. We used nanoparticle tracking analysis to compare the size of these vesicles and found that Pam3CSK4 grafted vesicles (pam-MEVs) were slightly larger (146 nm) as compared to MEVs (127 nm) (Figure 3.11a). We found that the zeta potential of pam-MEVs was -16.8 mV indicating improved stability in aqueous solution. To compare the capability of MEVs and pam-MEVs to reprogram M2 macrophages, we incubated M2 BMDMs separately with an equal number of MEVs or pam-MEVs and compared their cytokine production. While M2 macrophages show no detectable proinflammatory cytokines, those incubated with pam-MEVs showed substantial levels across most cytokines. Comparing cytokine levels we typically observe for M1 polarized macrophages, we saw that pam-MEV treatment shifted M2 macrophages to 20±2% (IFN- γ), 64±20% (IL-10), 50±4% (IL-12p70), 35±7% (IL-1 β), 20±2% (IL-6),

100±7% (KC/GRO) and 36±3% (TNF- α) of the average concentration seen for M1 macrophages (Figure). Similarly, M2 macrophages incubated with standard MEVs, exhibited values of 17±1% (IFN- γ), 51±11% (IL-10), 28±6% (IL-12p70), 20±8% (IL-1 β), 12±1% (IL-6), 79±16% (KC/GRO) and 7±1% (TNF- α) of the average concentration seen for M1 macrophages (Figure 3.11c). From these results, we found pam-MEVs treated M2 macrophages were more efficient at reprogramming M2 macrophages toward a proinflammatory phenotype than unmodified MEVs.

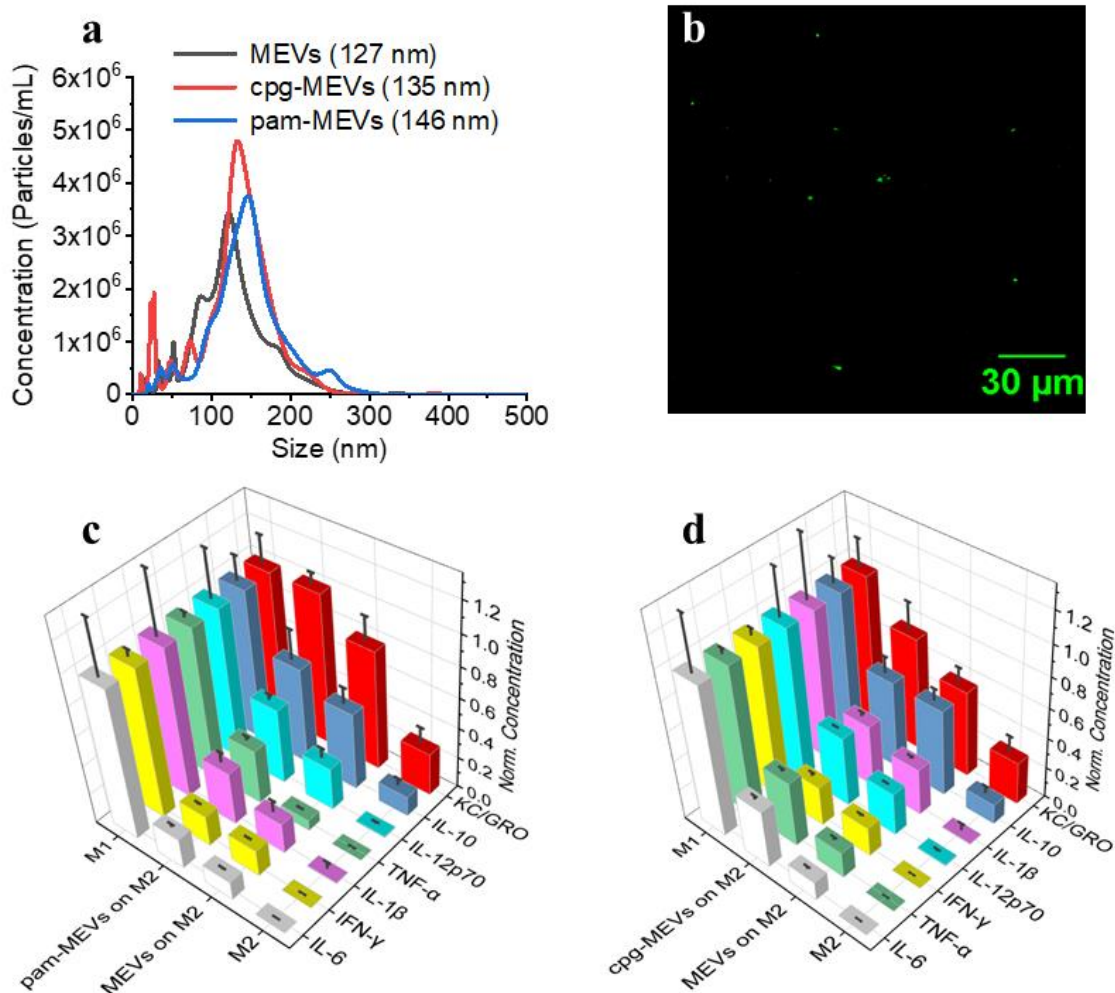


Figure 3.11 Programming MEVs with TLR-ligands for enhanced M2 macrophage reprogramming towards an M1 phenotype.

(a) Size distribution graph for MEVs, CpG oligonucleotide incorporated MEVs (cpg-MEVs), and Pam3CSK4 decorated MEVs (pam-MEVs). The mean diameter of MEVs (black), cpg-MEVs (red), and pam-MEVs (blue) is 127 nm, 135 nm, and 146 nm, respectively. (b) Fluorescence image of rhodamine labeled Pam3CSK4 decorated MEVs. (c) Comparison of the repolarization efficiency of pam-MEVs compared to regular MEVs. (d) Comparison of the repolarization efficiency of cpg-MEVs compared to regular MEVs.

The data is presented as the mean \pm SEM.

We also generated programmed nanovesicles by incorporating small molecule agonists on the vesicle surface. Cytosine-phosphorothioate-guanine oligodeoxynucleotides (CpG-ODN), a synthetic oligonucleotide, has sequence patterns that resemble bacterial DNA and has been found to activate antigen presenting cells (APCs) such as macrophages and dendritic cells²⁹³. CpG-ODN is recognized by the Toll-like receptor 9 (TLR-9) present in APCs²⁹⁴⁻²⁹⁶. CpG-ODN interaction with TLR-9 initiates signaling pathways that causes the APC to secrete several pro-inflammatory cytokines including IFN- γ , IL-12, TNF- α ²⁹⁴. Recent studies have shown that stimulation of macrophages with ODN1826, a Class B CpG oligonucleotide, increases their phagocytotic and anti-tumor activity¹²³. CpG-ODN treated macrophages produced high levels of pro-inflammatory cytokines compared to other immune-stimulant agonists upon interaction with macrophage¹²³. While CpG-ODN is a well-known immunostimulatory agonist, its efficacy is limited by its rapid degradation and inability to effectively be delivered to the intracellular compartment of APCs²⁹⁷. We incorporated ODN1826, a synthetic class B CpG oligonucleotide lipopeptides, into the membrane bilayer of the MEVs. To compare the capability of MEVs and cpg-MEVs to reprogram already polarized macrophages, we separately incubated M2 BMDMs with equal number of MEVs or cpg-MEVs and compared cytokine production. cpg-MEVs induced the production of cytokines to levels of 26 \pm 3% (IFN- γ), 58 \pm 11% (IL-10), 46 \pm 1% (IL-12p70), 41 \pm 3% (IL-1 β), 38 \pm 3% (IL-6), 75 \pm 18% (KC/GRO), and 43 \pm 2% (TNF- α) of the average concentration seen for M1 macrophages (Figure 3.11d). This was an improvement over the polarization induced by unmodified MEVs of 7%, 1%, 18%, 10%, 26%, 18%, 26% more efficient in the production of IFN- γ , IL-10, IL-12p70, IL-1 β , IL-6, KC/GRO and TNF- α , respectively. These results suggest MEV efficacy can be enhanced by incorporating polarization inducing ligands into the surface of the vesicle.

3.5 Conclusions

In conclusion, BMDMs can be used to generate exosome mimicking vesicles with high yield using nitrogen cavitation. Interactions of endogenous ligands present on the membrane bilayer of a vesicle with their corresponding receptors present on the target macrophage cause anti-inflammatory macrophages to repolarize towards a pro-inflammatory phenotype. Cell-engineered nanovesicles can be programmed to overexpress specific ligands on their surface that improve targeting and repolarization efficacy. Programmed nanovesicles, when interacting with the M2 macrophages can elicit enhanced immunomodulatory properties compared to non-programmed vesicles. This shows that programmed M1 macrophage-engineered nanovesicles can be used as a potential therapeutic platform to achieve enhanced re-polarization of tumor-supportive M2 macrophages towards a tumor-killing M1 phenotype.

CHAPTER 4. CELL-DERIVED VESICLES FOR IN VITRO AND IN VIVO TARGETED THERAPEUTIC DELIVERY

4.1 Chapter Summary

Engineering a therapeutic delivery system that would successfully transport therapeutics to the interior of the cell has always been a challenging project. Recent studies have focused on developing exosomes or liposome-based therapeutic delivery systems to deliver therapeutic cargo to the cell of interest^{138, 143, 245, 298}. Exosomes are lipid bilayer-enclosed compartments released by various eukaryotic cells^{261, 299}. These nanosized (50-100 nm) particles have been utilized as intercellular communicators, drug delivery vehicles and immune stimulators^{177, 300, 301}. Exosomes are highly biocompatible, less immunogenic, smaller in size, and exhibit cell targeting specificity^{143, 159, 201, 245, 298}. While exosome-based drug delivery system offers multiple advantages for their use in therapeutic delivery, use of exosomes is always a challenge for clinical applications because of their low production yield and cumbersome separation steps^{144, 302}. Liposomes are synthetic lipid bilayer vesicles often used as an alternative to exosomes^{135, 303}. While liposomes can be synthesized with smaller sizes, high yields, and the ability to be functionalized with surface moieties, these nanoparticles are prone to immune clearance when administered into the body¹²⁴. Here, we overcome the limitations of naturally produced exosomes as well as synthetic liposomes by generating cell-engineered vesicles (CEVs) artificially via disruption of the cellular membrane by nitrogen cavitation. CEVs can be generated at high yields and exhibit similar properties to exosomes. In this chapter, we also demonstrate that cell-engineered vesicles produced artificially by fragmenting cellular membranes can be effectively loaded with a variety of cargo, including fluorescent markers, chemotherapeutics, or any sort of cargo like proteins or genetic materials that can then be transported to the interior of the cell of interest. Cellular CEVs display cell targeting

specificity as well as the capability to carry both lipophilic as well as hydrophilic cargo into the interior of the cell. *In vitro*, we found that CEVs generated from cancer cells can reprogram immune cell phenotype when delivered *in vitro*. Furthermore, chemotherapeutic-loaded CEVs successfully deliver cancer therapeutics and exhibit greater cancer cell inhibition compared to the free drug in solution. Incorporating cancer cell targeting moieties into the vesicle membrane provided improved delivery and uptake of therapeutic loaded nanovesicles leading to greater efficacy. We also performed *in vivo* targeting and delivery in an animal utilizing fluorescently tagged nanovesicles to target tumor xenografts. Cell-engineered vesicles can be produced in large quantities and readily loaded with a multitude of payloads. Because of their propensity to selectively target the parent cell type, these vesicles may be useful for delivering therapeutics as well as other cargo both *in vitro* and *in vivo*.

4.2 Background

For the discovery of novel treatments and the comprehension of biological function, the efficient transport of cargos such as fluorescent probes, gene products, medications, and proteins to the inside of the cell is highly important³⁰⁴⁻³⁰⁷. Despite developments in fields like gene transfer³⁰⁸, targeted therapies, endogenous vesicle-based delivery methods^{139, 309}, and the use of peptides³¹⁰, one of the key obstacles to the development of treatments is the effective transport of cargo through the cell membrane. Endocytic routes are the most popular means of entering the cell's interior. While this offers a somewhat effective way to breach the cell membrane, it also causes the cargo to get trapped in endosomal vesicles. The payload must then evade from these vesicles, reducing the effectiveness of medicines as well as their potential³¹¹. This makes cargo delivery more difficult for both *in vivo* and cell culture-based applications. Ideal drug delivery systems

would enable cargo to be transported directly into the interior of the cell and protect the cargo from endocytic degradation.

Phospholipid bilayer-based vesicles have shown potential as therapeutic delivery vehicles able to enclose the payload and convey it to the inside of target cells^{312, 313}. Synthetic vesicles, like liposomes made of phospholipid membranes, are extremely simple to load and have the potential to be used as intracellular delivery systems both *in vitro* and *in vivo*^{135, 139, 314}. The inability of liposomes to carry drugs *in vivo* without being recognized by the immune system, however, limits their use. Naturally produced cellular vesicles are an appealing substitute. Exosomes, for instance, have drawn a lot of interest as therapeutic delivery systems to deliver cargo to the cell of interest since they are nonimmunogenic and only target certain cell types^{142, 242, 313, 315}. While cell specificity solves a significant issue with focused therapeutic administration, the use of exosomes as therapeutic delivery systems is limited by their inadequate synthesis. Exosomes have been used for the *in vitro* delivery of medicines and for the delivery of genes despite these drawbacks³¹⁶⁻³¹⁸. Recently, vesicles produced from cell organelle membranes were employed as exosome mimics and such vesicles preserved some of the targeting characteristics of exosomes^{183, 196, 319, 320}.

When developing intracellular delivery vectors, it is necessary to take several important considerations into account. The loading of the cargo has to be quick and simple, and the drug delivery system should be able to accommodate a diverse variety of different types of cargo. In this work, we generate cell-engineered vesicles (CEVs) that exhibit cell targeting specificity. We use these vesicles as general cell-delivery vehicles that can deliver their cargoes to the interior of the cells both *in vitro* and *in vivo*. We also developed therapeutic-loaded nanovesicles programmed with surface components designed to enhance their therapeutic delivery efficacy to cancer cells. Nanovesicles that are decorated with specific membrane-bound ligands are efficiently taken up by the target cell. We found that folate decorated therapeutics loaded nanovesicles exhibit increased cancer cell killing

ability compared to regular therapeutics loaded vesicles or the therapeutics in the solution. Overall, cell-engineered nanovesicles-based therapeutics show promise for both enhanced therapeutic delivery and the ability to reprogram immune cell polarization.

4.3 Methods

Generation of Empty Vesicles: Empty vesicles were generated from cells following the protocol as reported previously²¹². Briefly, cell media was aspirated off from the flask containing cells. 3 mL of PBS was then added to each flask, and cells were detached by scraping them and resuspended in PBS. The cell suspension from each flask was first collected into a 50 mL tube, and the total number of cells were then counted using a hemacytometer. The cell slurry collected in the previous step was then centrifuged at 1200 rpm at 4 °C for 5 minutes, and the obtained pellets were resuspended in 10 mL sucrose buffer solution (SBS) supplemented with protease inhibitor (10 mM HEPES, 250 mM sucrose, pH adjusted to 7.4 and one protease inhibitor mini tablet per 10 mL buffer). To fragment the cellular membrane and generate vesicles, cells were then subjected to a pressure of 300 psi for 5 minutes in a prechilled nitrogen gas decompressor (Parr Instruments Company, IL, USA) on ice. The fragmented cell mixture including vesicles was centrifuged at 4000xg for 10 minutes at 4 °C. Pellets obtained were discarded but the obtained supernatant centrifuged at 10,000xg for 20 minutes at 4 °C. The supernatant was then subjected to ultracentrifugation at 100,000xg for 65 minutes at 4 °C to collect the pellet containing nanovesicles. The pellet was then washed 5 times with PBS before resuspending them in 500 µL PBS.

Determination of Vesicle Size: To determine the effective diameter of vesicles, the vesicle suspension described above was diluted 1:4 in PBS. Approximately 3 mL of the diluted vesicle suspension was transferred into a cuvette and analyzed using dynamic light scattering (DLS).

Generation of Cisplatin-Loaded Vesicles: 60 million human lung cancer cells (A549 cells) were collected to generate A549-engineered vesicles for delivery. A549 cells were scraped from the culture into 20 mL of SBS. The cell slurry was then collected into a 50 mL conical tube and centrifuged at 2000 rpm for 2 minutes at 25 °C. The SBS obtained after centrifugation was aspirated off, and the pellet was resuspended in 8 mL of 8.33mM cisplatin in SBS. The cell solution was then subjected to fragmentation by nitrogen cavitation at 300 psi at 4 °C for 5 minutes. The cell slurry obtained after nitrogen cavitation was centrifuged at 4000xg for 10 minutes at 4 °C. The pellet resulting after centrifugation was discarded, while the supernatant was transferred to a 25 mL ultracentrifuge (UCF) tube and further centrifuged at 10,000xg for 20 minutes at 4 °C. The supernatant from the UCF tube was then transferred to a new 25 mL UCF tube and centrifuged at 100,000xg for 60 minutes at 4 °C. The pellet in the UCF tube was carefully washed with 500 µL SBS and the residual solution pipetted out and discarded. 750 µL of PBS was added to the UCF tube and the pellet resuspended via pipetting. Empty A549-engineered vesicles were generated in the exact same way except in the absence of cisplatin.

30,000 A549 cells were plated in each well of a 96-well cell culture plate and allowed to incubate for 24 hours in 200 µL of HEK media (Dulbecco's Modified Eagle's Medium (DMEM) supplemented with 10% FBS, 1% Glutamine and 1% PS) at 37 °C. After 24 hours of incubation, the growth media was replaced with 250 µL of fresh HEK media, empty vesicles in 250 µL of HEK media, HEK media containing 4.17 mM cisplatin, cisplatin loaded vesicles in HEK media. A549 cells were further incubated under these conditions for 24 hours, 48 hours and 72 hours wherein at each respective timepoint, the old media was aspirated off and 100 µL of optimem was added followed by 20 µL of alamar blue. The plate was further left to incubate for 45 minutes until uniform purple coloration was observed. This plate was then read using a FlexStation plate reader.

Determination of Cisplatin Concentration in Vesicles: Cisplatin concentration in vesicles was determined by first obtaining the concentration of platinum (Pt) present in

solution. At first 100, 10, 1, 0.1, and 0.01 ppm platinum standard solutions were prepared in 1% HNO₃ solution and were used to generate the standard curve using inductively coupled plasma optical emission spectroscopy (ICP-OES, Varian Vista Pro). Cisplatin-encapsulated vesicles were generated as discussed above in the presence of 8.33 mM cisplatin in SBS. The vesicle suspension was treated with (1%) Triton X-100 and concentrated HNO₃ to disrupt the vesicles' membranes and liberate the platinum encapsulated therein. This solution was further diluted and injected with 1% Yttrium in 1% HNO₃. The resulting emission and standard curve were used for determining the concentration of Pt in solution. The concentration of cisplatin was then determined from platinum concentration using a mole ratio.

Labeling Vesicles with DiI: To label vesicles, DiI was added to the vesicle resuspension such that the final concentration of the dye becomes 2 μM and left to incubate for 30 minutes at 37 °C. DiI is a lipophilic dye which becomes incorporated into the lipid bilayer of the vesicle. The free dye molecules were separated from the fluorescently labeled vesicles using a size exclusion spin column (PD MidiTrap). Briefly, the column was equilibrated by running 15 mL of PBS through the column followed by the column undergoing centrifugation at 1000xg for 2 minutes to flush any PBS remaining in the column. Then, 500 μL of vesicle solution was added dropwise on the center of the column from the top and centrifuged at 1000xg for 2 minutes. In doing so, free dye is trapped inside the column and only vesicles loaded with DiI are eluted.

Cell Targeting Specificity: HEK293T vesicles onto HEK293T and A549 cells: 64 million human embryonic kidney (HEK293T) cells were used to generate HEK293T-engineered vesicles for delivery. Cells were scraped from culture using a cell scraper in 20 mL of SBS. The cell solution obtained after scraping was collected into a 50 mL conical tube and pelleted at 2000 rpm at 25 °C for 2 minutes. In doing so all the cells present in solution after centrifugation settle down in the bottom of the tube. The supernatant was then carefully aspirated off such that the final volume of SBS was 10 mL. The solution was

pipetted up and down multiple times in order to homogeneously distribute cells in solution. The cell solution thus obtained was fragmented using nitrogen cavitation at 300 psi at 4 °C for 5 minutes. The resulting cell slurry was centrifuged at 4000xg for 10 minutes at 4 °C. The pellet was discarded, and the supernatant obtained from centrifugation was transferred to a 25 mL UCF tube for 10,000xg centrifugation for 20 minutes at 4 °C. The pellet obtained after this step was discarded and the supernatant from the UCF tube was then transferred to a new 25 mL UCF tube and centrifuged at 100,000xg for 60 minutes at 4 °C. The pellet collected inside of the UCF tube was washed multiple times with SBS before resuspending it in 100 µL of SBS. 2 µL of 1 mM DiI in 100% DMSO solution was added to the vesicle resuspension and allowed to incubate for 30 minutes at 37 °C which allowed CEVs to be labeled with DiI. Free dye which is still present in the vesicle resuspension after incubation was purified using a PD MidiTrap size exclusion column. 50 µL of purified vesicles were added to each glass bottom dish containing 90,000 HEK or A549 cells plated 24 hours prior. 54 million RAW264.7 (RAW) cells were used to generate RAW-engineered vesicles following the same procedure as above and were added to RAW and A549 cells as above.

The same protocol was followed as above for HCT116-engineered vesicles onto HCT116 cells and RAW-engineered vesicles onto HCT116 cells. 70.4 million HCT116 cells and 56.8 million RAW cells were used to generate vesicles. HCT116 cells being cancer cells divide at a faster rate than other noncancerous cells like RAW. Therefore only 50,000 HCT116 cells were plated onto glass bottom dishes compared to 90,000 RAW cells.

Folate-decorated MEVs: Bone marrow-derived macrophages (BMDMs) were obtained from 8-12 week old mice as discussed previously. Cells were resuspended in the standard medium (RPMI1640 supplemented with 10% fetal bovine serum (FBS), 5% penicillin/ streptomycin (PS), 1% glutamine, 1% HEPES(4-(2-hydroxyethyl)-1-piperazineethanesulfonic acid), 0.001% β-mercaptoethanol and 20% supernatant from sL929 cells), transferred into 75-cm² culture flasks, and allowed to grow for 2 days.

Starting on day 3, standard medium supplemented with 0.1% DSPE-PEG-Folate was then replaced every two days until day 7. Cells were re-plated on day 7 at a cell density of 1×10^6 cells/mL in re-plating media (Dulbecco's Modified Eagle's Medium (DMEM) supplemented with 10% FBS, 1% Glutamine and 1% PS). BMDMs were then stimulated to become M1 macrophages using LPS (20 ng/mL; Invivogen) and IFN- γ (20 ng/mL; eBioscience). Folate-decorated MEVs were generated using the nitrogen cavitation technique as discussed previously.

The decoration of folate ligands on the membrane of the M1 BMDMs was confirmed using the immunofluorescence technique. Briefly, folate decorated M1 BMDMs cultured in glass bottom dishes were first incubated with the folate primary antibody at 37 °C for 90 minutes. Cells were then washed with PBS three times and then incubated with the secondary antibody (goat anti-mouse IgG Alexa Fluor 488) at 37 °C for 90 minutes. A Nikon A1R laser scanning confocal microscope was used for fluorescence imaging of folate decorated-antibody treated-M1 macrophages. Folate-decorated MEVs were generated using folate-decorated M1 BMDMs as discussed previously. In order to confirm the presence of folate on the surface of MEVs, folate decorated MEVs were first resuspended in PBS and then allowed to incubate for 90 minutes at 37 °C with folate primary antibody. Primary antibody-treated folate MEVs were then incubated for 90 minutes at 37 °C with secondary antibody (goat anti mouse IgG Alexa Fluor 488). A fluorescence microscope was then used to confirm the presence of folate ligands on MEVs.

Cisplatin-loaded folate-decorated MEVs were generated using 100 million folate-decorated M1 BMDMs. Briefly, folate decorated M1 BMDMs were first resuspended in 8 mL of 8.33 mM cisplatin solution made in PBS supplemented with a protease inhibitor. To fragment the cells and generate cisplatin loaded folate decorated vesicles, the cell suspension was transferred to a prechilled nitrogen decompressor on ice and nitrogen cavitated at 300 psi for 5 min. The cell lysate obtained was then subjected to a series of centrifugation steps and purification steps as discussed previously to obtain pure folate

decorated cisplatin loaded MEVs. Inductively coupled plasma-optical emission spectrometry (ICPOES) was used to determine the concentration of cisplatin loaded in MEVs or folate-MEVs as discussed previously. First, we treated cisplatin-loaded MEVs with 1% Triton X-100 to dissolve the lipid bilayer, followed by a 70 % nitric acid treatment to release platinum from cisplatin. The resulting solution was further heated at 60 °C for 2 hours before diluting the nitric acid solution to 10 %. A standard curve using platinum standards in a 10% nitric acid solution was used to determine the platinum concentration.

In Vivo Xenograft: In order to validate the in vivo delivery of various CEVs into the tumor, immune-compromised nude mice were subcutaneously injected with A549 cancer cells (NSCLC, immortalized) in the right shoulder and monitored for 4-5 weeks until significant growth of the tumor was observed. CEVs were prepared using cultured A549, HEK and RAW cells following the procedure discussed earlier. These vesicles were then labeled with DiR, a lipophilic dye with an excitation maxima at 750 nm that can penetrate deep into the tissue rendering it suitable for in vivo imaging. Labeled vesicles were then administered to the mice intravenously and imaged after 24, 48 and 72 hours. Mice were anesthetized using isoflurane prior to imaging. An IVIS Spectrum In Vivo Imaging system was used to measure epifluorescence. The Fluorescence signal intensity was quantified using Living Image software (PerkinElmer).

4.4 Results and Discussions

4.4.1 Characterization of Cell-Engineered vesicles

We generated cell-engineered vesicles (CEVs) by subjecting eukaryotic cells in solution to high-pressure N₂ during nitrogen cavitation. The quick release of pressure causes the creation of gas bubbles that shatter the cellular membranes. Membrane fragments then reassemble to create vesicles. We performed a succession of centrifugation steps to isolate vesicles from the residual cell debris. Figure 4.1 depicts a schematic of the

vesicle formation and isolation procedure. The solution used to resuspend cells is encapsulated in the vesicles during cavitation, which is a benefit of this method. Thus, therapeutic, or other cargos are efficiently captured in the vesicles during vesicle production. Figure 4.2A depicts an image of vesicles generated by nitrogen cavitation from HEK cells in the presence of fluorescein, a fluorescent dye. The fluorescence image reveals punctate regions, indicating that the fluorophore is encapsulated within the vesicles. By encapsulating the cargo in a phospholipid bilayer, the payload is protected from untimely degradation. To demonstrate the adaptability of this method, we conducted a series of experiments using vesicles from human embryonic kidney cells (HEK), human colorectal cancer (HCT 116), human lung cancer (A549), bone marrow-derived macrophages (BMDMs) and macrophage-like cell lines (RAW 264.7).

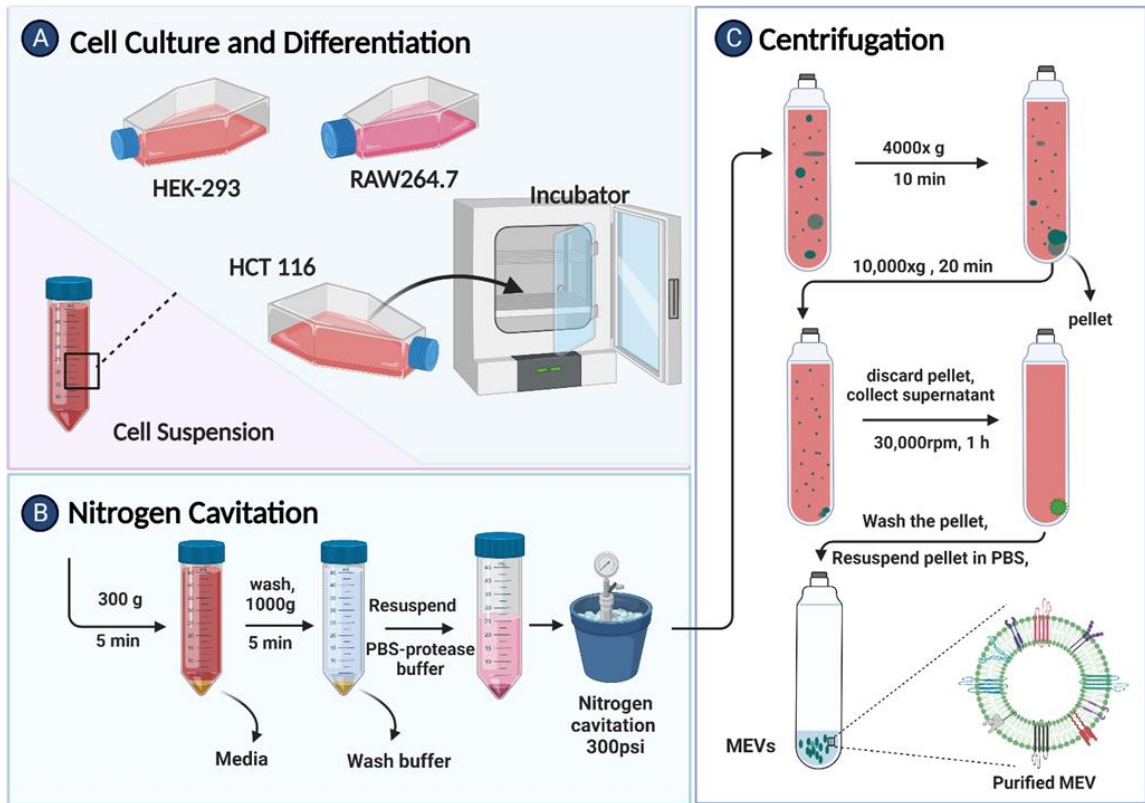


Figure 4.1 Schematic illustrating our approach of cell-engineered vesicle generation, loading, and isolation.

Cultured cells are nitrogen cavitated with cargo in free solution, then serially centrifuged to produce pure vesicles. Vesicles carry hydrophilic payloads enclosed during cavitation or lipophilic cargo anchored in the membrane of vesicles.

The biggest challenge of extracellular vesicles for their use in clinical applications is their low production yield. To assess the vesicle yield from nitrogen cavitation, we conducted fluorescence correlation spectroscopy (FCS). Vesicles were produced by nitrogen cavitation from roughly 40 million A549 cells in vitro. After isolating the vesicles, they were tagged with a lipophilic dialkylcarbocyanine fluorophore (DiI) that is nonfluorescent in aqueous solution but glows brilliantly when bound to a lipid bilayer. FCS detects changes in fluorescence as vesicles move across the focal volume. From the autocorrelation curve, both the diffusion time and the average number of molecules may be determined (Figure 4.2B). We used tetra speck beads to calibrate the FCS focal volume, and we found that nitrogen cavitation generated 1.3×10^{11} vesicles from 40 million cells. Thus, we were able to produce a high number of vesicles from a small number of cells.

We also performed nanoparticle tracking analysis (NTA) to determine the size distribution and concentration of cell-engineered vesicles. We found that the mean diameter of CEVs generated by nitrogen cavitation is between 50-100 nm, which is similar to the size distribution that is reported in the literature for endogenously released exosomes (100 to 150 nm). We also assessed the stability of CEVs by measuring their surface charge (zeta potential) while they were suspended in a PBS buffer. Vesicle preparations showed a -2.5 mV surface charge, indicating their stability in the solution. To understand the effect of pressure applied during nitrogen cavitation on the size distribution of the vesicles, we generated vesicles at varying nitrogen cavitation pressures of 250, 300, 600, and 900 psi. We obtained the smallest sized vesicles at 300 psi. In addition to producing vesicles that are similar in size to exosomes, the nitrogen cavitation process also maintains low heat and preserves both the sample and the cellular proteins from degradation. In this technique of vesicle generation all cells in solution are subjected to the same pressure, leading to rather homogenous vesicle formation.

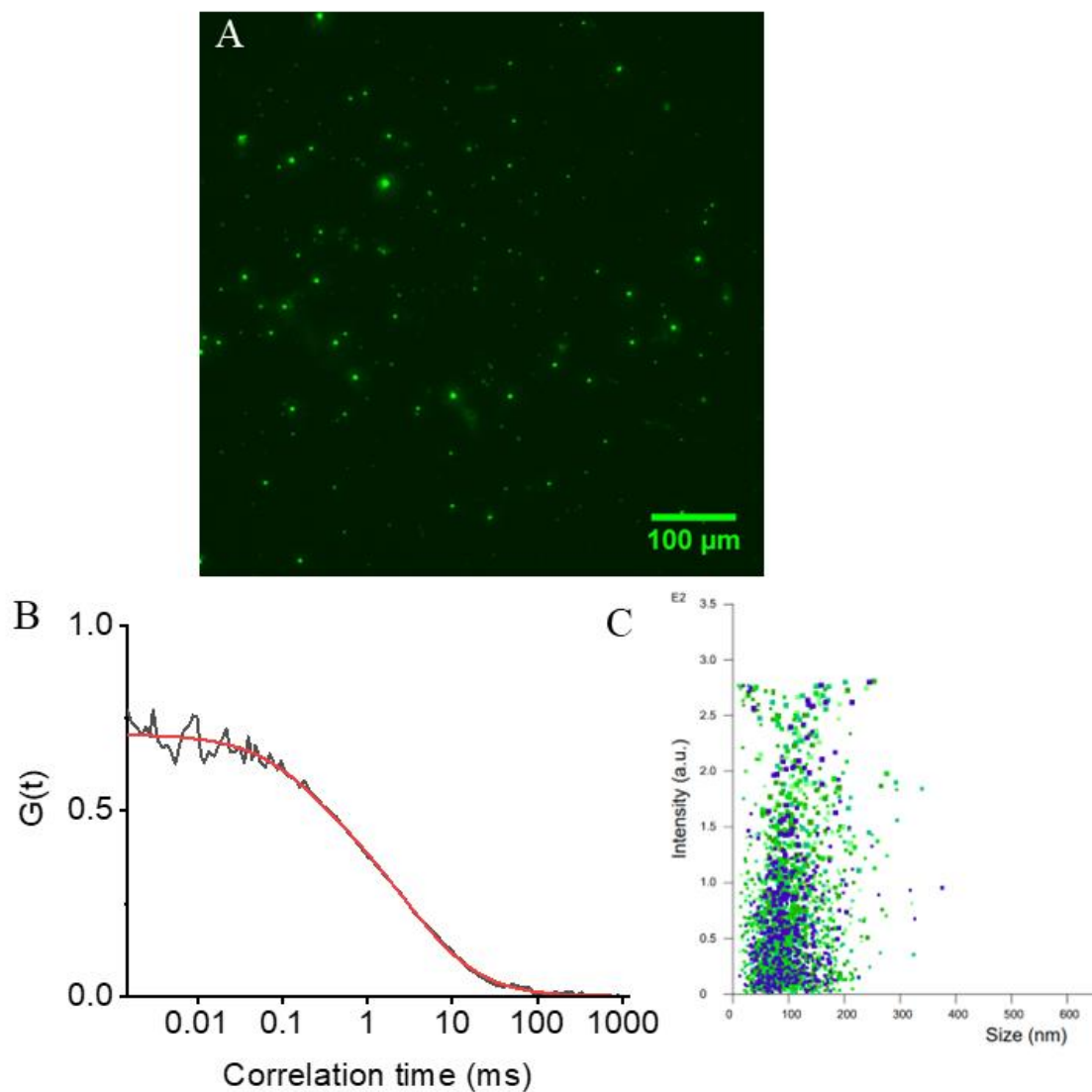


Figure 4.2 Cell-engineered vesicle characterization.

(A) Wide-field fluorescence image of fluorescein loaded CEVS. (B) Fluorescence correlation spectroscopy correlogram for determining the concentration of vesicles. (C) Size distribution of CEVs obtained from nanoparticle tracking analysis (NTA).

4.4.2 Targeting Specificity of CEVs Across Various Cell Types

Previous studies have shown that exosomes and vesicles derived from tumor cells preferentially target cells from which they were regenerated. In order to study the ability of CEVs to target the same cell from which they were regenerated, multiple experiments were carried out in which engineered vesicles generated from a specific cell type were delivered to the cell from which it originated versus other cell types. First, engineered vesicles were generated from cultured HEK cells and labeled with DiI. We then determined the efficiency of delivery to both HEK and A549 cells by measuring the fluorescence signal at various time points. We found that after 2 hours of interaction of the same number of HEK-engineered vesicles with HEK and A549 cells, HEK cells were found to have 10-fold increase in fluorescence compared to A549 cells (Figure 4.3A). Next, we used cultured RAW cells to generate RAW CEVs by nitrogen cavitation and found that RAW CEVs were delivered eight times more readily to RAW cells in comparison to A549 cells (Figure 4.3B). These results further demonstrate that CEVs exhibit cell targeting specificity like exosomes.

We further performed an experiment to compare the delivery of different vesicles to the same cell type. For this we generated DiI-labeled CEVs from both HCT as well as RAW cells and delivered them to HCT cells, measuring the fluorescence signal over time. In this study HCT CEVs too were preferentially taken up by HCT cells. The interesting result is that although HCT-engineered vesicles were more efficient at delivering cargo to HCT cells as compared to RAW vesicles, RAW CEVs still exhibited targeting properties for HCT cells (Figure 4.3C). Based on these results we were able to show that CEVs, like exosomes, have an affinity to deliver their cargo preferentially to those cells from which they originated. Wide field imaging shows the greater uptake of RAW-engineered vesicles by RAW cells and relatively low uptake by A549 cells (Figure 4.3D-E), illustrating greater

specificity for delivery to RAW cells. Although cancer CEVs specifically target cells from which they were originated, there is some a discrepancy among scientists as to the use of CEVs in clinical application due to the potential threat of these vesicles increasing the metastatic potential in vivo. On the other hand, we proposed that RAW CEVs, having only a 3-fold decrease in targeting A549 cells compared to RAW cells, can be used as a general drug delivery vehicle to deliver cargo to cancer cells.

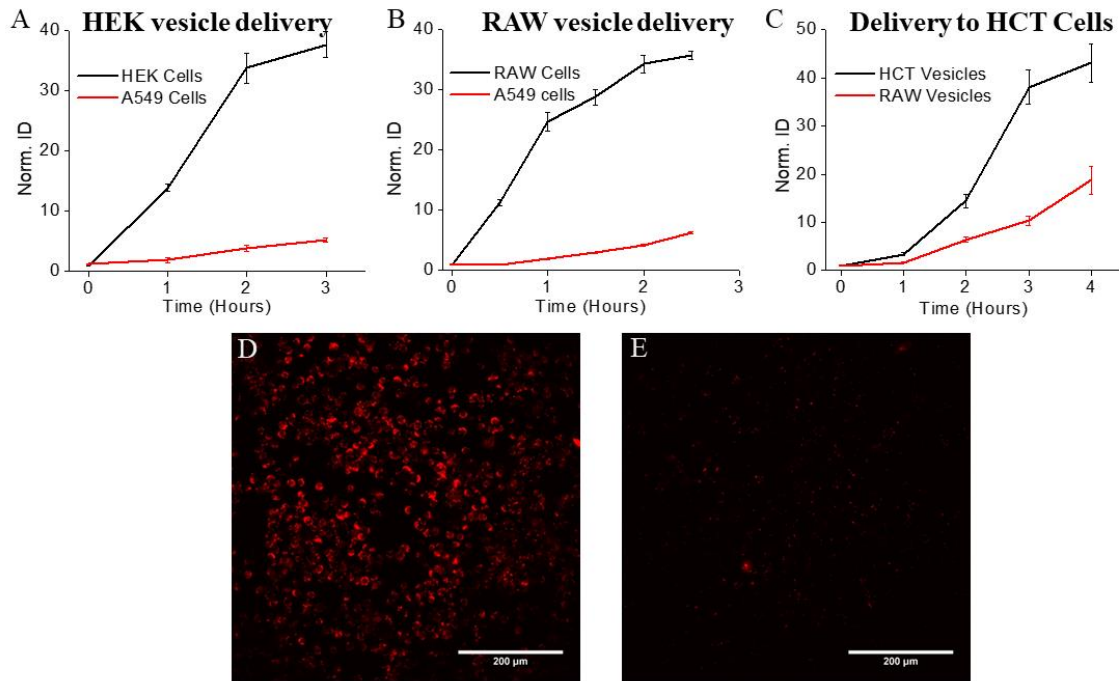


Figure 4.3 Cell targeting specificity of cell-engineered vesicles.

(A) Comparison of HEK vesicles delivered to HEK cells (black) versus HEK vesicles delivered to A549 cells (red). (B) Comparison of RAW vesicles delivered to RAW cells (black) versus RAW vesicles delivered to A549 cells (red). (C) Comparison of HCT vesicles delivered to HCT cells (black) versus RAW vesicles delivered to HCT cells (red). (D) Widefield fluorescence image of DiI labeled RAW vesicles delivered to RAW cells after 2.5 hours showing clear loading. (E) Widefield fluorescence image of DiI-labeled RAW vesicles delivered to A549 cells after 2.5 hours showing limited cellular uptake. Norm ID is the integrated density of the image normalized to the time 0 value. Each data point is the average of 5 experiments. A student's t-test was used to determine significance between end points. Each end point was significant with a p value <.001.

4.4.3 In Vitro Delivery of Hydrophilic Cargo

Previous studies have used exosomes to deliver cargo to the recipient cells. However, poor yield and difficulty in loading therapeutics into the exosome are some of the challenges associated with their use in clinical applications. To illustrate the adaptability of our vesicle-based delivery system, we generated vesicles that encapsulated fluorescein, a green-emitting fluorophore, in order to observe the transport of cargo to the interior of the cell. DiD, a lipophilic dye, was then used to label the membranes of these fluorescein-loaded vesicles. This enabled us to observe vesicle contents being delivered to the cytoplasm and the vesicle membrane being integrated with the membrane of the recipient cells. We incubated HEK cells with fluorescein-loaded DiD-labeled vesicles for 45 minutes to allow cells to take up these vesicles. Vesicles still present in the media solution were removed by rinsing the cells, and confocal imaging was conducted. We observed a clear fluorescence that spread throughout the cytosol, indicating vesicles successfully delivered the hydrophilic cargo, fluorescein, to the interior of the cell (Figure 4.4). Also, we saw DiD fluorescence in some parts of the cell membrane, which shows that vesicles first fuse with the cell membrane and then release their contents into the cell. These results demonstrate that CEVs can be used to successfully deliver cargo to the interior of the cell.

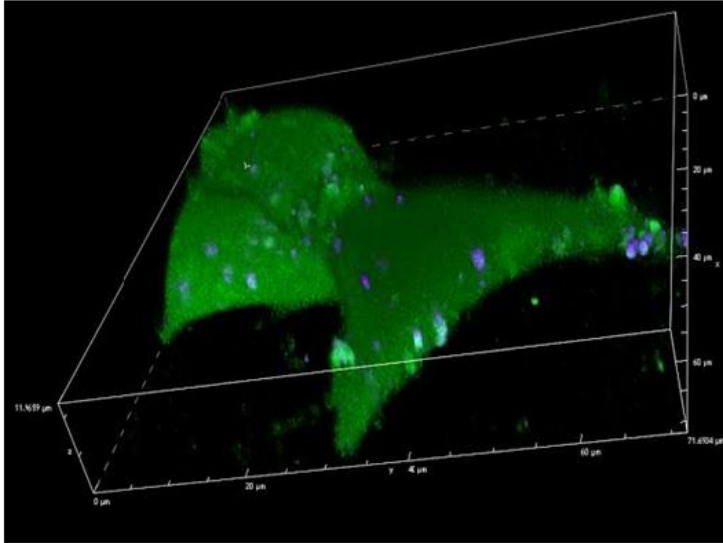


Figure 4.4 Confocal image of HEK cells showing vesicle mediated cargo delivery.

Cell-engineered vesicles were loaded with fluorescein (inside) and then labeled with DiD (lipid bilayer) prior to incubating them with HEK cells. After vesicle uptake, the interior of the cell is packed with fluorescein.

4.4.4 Immunomodulatory Properties of A549 cell generated CEVs

Recent studies have utilized exosomes released from cancer cells or immune cells to reprogram the immune cell phenotype of the recipient cell. Lower yield, and cumbersome isolation steps pose a barrier for their clinical translation. Here, we performed a series of experiments to see if cell-engineered vesicles generated from human lung cancer (A549) can trigger immune cell activation when they interact with the immune cells. In order to study the ability of engineered vesicles to flip the phenotype of macrophages we performed a series of experiments in vitro. At first, we induced M1 bone marrow-derived macrophage polarization via stimulation with a lipopolysaccharide (LPS) and an interferon gamma (IFN- γ). Similarly, we induced M2 macrophage polarization using IL-4. A549 CEVs were generated using nitrogen cavitation from cultured A549 cells. We added A549 CEVs (A549EVs) to cultured, unstimulated M0 macrophages, pro-inflammatory M1 macrophages and anti-inflammatory M2 macrophages and left to incubate for 24 hours at 37 °C. At first, we compared the cytokine production from M0 macrophages, M1 macrophages and M2 macrophages incubated with A549EVs (Figure 4.5A). The supernatant was collected from the cell culture of each sample and proinflammatory cytokines were analyzed using an MSD assay of the cell culture supernatant. We observed proinflammatory cytokine expression by M1 macrophages whereas almost zero expression of such markers was seen for M0 macrophages. We also observed a clear increase in the levels all the pro-inflammatory markers for M0 macrophages that had been incubated with A549EVs (Figure 4.5B). These result show that A549EVs can stimulate M0 macrophage towards M1 macrophages. In similar studies we have found that A549EVs somehow suppress the pro-inflammatory property of M1 macrophages but repolarize M2 macrophages towards a pro-inflammatory phenotype (Figure 4.5C).

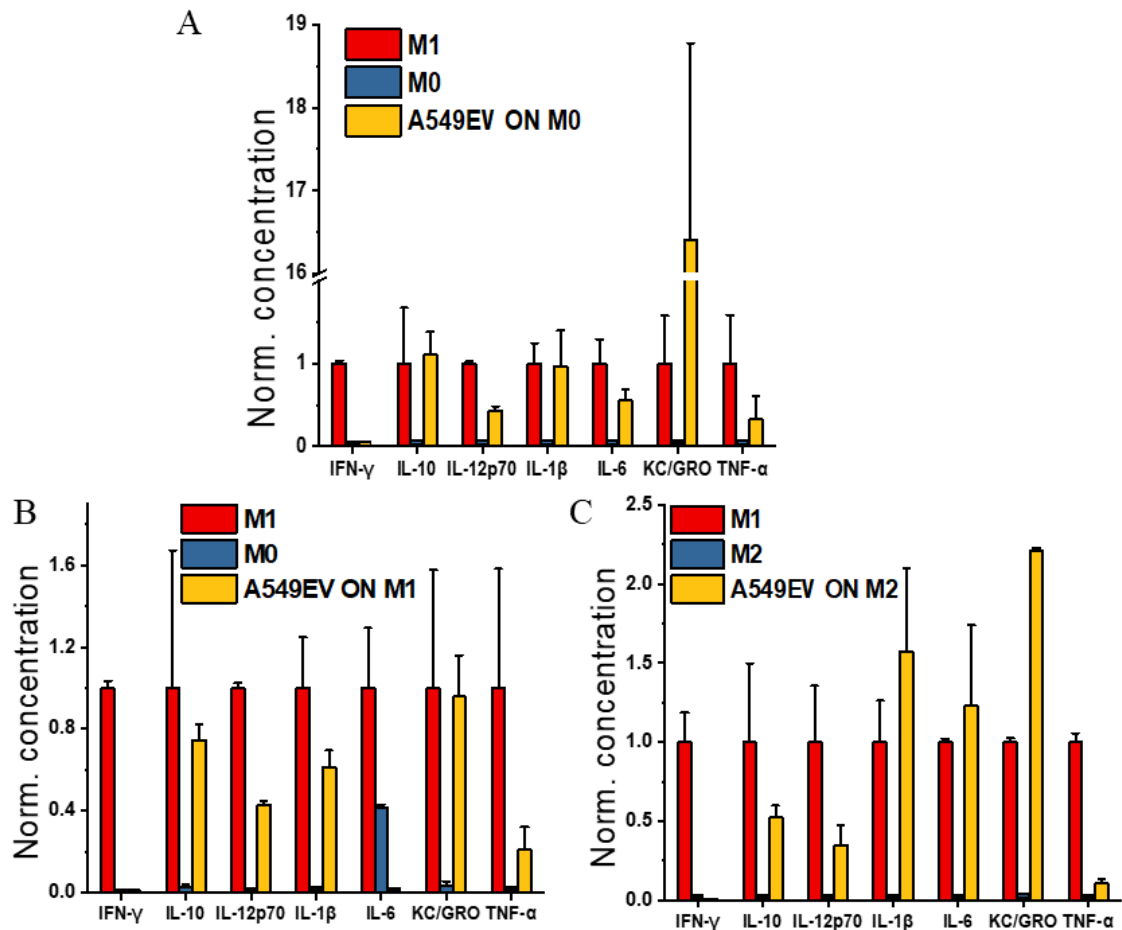


Figure 4.5 Polarization of M0, M1 and M2 macrophages in vitro by A549EVs.

(A) Polarization of M0 macrophages towards M1 macrophages in vitro when left to incubate with A549EVs. (B) Quantification of pro-inflammatory cytokine expression by M1 macrophages when left to incubate the with A549EVs in vitro. (C) Polarization of M2 macrophages towards M1 macrophages in vitro when treated with A549EVs. Each graph represents an MSD assay evaluation of macrophage-conditioned media for pro-inflammatory markers IFN- γ , IL-10, IL-12p70, IL-1 β , IL-6, and KC/GRO, typical cytokines release by M1 macrophages. Each data point is the average of at least 3 experiments.

4.4.5 CEV-mediated Chemotherapeutic Delivery to Cancer Cells

In the face of the growing danger posed by tumors, it has always been a difficult task to develop a versatile DDS that can be used for effective therapeutic delivery to cancer cells. In particular, it has been difficult to develop a DDS that demonstrates enhanced cancer cell targeting capability. Many different DDS platforms, including polymer assembly, inorganic materials composites, liposomes, and hydrogels, have been used for therapeutic delivery onto cancer cells over the last few decades. While these DDS have paved the way for the further development of novel DDS, their inherent flaws, including intricate functionalization techniques, a need to improve their stability *in vivo*, and possible metal toxicity, limit their use in clinical applications. Because of this, there is a pressing need to develop new DDS with superior biocompatibility and ease of incorporation of cell-targeting and therapeutic components. In addition, these new DDS should be generated using simple and bio-friendly preparation techniques. While endogenously produced exosomes have been increasingly employed as innovative DDS for tumor diagnostics and treatment, exosomes are produced in low quantities, involve cumbersome purification steps, and difficult to functionalize with cell targeting moieties. To overcome these limitations, we developed therapeutic-loaded CEVs and exploited them for cisplatin delivery into cancer cells. Cell-engineered vesicles can be generated with high yields and can be easily loaded with therapeutics during nitrogen cavitation.

We performed a series of experiments to evaluate the efficacy of chemotherapeutic-loaded CEVs delivery to cancer cells. First, cisplatin loaded A549 engineered vesicles were generated in the presence of 8.33 mM cisplatin in sucrose buffer solution (SBS). We measured the concentration of cisplatin-encapsulated inside of the vesicles using ICP-OES. We found that 1×10^{11} CEVs can encapsulate 3 μg of cisplatin. We further investigated the stability of such cisplatin-loaded vesicles by measuring the cisplatin leaking into the solution for 3 consecutive days and found that vesicles are stable at 37 °C for two days as

we found no apparent leakage of cisplatin from these vesicles for 48 hours. As a control study we first treated A549 cells with empty A549 CEVs and compared the viability of A549 cells in absence and presence of vesicles. We found the presence of empty vesicles does not alter the viability of A549 cells (Figure 4.6). In addition to this, we further compared the effect of free cisplatin and cisplatin-loaded vesicles to A549 cells. The concentration of cisplatin delivered through vesicles was maintained the same as cisplatin in free solution. At 24 hours we found that cisplatin-loaded engineered vesicles were able to cause 70% cell death while free cisplatin caused no apparent cell death. Similarly, at 48 hours cisplatin loaded CEVs resulted in 90% cell death whereas free cisplatin caused only 15 % cell death. This low concentration of free cisplatin resulted in no apparent cell death at 24 hours, while cisplatin-loaded vesicles resulted in 70% cell death. By the 48-hour time point, loaded cell-derived vesicles resulted in 90% cell death, while free cisplatin resulted in 15% cell death. At 72 hours cisplatin-loaded vesicles maintained 90% cell death while free cisplatin caused 50% cell death. These results clearly showed that cisplatin loaded CEVs were much more effective in causing cell death at very low concentration compared to free cisplatin by delivering their cargo effectively inside of the cell.

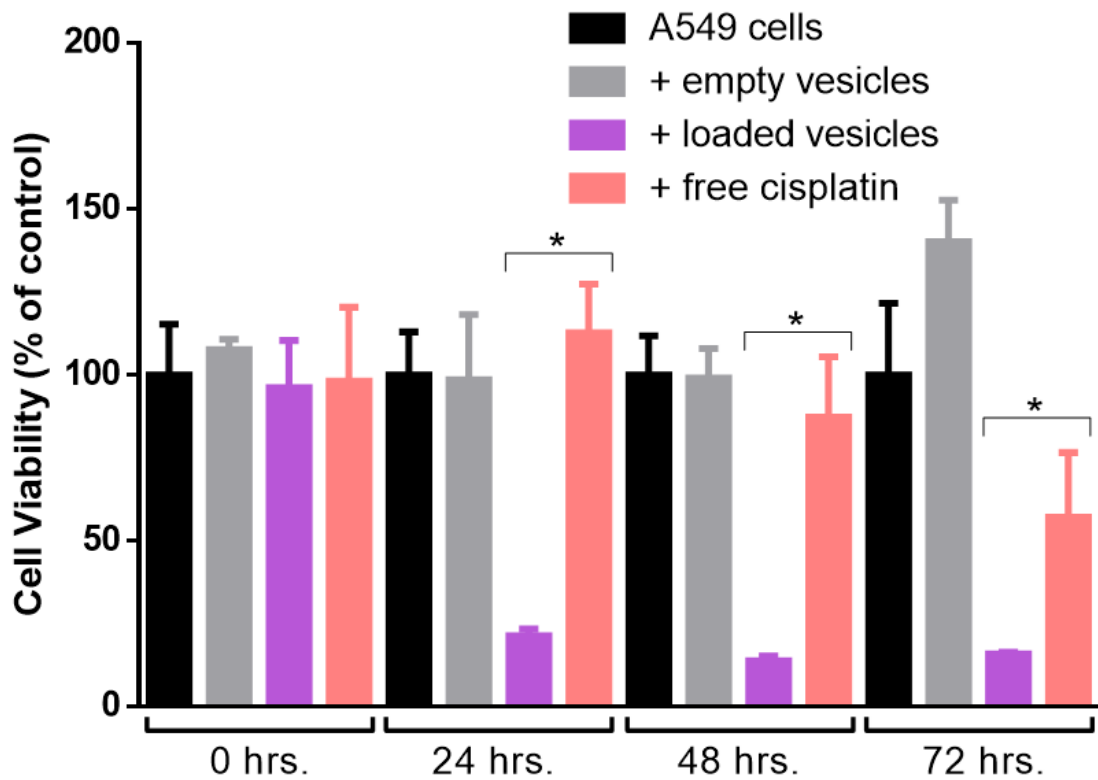


Figure 4.6 Efficacy of cisplatin loaded vesicles.

Comparison of cell growth at time 0, 24 hours, 48 hours, and 72 hours for A549 cells with no treatment (black), treated with empty vesicles (gray), with carboplatin loaded vesicles (purple), and free cisplatin in solution (pink). Empty vesicles have no effect on cell growth while both free cisplatin and loaded vesicles show similar efficacy in killing A549 cells. Each data point is the average of 5 experiments. A student's t-test was used to determine significance. * Indicates a p value <.001.

In order to improve the targeting efficiency as well as cancer killing ability of therapeutic-loaded CEVs we generated folate ligands decorated engineered vesicles. Folate ligands can interact with folate receptors that are ubiquitously present in cancer cells. Folate receptor (FR) is a membrane glycoprotein that is highly expressed in tumor cells including ovarian, lung, brain, and breast cancers³²¹⁻³²⁴. Folate ligands are often incorporated onto the surface of drug delivery systems such as liposomes and micro vesicles to enhance their targeting to cancer cells. Recently, Zhu et al. incorporated folate into the phospholipid membrane of micro vesicles (size 792nm) generated from CAL27, an oral adenosquamous carcinoma cell line, and showed improved targeting toward breast cancer.²⁶⁹ Although, the engineering of micro vesicles and lipid based particles seems promising, they still suffer from challenges such as lower yields, bigger size, and an inability to evade immune clearance when delivered *in vivo*. We generated folate decorated macrophage engineered vesicles (MEVs) vesicles to determine the effect on targeting lung cancer(A549) cells.

Folate ligands were allowed to incorporate onto the macrophage membrane through a phospholipid substitution technique as described previously³²⁵. We found that when macrophages are allowed to proliferate in standard media supplemented with 1,2-distearoyl-sn-glycero-3-phosphoethanolamine-N-(folate(polyethylene glycol)-2000) ammonium salt (DSPE-PEG-Folate), DSPE-PEG-Folate is incorporated into the macrophage membrane during cell division. We confirmed folate decoration on macrophage using fluorescence microscopy. Fluorescence images of folate-decorated macrophages are displayed in Figure 4.7A. We next polarized folate decorated BMDMs to an M1 phenotype and generated folate decorated MEVs (folate-MEVs). The presence of folate ligands on MEVs was confirmed using fluorescence microscopy (Figure 4.7C). We used Nanoparticle Tracking Analysis (NTA) and Dynamic Light Scattering (DLS) to measure the size, particle number, and the zeta potential of the MEVs. Folate decorated MEVs have a diameter of 100-200 nm with a zeta potential of -17.2 mV. We next

performed a set of experiments to determine if folate-MEVs exhibit greater cancer cell targeting properties compared to the regular MEVs. We generated folate decorated MEVs and regular MEVs and then labeled them with a lipophilic dye, DiI. We added 1×10^{11} DiI labeled folate-MEVs or DiI labeled MEVs to 30,000 A549 cells in culture and incubated them at 37 °C. We then determined the efficacy of delivery of DiI labeled vesicles to the A549 cells by measuring the increase fluorescence intensity at time points over 2.5 hours. Folate decorated MEVs exhibit almost 20% higher targeting ability to A549 cells compared to non-decorated MEVs (Figure 4.8A-C). We further generated cisplatin loaded MEVs and cisplatin loaded folate decorated MEVs and compared the half-maximal inhibitory concentration (IC_{50}) values of cisplatin in media, cisplatin loaded vesicles, and cisplatin loaded folate decorated vesicles. The IC_{50} values of cisplatin loaded MEVs ($IC_{50} = 4.3 \mu M$) was 40 % less than cisplatin in media ($IC_{50} = 7.2 \mu M$) (Figure 4.8D-E). Cisplatin loaded folate decorated MEVs ($IC_{50} = 3.2 \mu M$) have an IC_{50} value 20 % less than cisplatin loaded MEVs (Figure 4.8E-F). These results show that folate decoration of MEVs not only improves the targeting ability to the cancer cells but also increases the therapeutic efficacy.

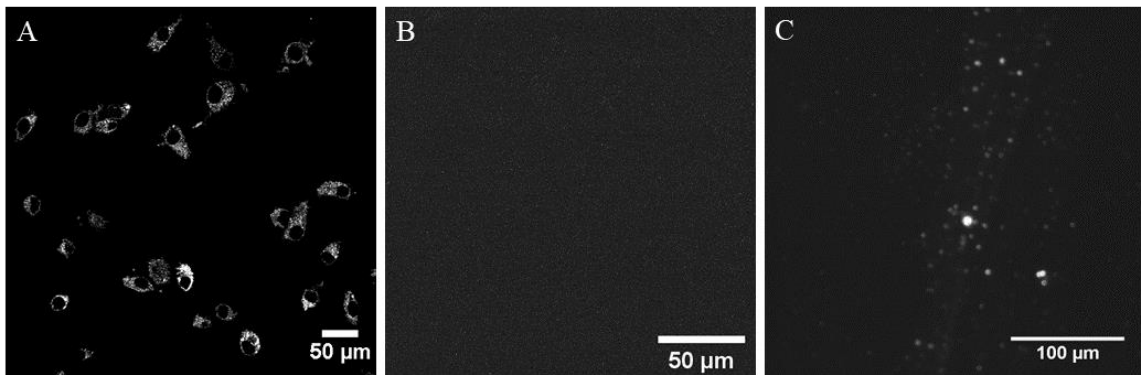


Figure 4.7 Programming BMDMs and MEVs with folate ligands.

(A) Fluorescence image of BMDMs expressing folate ligands. (B) BMDMs control. (C) MEVs generated using folate decorated BMDMs express folate ligands on their surface.

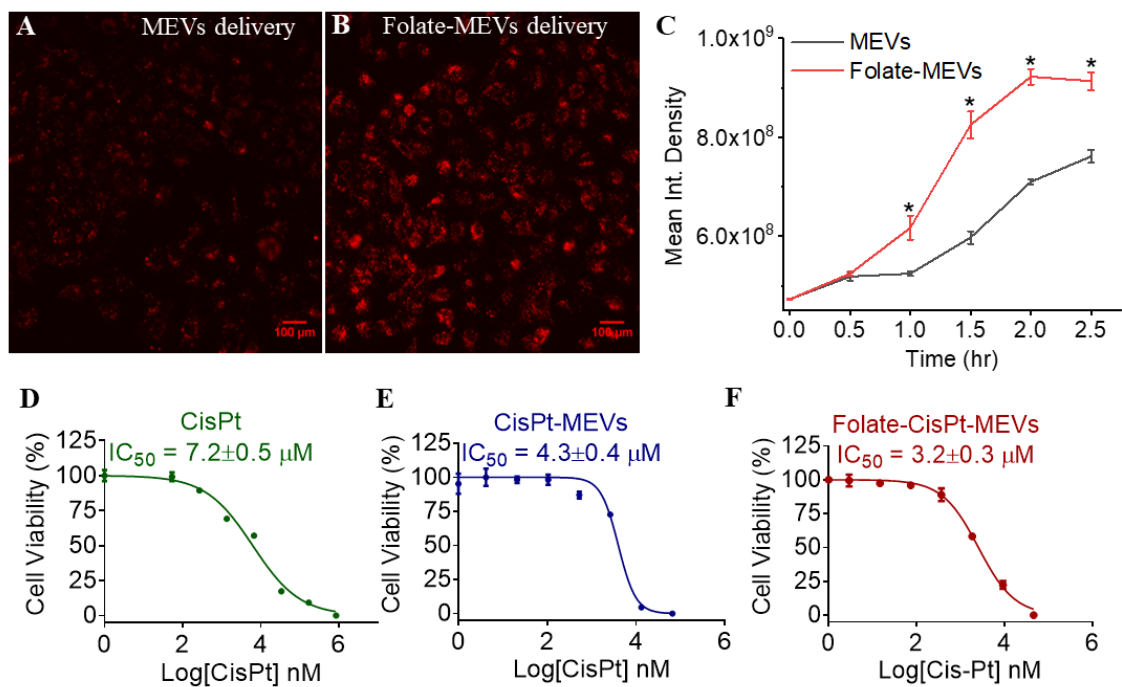


Figure 4.8 Programming MEVs with folate ligands for A549 cell targeting.

(A-B) Fluorescence image showing folate decorated MEVs are taken up more efficiently compared to regular MEVs. (C) Quantification of uptake of MEVs and folate-MEVs by A549 cell. (D,E,F) IC₅₀ values for cisplatin-media solution, cisplatin loaded MEVs, and folate decorated cisplatin loaded MEVs onto A549 cells.

4.4.6 In Vivo Targeting and Delivery of Vesicles

Our previous experiments demonstrate that cell-engineered vesicles mimic exosomes and can deliver cargo to the targeted cell in vitro. An ideal drug delivery vehicle should be biocompatible, less immunogenic, stable over a prolonged period while circulating in the blood, safe, and able to deliver therapeutics in vivo. We next performed a series of experiments to assess the utility of cell-engineered vesicles in delivering cargo to a specific tissue in a live animal. First, we implanted a xenograft containing A549 carcinoma cells into an immune-compromised nude mouse by subcutaneous injection of A549 cells. When the tumor had reached a sufficient size, we created cell-engineered vesicles and conducted a positive control experiment. In this work, DiR-labeled cell-engineered vesicles were injected directly into the tumor xenograft. The animal was scanned using in vivo imaging equipment, and successive imaging sessions were compared to investigate the uptake and distribution of DiR-labeled CEVs into the tumor xenograft. Next, we administered a solution containing DiR dye molecules through the tail vein of another animal with a xenograft and discovered no detectable dyes in the tumor. Finally, we generated CEVs from A549 cells, labeled them with DiR, and then performed tail vein injection of CEVs into the mouse carrying a xenograft. Images of the mouse demonstrated that vesicles do reach the tumor. These results confirmed our idea that cell-derived vesicles produced by nitrogen cavitation may be used to selectively deliver drugs to malignancies.

After confirming the utility of CEVs in delivering cargo to the tumor xenograft, we next performed a series of similar experiments using CEVs from multiple cell lines and checked whether CEVs exhibit tumor xenograft targeting specificity in vivo. We generated vesicles from human embryonic kidney cells (HEK), human lung cancer (A549), and labeled them separately with a membrane dye, DiR. Dye-labeled vesicles were purified from free dye using PD midi-prep size exclusion columns. We found that DiR alone when injected into the mice as a control showed nonspecific accumulation whereas HEK-

engineered vesicles accumulated in the area of bladder and were not able to reach the tumor (Figure 4.9A&B). However, A549 cell-engineered vesicles were able to specifically target the A549 tumor xenograft inside a live animal (Figure 4.9C). These results demonstrate that cell engineered vesicles exhibit tumor cell targeting specificity in vivo.

While A549 CEVs are able to specifically target a tumor inside the body of an animal, use of these vesicles in clinical application is concerning due to the fact that these vesicles may carry genetic materials belonging to the parent cells, which when administered into the body, may induce the proliferation of cancer¹⁸⁶⁻¹⁸⁸ instead of curing cancer. An alternative to using cancer cell-engineered vesicles could be to use vesicles from macrophages. Immune cells such as macrophages are widespread in the tumor microenvironment. Because CEVs exhibit targeting specificity, we expect that CEVs generated using macrophage-like cell lines (RAW 264.7) could specifically target tumor tissue. We next generated vesicles from RAW 264.7 cells and labeled them with DiR. When these vesicles were administered into the mice with tumor xenograft through the tail vein, we found that RAW cell-engineered vesicles were able to specifically target the A549 tumor xenograft inside a live animal (Figure 4.9D). These results demonstrate that cell engineered vesicles from macrophages offer better alternatives to CEVs from cancer cells to deliver cargo specifically to the tumor tissue.

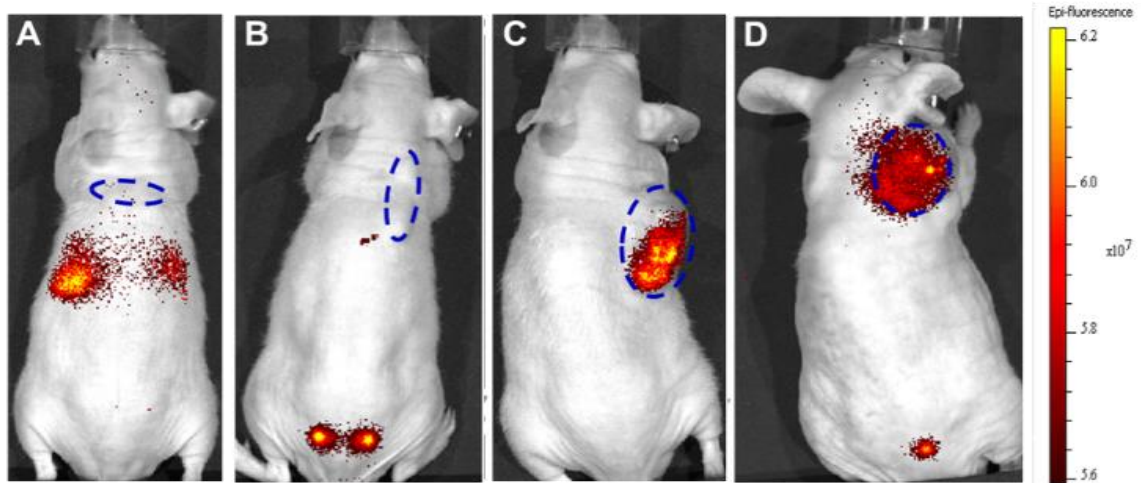


Figure 4.9 CEVs can reach the tumor xenograft in ice.

Mice bearing A549 xenografts on the right shoulder (dashed blue ovals) were injected with (A). dye (DiR) alone (B). dye labeled vesicles derived from HEK cells (C). dye labeled vesicles derived from A549 cells, and (D). dye labeled vesicles derived from RAW264.7 cells demonstrating RAW vesicles specifically targeted the A549 xenograft.

4.5 Conclusion

Existing therapeutic delivery strategies often involve systemic therapeutic administration into the human body. This results in the interaction of drugs with both benign as well as malignant cells, which leads to unwanted side effects. While exosome or liposome-based therapeutic delivery systems have shown promise for their use in targeted therapeutic delivery, low production yields and high isolation costs associated with exosomes and immune clearance for liposomes have been challenges for their use in clinical applications.

Here, we developed novel cell-engineered vesicles (CEVs) from multiple cell types using the nitrogen cavitation technique. CEVs were generated with high yields and mimic the useful properties of exosomes. The size distribution of vesicles generated using nitrogen cavitation is similar to the size distribution reported for exosomes and liposomes. Similar to exosomes, CEVs exhibit a negative zeta potential value and are stable over a prolonged period of time. These vesicles can be loaded with virtually any cargo and can be specifically delivered to the cell of interest both *in vitro* and *in vivo*. Because vesicles can be generated under minimal temperature conditions, CEVs maintain the stability of biological as well as therapeutic cargo. Overall, CEVs can be generated with high yield, easily loaded with therapeutics, and can specifically target tumor tissue *in vivo*. All these useful features of CEVs allow us to use them as a novel drug delivery vehicle that could selectively transport drug molecules to the cell of interest both *in vitro* and *in vivo*.

Effective delivery of chemotherapeutics to cancer cells is one of the main challenges of the existing drug delivery system. Chemotherapeutics-loaded cell-engineered vesicles aid in overcoming this challenge by efficiently delivering therapeutics to the recipient cell. Cancer therapeutic-loaded CEVs kill cancer cells at low drug doses

compared to free drugs in solution. In addition, CEVs can be programmed to express cell-targeting ligands on their surface, which enables improved cancer cell targeting ability. Furthermore, the cancer cell killing effect can be increased by using therapeutic-loaded programmed-CEVs compared to regular therapeutic-loaded cell engineered vesicles.

Besides delivering both lipophilic as well as hydrophilic cargo successfully under in vitro conditions, we next used CEVs for targeting tumor tissue in the animal. Dye-labeled CEVs generated from both cancer cells and macrophages, when administered through the tail vein injection, localize specifically to the tumor tissue into animals that had tumors grafted onto them. Immune These preliminary results demonstrate the utility of CEVs in delivering cargo efficiently to the tumor site in an animal. Overall CEVs can be used as drug delivery systems both in vitro and in vivo.

Recently, we have focused on utilizing chemotherapeutic-loaded CEVs for treating ovarian and osteosarcoma tumor xenografts in mice. In the near future, we plan to expand our research by isolating cancer cells from a patient and growing those cells in vitro. We plan to use some of the cultured cells for developing tumor xenografts in mice and use the remainder for generating therapeutic-loaded CEVs for delivering them back to the tumor xenograft. We will compare the efficacy of such vesicles in treating cancer compared to the drug in solution. We hope CEVs will demonstrate greater therapeutic efficacy in vivo and eliminate the off-target effect brought about by systemic administration of chemotherapy.

CHAPTER 5. CONCLUSIONS AND FUTURE DIRECTIONS

One of the main objectives of my graduate research was to develop potential immunomodulatory and therapeutic delivery nanocarriers that could controllably modulate immune cell phenotype and deliver therapeutic cargo to the interior of the cell. Immune cells like macrophages, dendritic cells, and microglia, among others, can show a continuum of polarization states that range from pro-inflammatory to anti-inflammatory⁷⁹. The presence of a particular phenotype is linked to the advancement of numerous disease conditions¹²⁷. For example, depending on the phenotype that macrophages exhibit in the tissue microenvironment, macrophages can either contribute to the development or suppression of cancer, inflammatory conditions, and infectious diseases^{123, 224, 227, 268}. Various factors, including cytokines, chemokines, and immune checkpoints expressed by cancer cells in the tumor microenvironment, cause tumor associated macrophages to exhibit an anti-inflammatory (M2) phenotype^{76, 77, 80}. M2 macrophages then produce various cytokines, chemokines, and growth factors that contribute to angiogenesis, tissue remodeling, chemoresistance, and metastasis⁷⁷. In addition, M2-TAMs express immune checkpoints like PD-L1 and PD-L2 that inhibit the adaptive immune response against tumors³²⁶⁻³²⁸. Additionally, macrophages play a significant part in the inflammatory response, such as that which occurs after a spinal cord injury (SCI)²³⁴. Following a spinal cord injury, the blood-brain barrier is disrupted, which allows for the fast invasion of peripheral macrophages into the spinal cord²³⁵. These macrophages participate in both pathogenic and reparative processes²³⁵. Pro-inflammatory macrophages are to blame for neurodegeneration and tissue loss after an SCI. On the other hand, anti-inflammatory macrophages are responsible for tissue reorganization and axon regeneration^{223, 237, 238, 264}.

The ability to therapeutically modulate macrophage phenotypes between M1 and M2 polarizations is one of the prospective treatments that has the potential to treat a number of diseases, including traumatic injury, wound healing, and cancer^{87, 131, 239, 241, 242, 261}. For instance, repolarizing M1 macrophages toward M2 phenotypes and thereby lowering the potential neurotoxic effects of M1 macrophages could be an effective method for treating stroke and spinal cord injuries (SCI)^{329, 330}. In a similar way, repolarizing M2 tumor-associated macrophages (M2-TAMs) toward an M1 phenotype that promotes inflammation is an appealing way to make cancer more susceptible to chemo-immunotherapy^{125, 201}. Recently, researchers have focused on developing therapeutics to specifically modulate the physiology of macrophages^{242, 329-331}. Previous approaches that involve systemic administration of several receptor agonists for immune cell modulation are recognized by various immune cell types, resulting in systemic toxicity^{123, 278, 332}. In addition, the utilization of small molecules in therapeutic applications is undermined by their quick degeneration, failure to boost anti-tumor actions in recipient macrophages, and increasing toxicity when utilized for extended durations²⁷⁸.

Nanomedicine provides a diverse platform of biocompatible and biodegradable technologies that are capable of delivering traditional therapeutic medicines *in vivo*, optimizing their release profiles while simultaneously boosting their bioavailability and concentration surrounding the target tissue⁵⁷. For example, liposomes loaded with therapeutics have been employed as nanocarriers as an alternative to systemic administration of small molecules and TLR-agonists^{303, 333}. Nevertheless, liposomes display non-specific targeting and are susceptible to clearance by the immune system¹²⁴. An ideal drug carrier should be able to evade phagocytosis and destruction by the body's immune system, selectively reach the targeted tissue of the body, and infiltrate the cellular system to distribute the cargo for a sustained length of time¹⁴⁴. As an alternative to liposomes, endogenously released exosomes from immune cells have been used. Exosomes can specifically target distal tissue and program immune cell modulation^{300, 334}. They have

most of the qualities of an ideal nanocarrier and have shown potential promise as a therapeutic platform against several diseases, including cancer. Exosomes released by M1 macrophages can specifically target distal tumor tissue and program M2 macrophages towards an M1 phenotype^{125, 242, 331}. Similarly, exosomes isolated from M2 macrophages can reprogram macrophages from M1 to M2 phenotypes at the wound site and promote angiogenesis, re-epithelialization, and collagen deposition³²⁹. Although exosomes have a natural targeting specificity and the capacity to change the phenotype of macrophages, exosome-based treatments are challenged by poor manufacturing yield and the difficulty of separating them^{302, 335}. Artificially engineered nanovesicles from immune cells could be a better alternative to exosomes or liposomes, as these nanovesicles offer a number of benefits, including a high yield, the capability to target the cells from which they were made, and the potential to alter the polarization of immune cells^{127, 144, 212}.

In chapter 1, we developed macrophage-engineered nanovesicles as a therapeutic platform by fragmenting cellular membranes using nitrogen cavitation. We performed a series of experiments to see if these vesicles exhibit exosome-like properties. Nitrogen cavitation techniques use N₂ to fragment mouse bone marrow-derived macrophages and form vesicles. Vesicles were purified from cell lysate by serial centrifugation. MEVs have the ability to be manufactured with high yields, conveniently loaded with diagnostic compounds or chemotherapeutics, and delivered to macrophages. We found that macrophage engineered vesicles, MEVs, can be used as nanocarriers that are capable of modulating macrophages and microglia to M1- or M2-phenotypes. In general, the capacity of MEVs to controllably regulate the inflammatory phenotypes of macrophages and microglia shows that they have great potential as possible delivery vehicles for both medicines and other kinds of molecules. These phenotypes are determined by the interactions between MEVs and the macrophage (e.g., neurotoxicity, tumor migration). This demonstrates that MEVs have the potential to function as an innovative and alternative therapy to target and reprogram macrophages.

Cell-engineered vesicle-based treatments overcome number of obstacles that restrict other nanoscale medicines. However, CEVs would be more successful with more efficiency in repolarizing anti-inflammatory macrophages to a proinflammatory phenotype or vice versa. One strategy for enhancing the therapeutic delivery effectiveness or macrophage reprogramming potential of drug delivery systems, such as cell-engineered vesicles, is to modify the properties of their surface with specific moieties that provide increased immunomodulatory characteristics. In chapter 2, we performed a series of experiments to first identify the possible proteins that could be anchored in MEVs and play a crucial role in re-polarizing M2 macrophages to M1 macrophages. We conclude that membrane proteins present on MEVs determine their uptake and ability to reprogram target macrophages. We next performed transfection to increase the expression level of the specific membrane-bound proteins in M1 macrophages and used those macrophages to generate programmed cell-engineered vesicles. We found that programmed cell-engineered nanovesicles over-expressing ligands could more effectively modulate the phenotype of immune cells. We programmed MEVs with the overexpression of several ligands, including TNF- α , CCL5, and ICAM1. We also developed programmed MEVs by incorporating already known M1 polarizing ligands such as PAM3CSK4 and CpG-ODN, and we found that compared to regular MEVs, programmed MEVs can execute enhanced immunomodulatory properties. We found that MEVs could successfully target cells present in the tumor micro-environment. In the future it is important to characterize the macrophage phenotype in the tumor microenvironment before and after vesicle delivery. This would allow us to study the MEV-mediated repolarization of immune cells present in the tumor microenvironment. In the future, we plan to study the effect of vesicle based M2 to M1 polarization on tumor regulation.

MEV-mediated repolarization of macrophages from one phenotype to another is one has the potential to provide different types of therapy for a number of ailments. For instance, repolarizing the macrophages that relate to the tumor towards a phenotype that is

more pro-inflammatory is an appealing method for making cancer more susceptible to immunotherapy. In a similar vein, repolarizing pro-inflammatory macrophages toward anti-inflammatory phenotypes and so lowering the potential neurotoxic effects of M1 macrophages could be an effective method for treating stroke and spinal cord injuries (SCI). By programming nanovesicles, we were able to enhance their immunomodulatory properties. We next aim to use programmed vesicles generated from M1 BMDMs for in vivo experiments. We hope programmed MEVs will successfully reprogram M2 TAMs present in the tumor microenvironment towards an M1 phenotype. We aim to perform immunohistochemistry experiments to analyze the expression of M1 markers in tumor-residing macrophages after vesicle delivery. We will also deliver TLR agonist-loaded vesicles to target macrophages in the tumor microenvironment, aiming to increase MEV-mediated macrophage reprogramming efficiency. Similarly, MEVs derived from M2-BMDMs will be injected into spinal cord injured mice. We hope that M2 MEVs will be able to facilitate the repair of spinal cord injuries.

In chapter 3, we employed CEVs for therapeutic delivery into the interior of cancer cells. Existing therapeutic delivery methods often utilize systemic therapeutic administration inside the body. This causes undesirable medication interactions with both benign and malignant cells, resulting in undesired side effects³³⁶. Although therapeutic-loaded nanoparticles have been utilized for targeted drug delivery, poor manufacturing yields and expensive isolation procedures have posed obstacles to their clinical usage³³⁵. We made unique cell-engineered vesicles (CEVs) from different types of cells using the nitrogen cavitation method. CEVs are produced in large quantities and resemble the advantageous features of exosomes. We found that the size distribution of vesicles formed by nitrogen cavitation is comparable to that of exosomes and liposomes. CEVs have a negative zeta potential value and are stable over prolonged time. These vesicles may be loaded with nearly any payload and delivered precisely to the target cell in vitro and in vivo. All these characteristics of CEVs enable us to employ them as a unique drug delivery

nanocarrier that might selectively transport drug molecules to the target cell *in vitro* and *in vivo*.

One of the greatest problems of the current medication delivery system is the efficient delivery of chemotherapeutics to cancer cells. By effectively delivering treatments to the cell of interest, chemotherapeutic-loaded cell-engineered vesicles could assist in overcoming this obstacle because, compared to free drugs in solution, cancer therapeutic-loaded CEVs kill cancer cells at lower drug concentrations. Additionally, CEVs may be designed to express cell-targeting ligands on their surface, therefore enhancing their potential to target cancer cells. Use of therapeutically loaded programmed-CEVs as opposed to conventional therapeutically loaded cell engineered vesicles can also boost the cancer cell-killing efficacy.

In addition to effectively delivering both lipophilic and hydrophilic cargo under *in vitro* conditions, we employed CEVs to target tumor tissue in the animal. When these CEVs are injected into the tail veins of tumor-bearing animals, they selectively localize to the tumor tissue. Immune These early results suggest that CEVs can successfully deliver cargo to the site of a tumor in an animal. Overall, CEVs may be exploited both *in vitro* and *in vivo* as drug delivery methods.

Based on our studies, we found that nitrogen cavitation technique-based vesicle formation technology offers numerous benefits over existing mechanical disruption strategies. First, as opposed to sonication or extrusion-based approaches, biological samples are kept at a lower temperature throughout the vesicle production process. This not only serves to preserve the chemical composition of the cell medium, but also the biological integrity of the produced vesicles. The nitrogen cavitation process is less constrained by cell size, sample size, and sample concentration due to the fact that nitrogen bubbles are generated inside each individual cell during decompression. Nitrogen cavitation also yields more trustworthy results since the force applied by the N₂ gas at greater pressure is distributed uniformly throughout the sample, which can be repeated at

comparable pressures. A third advantage of this method is that the solution in which cells are suspended during cavitation is contained inside the vesicles. Consequently, during the creation of vesicles, pharmaceuticals and other cargos may be effectively encapsulated. In addition, a comprehensive investigation of size, shape, and protein markers demonstrated that nitrogen cavitation-generated nanovesicles are similar to naturally occurring endogenously produced extracellular vesicles. Overall, nitrogen cavitation is a novel methodology for efficiently manufacturing exosome-like cell-engineered nanovesicles for therapeutic purposes, and this technology might be used to a wide range of cell types for the development of customized nanomedicine.

We have recently emphasized the use of CEVs loaded with chemotherapeutics to treat ovarian and osteosarcoma tumor xenografts in mice. In the near future, we want to broaden our study by isolating a patient's cancer cells and cultivating them *in vitro*. We want to employ a portion of the grown cells to generate tumor xenografts in mice, while the rest will be used to generate therapeutic-loaded CEVs for re-administration to the tumor xenograft. We will compare the effectiveness of these vesicles in treating cancer to that of cisplatin in solution. We anticipate that CEVs will display improved therapeutic effectiveness *in vivo* and reduce the harmful side effects stemming from systemic administration of chemotherapy. In addition, we plan to deliver folate-decorated, therapeutic-loaded vesicles into the mice with the tumor once every week for one month and evaluate the therapeutic efficacy of nanovesicles in reducing the size of the tumor and eventually eliminating it from the mice. We will also study if these vesicles are safe to deliver for a prolonged period of time. We will also evaluate the activity of CEVs generated using primary human monocytes since therapeutic applications would need MEVs generated from cells suitable for administration to human patients.

REFERENCE

1. Debela, D. T.; Muzazu, S. G.; Heraro, K. D.; Ndalama, M. T.; Mesele, B. W.; Haile, D. C.; Kitui, S. K.; Manyazewal, T., New approaches and procedures for cancer treatment: Current perspectives. *SAGE open medicine* **2021**, *9*, 20503121211034366.
2. Gunjal, P.; Schneider, G.; Kakar, S.; Kucia, M.; Ratajczak, M., Evidence for Induction of a Tumor-Metastasis-Receptive Microenvironment in Bone Marrow and Other Organs As an Unwanted and Underestimated Side Effect of Chemotherapy/Radiotherapy. *Blood* **2014**, *124* (21).
3. Arruebo, M.; Vilaboa, N.; Sáez-Gutierrez, B.; Lambea, J.; Tres, A.; Valladares, M.; González-Fernández, A., Assessment of the evolution of cancer treatment therapies. *Cancers (Basel)* **2011**, *3* (3), 3279-330.
4. Baskar, R.; Lee, K. A.; Yeo, R.; Yeoh, K. W., Cancer and radiation therapy: current advances and future directions. *Int. J. Med. Sci.* **2012**, *9* (3), 193-9.
5. Jackson, S. P.; Bartek, J., The DNA-damage response in human biology and disease. *Nature* **2009**, *461* (7267), 1071-8.
6. Dewey, W. C.; Furman, S. C.; Miller, H. H., Comparison of lethality and chromosomal damage induced by x-rays in synchronized Chinese hamster cells in vitro. *Radiat. Res.* **1970**, *43* (3), 561-81.
7. Hendry, J. H.; West, C. M., Apoptosis and mitotic cell death: their relative contributions to normal-tissue and tumour radiation response. *Int. J. Radiat Biol.* **1997**, *71* (6), 709-19.
8. Lisa, M. C.; Zena, W., Inflammation and cancer. *Nature* **2002**, *420* (6917), 860.
9. Rubin, P.; Johnston, C. J.; Williams, J. P.; McDonald, S.; Finkelstein, J. N., A perpetual cascade of cytokines postirradiation leads to pulmonary fibrosis. *Int. J. Radiat. Oncol. Biol. Phys.* **1995**, *33* (1), 99-109.
10. Darby, S. C.; Ewertz, M.; McGale, P.; Bennet, A. M.; Blom-Goldman, U.; Brønnum, D.; Correa, C.; Cutter, D.; Gagliardi, G.; Gigante, B.; Jensen, M. B.; Nisbet, A.; Peto, R.; Rahimi, K.; Taylor, C.; Hall, P., Risk of ischemic heart disease in women after radiotherapy for breast cancer. *N. Engl. J. Med.* **2013**, *368* (11), 987-98.
11. Cooper, J. S.; Fu, K.; Marks, J.; Silverman, S., Late effects of radiation therapy in the head and neck region. *Int. J. Radiat. Oncol. Biol. Phys.* **1995**, *31* (5), 1141-64.
12. Stone, H. B.; Coleman, C. N.; Anscher, M. S.; McBride, W. H., Effects of radiation on normal tissue: consequences and mechanisms. *Lancet Oncol.* **2003**, *4* (9), 529-36.
13. Hoskin, P., The price of anticancer intervention. Secondary malignancies after radiotherapy. *Lancet Oncol.* **2002**, *3* (9), 577-8.

14. Hall, E. J., Intensity-modulated radiation therapy, protons, and the risk of second cancers. *Int. J. Radiat. Oncol. Biol. Phys.* **2006**, *65* (1), 1-7.
15. DeVita, V. T., Jr.; Chu, E., A history of cancer chemotherapy. *Cancer Res.* **2008**, *68* (21), 8643-53.
16. van den Boogaard, W. M. C.; Komninos, D. S. J.; Vermeij, W. P., Chemotherapy Side-Effects: Not All DNA Damage Is Equal. *Cancers (Basel)* **2022**, *14* (3).
17. Kitao, H.; Iimori, M.; Kataoka, Y.; Wakasa, T.; Tokunaga, E.; Saeki, H.; Oki, E.; Maehara, Y., DNA replication stress and cancer chemotherapy. *Cancer Sci.* **2018**, *109* (2), 264-271.
18. Haley, B.; Frenkel, E., Nanoparticles for drug delivery in cancer treatment. *Urologic Oncology: Seminars and Original Investigations* **2008**, *26* (1), 57-64.
19. Mark, E. D.; Zhuo, C.; Dong, M. S., Nanoparticle therapeutics: an emerging treatment modality for cancer. *Nature Reviews Drug Discovery* **2008**, *7* (9), 771.
20. McCormick, R. E., Possible acceleration of aging by adjuvant chemotherapy: a cause of early onset frailty? *Med. Hypotheses* **2006**, *67* (2), 212-5.
21. Guida, J. L.; Ahles, T. A.; Belsky, D.; Campisi, J.; Cohen, H. J.; DeGregori, J.; Fuldner, R.; Ferrucci, L.; Gallicchio, L.; Gavrillov, L.; Gavrillova, N.; Green, P. A.; Jhappan, C.; Kohanski, R.; Krull, K.; Mandelblatt, J.; Ness, K. K.; O'Mara, A.; Price, N.; Schrack, J.; Studenski, S.; Theou, O.; Tracy, R. P.; Hurria, A., Measuring Aging and Identifying Aging Phenotypes in Cancer Survivors. *J. Natl. Cancer Inst.* **2019**, *111* (12), 1245-1254.
22. Armenian, S. H.; Gibson, C. J.; Rockne, R. C.; Ness, K. K., Premature Aging in Young Cancer Survivors. *JNCI: Journal of the National Cancer Institute* **2019**, *111* (3), 226-232.
23. Cupit-Link, M. C.; Kirkland, J. L.; Ness, K. K.; Armstrong, G. T.; Tchkonina, T.; LeBrasseur, N. K.; Armenian, S. H.; Ruddy, K. J.; Hashmi, S. K., Biology of premature ageing in survivors of cancer. *ESMO open* **2017**, *2* (5), e000250-e000250.
24. Mansoori, B.; Mohammadi, A.; Davudian, S.; Shirjang, S.; Baradaran, B., The Different Mechanisms of Cancer Drug Resistance: A Brief Review. *Advanced pharmaceutical bulletin* **2017**, *7* (3), 339-348.
25. Housman, G.; Byler, S.; Heerboth, S.; Lapinska, K.; Longacre, M.; Snyder, N.; Sarkar, S., Drug resistance in cancer: an overview. *Cancers (Basel)* **2014**, *6* (3), 1769-1792.
26. Wu, T.; Qi, Y.; Zhang, D.; Song, Q.; Yang, C.; Hu, X.; Bao, Y.; Zhao, Y.; Zhang, Z., Bone Marrow Dendritic Cells Derived Microvesicles for Combinational Immunotherapy against Tumor. *Advanced Functional Materials* **2017**, *27* (42), n/a-n/a.
27. Barber, F. D., Adverse Events of Oncologic Immunotherapy and Their Management. *Asia-Pacific Journal of Oncology Nursing* **2019**, *6* (3), 212-226.

28. Alatrash, G.; Jakher, H.; Stafford, P. D.; Mittendorf, E. A., Cancer immunotherapies, their safety and toxicity. *Expert Opin. Drug Saf.* **2013**, *12* (5), 631-45.
29. Hanahan, D.; Weinberg, R. A., Hallmarks of cancer: the next generation. *Cell* **2011**, *144* (5), 646-74.
30. Ventola, C. L., Cancer Immunotherapy, Part 1: Current Strategies and Agents. *P & T : a peer-reviewed journal for formulary management* **2017**, *42* (6), 375-383.
31. Hu, R.; George, D. J.; Zhang, T., What is the role of sipuleucel-T in the treatment of patients with advanced prostate cancer? An update on the evidence. *Ther. Adv. Urol.* **2016**, *8* (4), 272-278.
32. Graff, J. N.; Chamberlain, E. D., Sipuleucel-T in the treatment of prostate cancer: an evidence-based review of its place in therapy. *Core evidence* **2015**, *10*, 1-10.
33. Yagiela, J. A.; Neidle, E. A.; Dowd, F. J., *Pharmacology and therapeutics for dentistry*. Mosby Incorporated: 1998; Vol. 4.
34. Stanculeanu, D. L.; Daniela, Z.; Lazescu, A.; Bunghez, R.; Anghel, R., Development of new immunotherapy treatments in different cancer types. *J. Med. Life* **2016**, *9* (3), 240-248.
35. Jarboe, J.; Gupta, A.; Saif, M. W., Therapeutic human monoclonal antibodies against cancer. *Methods Mol. Biol.* **2014**, *1060*, 61-77.
36. Guan, M.; Zhou, Y. P.; Sun, J. L.; Chen, S. C., Adverse events of monoclonal antibodies used for cancer therapy. *BioMed research international* **2015**, *2015*, 428169.
37. Gharwan, H.; Groninger, H., Kinase inhibitors and monoclonal antibodies in oncology: clinical implications. *Nat. Rev. Clin. Oncol.* **2016**, *13* (4), 209-27.
38. Callahan, C.; Baniewicz, D.; Ely, B., CAR T-Cell Therapy: Pediatric Patients With Relapsed and Refractory Acute Lymphoblastic Leukemia. *Clin. J. Oncol. Nurs.* **2017**, *21* (2 Suppl), 22-28.
39. Bayer, V.; Amaya, B.; Baniewicz, D.; Callahan, C.; Marsh, L.; McCoy, A. S., Cancer Immunotherapy: An Evidence-Based Overview and Implications for Practice. *Clin. J. Oncol. Nurs.* **2017**, *21* (2 Suppl), 13-21.
40. Zheng, P. P.; Kros, J. M.; Li, J., Approved CAR T cell therapies: ice bucket challenges on glaring safety risks and long-term impacts. *Drug Discov Today* **2018**, *23* (6), 1175-1182.
41. Frey, N., Cytokine release syndrome: Who is at risk and how to treat. *Best Pract. Res. Clin. Haematol.* **2017**, *30* (4), 336-340.
42. Lee, D. W.; Gardner, R.; Porter, D. L.; Louis, C. U.; Ahmed, N.; Jensen, M.; Grupp, S. A.; Mackall, C. L., Current concepts in the diagnosis and management of cytokine release syndrome. *Blood* **2014**, *124* (2), 188-95.
43. Bonifant, C. L.; Jackson, H. J.; Brentjens, R. J.; Curran, K. J., Toxicity and management in CAR T-cell therapy. *Molecular therapy oncolytics* **2016**, *3*, 16011.

44. Cappelli, L. C. M. D. M. H. S.; Shah, A. A. M. D. M. H. S.; Bingham, C. O. M. D., Immune-Related Adverse Effects of Cancer Immunotherapy— Implications for Rheumatology. *Rheum. Dis. Clin. North Am.* **2016**, *43* (1), 65-78.
45. Brahmer, J. R.; Hammers, H.; Lipson, E. J., Nivolumab: targeting PD-1 to bolster antitumor immunity. *Future Oncol.* **2015**, *11* (9), 1307-26.
46. Dine, J.; Gordon, R.; Shames, Y.; Kasler, M. K.; Barton-Burke, M., Immune Checkpoint Inhibitors: An Innovation in Immunotherapy for the Treatment and Management of Patients with Cancer. *Asia Pac J Oncol Nurs* **2017**, *4* (2), 127-135.
47. Thallinger, C.; Füreder, T.; Preusser, M.; Heller, G.; Müllauer, L.; Höller, C.; Prosch, H.; Frank, N.; Swierzewski, R.; Berger, W.; Jäger, U.; Zielinski, C., Review of cancer treatment with immune checkpoint inhibitors : Current concepts, expectations, limitations and pitfalls. *Wien. Klin. Wochenschr.* **2018**, *130* (3-4), 85-91.
48. Gordon, R.; Kasler, M. K.; Stasi, K.; Shames, Y.; Errante, M.; Ciccolini, K.; Skripnik Lucas, A.; Raasch, P.; Fischer-Carlidge, E., Checkpoint Inhibitors: Common Immune-Related Adverse Events and Their Management. *Clin. J. Oncol. Nurs.* **2017**, *21* (2 Suppl), 45-52.
49. Haanen, J.; Carbonnel, F.; Robert, C.; Kerr, K. M.; Peters, S.; Larkin, J.; Jordan, K., Management of toxicities from immunotherapy: ESMO Clinical Practice Guidelines for diagnosis, treatment and follow-up. *Ann. Oncol.* **2017**, *28* (suppl_4), iv119-iv142.
50. Brahmer, J. R.; Lacchetti, C.; Thompson, J. A., Management of Immune-Related Adverse Events in Patients Treated With Immune Checkpoint Inhibitor Therapy: American Society of Clinical Oncology Clinical Practice Guideline Summary. *J. Oncol. Pract.* **2018**, *14* (4), 247-249.
51. Ventola, C. L., Cancer Immunotherapy, Part 3: Challenges and Future Trends. *P&T (Lawrenceville, N.J.)* **2017**, *42* (8), 514-521.
52. Chiriva-Internati, M.; Bot, A., A new era in cancer immunotherapy: discovering novel targets and reprogramming the immune system. *Int. Rev. Immunol.* **2015**, *34* (2), 101-3.
53. Zugazagoitia, J.; Guedes, C.; Ponce, S.; Ferrer, I.; Molina-Pinelo, S.; Paz-Ares, L., Current Challenges in Cancer Treatment. *Clin. Ther.* **2016**, *38* (7), 1551-66.
54. Adams, K. T., Cancer Immunotherapies--and Their Cost--Take Center Stage at ASCO's 2015 Annual Meeting. *Manag. Care* **2015**, *24* (7), 30-2.
55. Karlitepe, A.; Ozalp, O.; Avci, C. B., New approaches for cancer immunotherapy. *Tumour Biol.* **2015**, *36* (6), 4075-8.
56. Pucci, C.; Martinelli, C.; Ciofani, G., Innovative approaches for cancer treatment: current perspectives and new challenges. *Ecancermedalscience* **2019**, *13*, 961.
57. Martinelli, C.; Pucci, C.; Ciofani, G., Nanostructured carriers as innovative tools for cancer diagnosis and therapy. *APL bioengineering* **2019**, *3* (1), 011502.

58. Bazak, R.; Houri, M.; El Achy, S.; Kamel, S.; Refaat, T., Cancer active targeting by nanoparticles: a comprehensive review of literature. *J. Cancer Res. Clin. Oncol.* **2015**, *141* (5), 769-84.
59. Lebedeva, I. V.; Su, Z. Z.; Sarkar, D.; Fisher, P. B., Restoring apoptosis as a strategy for cancer gene therapy: focus on p53 and mda-7. *Semin. Cancer Biol.* **2003**, *13* (2), 169-78.
60. Shanker, M.; Jin, J.; Branch, C. D.; Miyamoto, S.; Grimm, E. A.; Roth, J. A.; Ramesh, R., Tumor suppressor gene-based nanotherapy: from test tube to the clinic. *Journal of drug delivery* **2011**, *2011*, 465845.
61. Vaishnav, A. K.; Gollob, J.; Gamba-Vitalo, C.; Hutabarat, R.; Sah, D.; Meyers, R.; de Fougerolles, T.; Maraganore, J., A status report on RNAi therapeutics. *Silence* **2010**, *1* (1), 14.
62. Hervault, A.; Thanh, N. T., Magnetic nanoparticle-based therapeutic agents for thermo-chemotherapy treatment of cancer. *Nanoscale* **2014**, *6* (20), 11553-73.
63. Brace, C., Thermal tumor ablation in clinical use. *IEEE pulse* **2011**, *2* (5), 28-38.
64. Aerts, H. J., The Potential of Radiomic-Based Phenotyping in Precision Medicine: A Review. *JAMA oncology* **2016**, *2* (12), 1636-1642.
65. Yu, K. H.; Zhang, C.; Berry, G. J.; Altman, R. B.; Ré, C.; Rubin, D. L.; Snyder, M., Predicting non-small cell lung cancer prognosis by fully automated microscopic pathology image features. *Nat Commun* **2016**, *7*, 12474.
66. Grove, O.; Berglund, A. E.; Schabath, M. B.; Aerts, H. J.; Dekker, A.; Wang, H.; Velazquez, E. R.; Lambin, P.; Gu, Y.; Balagurunathan, Y.; Eikman, E.; Gatenby, R. A.; Eschrich, S.; Gillies, R. J., Quantitative computed tomographic descriptors associate tumor shape complexity and intratumor heterogeneity with prognosis in lung adenocarcinoma. *PLoS One* **2015**, *10* (3), e0118261.
67. Kong, J.; Cooper, L. A.; Wang, F.; Gao, J.; Teodoro, G.; Scarpace, L.; Mikkelsen, T.; Schniederjan, M. J.; Moreno, C. S.; Saltz, J. H.; Brat, D. J., Machine-based morphologic analysis of glioblastoma using whole-slide pathology images uncovers clinically relevant molecular correlates. *PLoS One* **2013**, *8* (11), e81049.
68. Jin, M.-Z.; Jin, W.-L., The updated landscape of tumor microenvironment and drug repurposing. *Signal Transduction and Targeted Therapy* **2020**, *5* (1), 166.
69. Maman, S.; Witz, I. P., A history of exploring cancer in context. *Nat. Rev. Cancer* **2018**, *18* (6), 359-376.
70. Baghban, R.; Roshangar, L.; Jahanban-Esfahlan, R.; Seidi, K.; Ebrahimi-Kalan, A.; Jaymand, M.; Kolahian, S.; Javaheri, T.; Zare, P., Tumor microenvironment complexity and therapeutic implications at a glance. *Cell Communication and Signaling* **2020**, *18* (1), 59.
71. Jahanban-Esfahlan, R.; Seidi, K.; Zarghami, N., Tumor vascular infarction: prospects and challenges. *Int. J. Hematol.* **2017**, *105* (3), 244-256.

72. Mbeunkui, F.; Johann, D. J., Jr., Cancer and the tumor microenvironment: a review of an essential relationship. *Cancer Chemother. Pharmacol.* **2009**, *63* (4), 571-82.
73. Korneev, K. V.; Atretkhany, K. N.; Drutskaya, M. S.; Grivennikov, S. I.; Kuprash, D. V.; Nedospasov, S. A., TLR-signaling and proinflammatory cytokines as drivers of tumorigenesis. *Cytokine* **2017**, *89*, 127-135.
74. Alfarouk, K. O.; Muddathir, A. K.; Shayoub, M. E., Tumor acidity as evolutionary spite. *Cancers (Basel)* **2011**, *3* (1), 408-14.
75. Ghoshdastider, U.; Rohatgi, N.; Mojtabavi Naeini, M.; Baruah, P.; Revkov, E.; Guo, Y. A.; Rizzetto, S.; Wong, A. M. L.; Solai, S.; Nguyen, T. T.; Yeong, J. P. S.; Iqbal, J.; Tan, P. H.; Chowbay, B.; Dasgupta, R.; Skanderup, A. J., Pan-Cancer Analysis of Ligand-Receptor Cross-talk in the Tumor Microenvironment. *Cancer Res.* **2021**, *81* (7), 1802-1812.
76. Schweer, D.; McAtee, A.; Neupane, K.; Richards, C.; Ueland, F.; Kolesar, J., Tumor-Associated Macrophages and Ovarian Cancer: Implications for Therapy. *Cancers (Basel)* **2022**, *14* (9), 2220.
77. Hourani, T.; Holden, J. A.; Li, W.; Lenzo, J. C.; Hadjigol, S.; O'Brien-Simpson, N. M., Tumor Associated Macrophages: Origin, Recruitment, Phenotypic Diversity, and Targeting. *Front. Oncol.* **2021**, *11*, 788365.
78. Mills, C. D., Anatomy of a discovery: m1 and m2 macrophages. *Front. Immunol.* **2015**, *6*, 212.
79. Mosser, D. M.; Edwards, J. P., Exploring the full spectrum of macrophage activation. *Nat. Rev. Immunol.* **2008**, *8* (12), 958-69.
80. Boutilier, A. J.; ElSawa, S. F., Macrophage Polarization States in the Tumor Microenvironment. *International journal of molecular sciences* **2021**, *22* (13), 6995.
81. Hadrup, S.; Donia, M.; Thor Straten, P., Effector CD4 and CD8 T cells and their role in the tumor microenvironment. *Cancer Microenviron.* **2013**, *6* (2), 123-33.
82. Susek, K. H.; Karvouni, M.; Alici, E.; Lundqvist, A., The Role of CXC Chemokine Receptors 1-4 on Immune Cells in the Tumor Microenvironment. *Front. Immunol.* **2018**, *9*, 2159.
83. Fan, Z.; Yu, P.; Wang, Y.; Wang, Y.; Fu, M. L.; Liu, W.; Sun, Y.; Fu, Y. X., NK-cell activation by LIGHT triggers tumor-specific CD8+ T-cell immunity to reject established tumors. *Blood* **2006**, *107* (4), 1342-51.
84. MacMicking, J.; Xie, Q. W.; Nathan, C., Nitric oxide and macrophage function. *Annu. Rev. Immunol.* **1997**, *15*, 323-50.
85. Zhang, M.; He, Y.; Sun, X.; Li, Q.; Wang, W.; Zhao, A.; Di, W., A high M1/M2 ratio of tumor-associated macrophages is associated with extended survival in ovarian cancer patients. *Journal of ovarian research* **2014**, *7*, 19.
86. Lopez-Gonzalez, J. S.; Avila-Moreno, F.; Prado-Garcia, H.; Aguilar-Cazares, D.; Mandoki, J. J.; Meneses-Flores, M., Lung carcinomas decrease the number of

- monocytes/macrophages (CD14+ cells) that produce TNF-alpha. *Clin. Immunol.* **2007**, *122* (3), 323-9.
87. Ma, J.; Liu, L.; Che, G.; Yu, N.; Dai, F.; You, Z., The M1 form of tumor-associated macrophages in non-small cell lung cancer is positively associated with survival time. *BMC Cancer* **2010**, *10*, 112.
 88. Jackute, J.; Zemaitis, M.; Pranys, D.; Sitkauskiene, B.; Miliauskas, S.; Vaitkiene, S.; Sakalauskas, R., Distribution of M1 and M2 macrophages in tumor islets and stroma in relation to prognosis of non-small cell lung cancer. *BMC Immunol.* **2018**, *19* (1), 3.
 89. Alves, A. M.; Diel, L. F.; Lamers, M. L., Macrophages and prognosis of oral squamous cell carcinoma: A systematic review. *J. Oral Pathol. Med.* **2018**, *47* (5), 460-467.
 90. Edin, S.; Wikberg, M. L.; Oldenborg, P. A.; Palmqvist, R., Macrophages: Good guys in colorectal cancer. *Oncoimmunology* **2013**, *2* (2), e23038.
 91. Guo, L.; Cheng, X.; Chen, H.; Chen, C.; Xie, S.; Zhao, M.; Liu, D.; Deng, Q.; Liu, Y.; Wang, X.; Chen, X.; Wang, J.; Yin, Z.; Qi, S.; Gao, J.; Ma, Y.; Guo, N.; Shi, M., Induction of breast cancer stem cells by M1 macrophages through Lin-28B-let-7-HMGA2 axis. *Cancer Lett* **2019**, *452*, 213-225.
 92. Lan, C.; Huang, X.; Lin, S.; Huang, H.; Cai, Q.; Wan, T.; Lu, J.; Liu, J., Expression of M2-polarized macrophages is associated with poor prognosis for advanced epithelial ovarian cancer. *Technol. Cancer Res. Treat.* **2013**, *12* (3), 259-67.
 93. Chen, Y.; Song, Y.; Du, W.; Gong, L.; Chang, H.; Zou, Z., Tumor-associated macrophages: an accomplice in solid tumor progression. *J. Biomed. Sci.* **2019**, *26* (1), 78.
 94. Komohara, Y.; Fujiwara, Y.; Ohnishi, K.; Takeya, M., Tumor-associated macrophages: Potential therapeutic targets for anti-cancer therapy. *Adv Drug Deliv Rev* **2016**, *99* (Pt B), 180-185.
 95. Parker, K. H.; Sinha, P.; Horn, L. A.; Clements, V. K.; Yang, H.; Li, J.; Tracey, K. J.; Ostrand-Rosenberg, S., HMGB1 enhances immune suppression by facilitating the differentiation and suppressive activity of myeloid-derived suppressor cells. *Cancer Res.* **2014**, *74* (20), 5723-33.
 96. Anderson, K. M.; Czinn, S. J.; Redline, R. W.; Blanchard, T. G., Induction of CTLA-4-mediated anergy contributes to persistent colonization in the murine model of gastric *Helicobacter pylori* infection. *J. Immunol.* **2006**, *176* (9), 5306-13.
 97. Matsunaga, T.; Saito, H.; Ikeguchi, M., Increased B7-H1 and B7-H4 Expressions on Circulating Monocytes and Tumor-Associated Macrophages are Involved in Immune Evasion in Patients with Gastric Cancer. *Yonago Acta Med.* **2011**, *54* (1), 1-10.

98. Bloch, O.; Crane, C. A.; Kaur, R.; Safaee, M.; Rutkowski, M. J.; Parsa, A. T., Gliomas promote immunosuppression through induction of B7-H1 expression in tumor-associated macrophages. *Clin. Cancer Res.* **2013**, *19* (12), 3165-75.
99. Jeong, H.; Kim, S.; Hong, B. J.; Lee, C. J.; Kim, Y. E.; Bok, S.; Oh, J. M.; Gwak, S. H.; Yoo, M. Y.; Lee, M. S.; Chung, S. J.; Defrêne, J.; Tessier, P.; Pelletier, M.; Jeon, H.; Roh, T. Y.; Kim, B.; Kim, K. H.; Ju, J. H.; Kim, S.; Lee, Y. J.; Kim, D. W.; Kim, I. H.; Kim, H. J.; Park, J. W.; Lee, Y. S.; Lee, J. S.; Cheon, G. J.; Weissman, I. L.; Chung, D. H.; Jeon, Y. K.; Ahn, G. O., Tumor-Associated Macrophages Enhance Tumor Hypoxia and Aerobic Glycolysis. *Cancer Res.* **2019**, *79* (4), 795-806.
100. Obermajer, N.; Muthuswamy, R.; Odunsi, K.; Edwards, R. P.; Kalinski, P., PGE(2)-induced CXCL12 production and CXCR4 expression controls the accumulation of human MDSCs in ovarian cancer environment. *Cancer Res.* **2011**, *71* (24), 7463-70.
101. Allavena, P.; Mantovani, A., Immunology in the clinic review series; focus on cancer: tumour-associated macrophages: undisputed stars of the inflammatory tumour microenvironment. *Clin. Exp. Immunol.* **2012**, *167* (2), 195-205.
102. Riabov, V.; Gudima, A.; Wang, N.; Mickley, A.; Orekhov, A.; Kzhyshkowska, J., Role of tumor associated macrophages in tumor angiogenesis and lymphangiogenesis. *Front. Physiol.* **2014**, *5*, 75.
103. Yin, M.; Shen, J.; Yu, S.; Fei, J.; Zhu, X.; Zhao, J.; Zhai, L.; Sadhukhan, A.; Zhou, J., Tumor-Associated Macrophages (TAMs): A Critical Activator In Ovarian Cancer Metastasis. *Onco Targets Ther.* **2019**, *12*, 8687-8699.
104. Nowak, M.; Klink, M., The Role of Tumor-Associated Macrophages in the Progression and Chemoresistance of Ovarian Cancer. *Cells* **2020**, *9* (5).
105. Hagemann, T.; Wilson, J.; Kulbe, H.; Li, N. F.; Leinster, D. A.; Charles, K.; Klemm, F.; Pukrop, T.; Binder, C.; Balkwill, F. R., Macrophages induce invasiveness of epithelial cancer cells via NF-kappa B and JNK. *J. Immunol.* **2005**, *175* (2), 1197-205.
106. Kulbe, H.; Thompson, R.; Wilson, J. L.; Robinson, S.; Hagemann, T.; Fatah, R.; Gould, D.; Ayhan, A.; Balkwill, F., The inflammatory cytokine tumor necrosis factor-alpha generates an autocrine tumor-promoting network in epithelial ovarian cancer cells. *Cancer Res.* **2007**, *67* (2), 585-92.
107. Boutilier, A. J.; Elsawa, S. F., Macrophage Polarization States in the Tumor Microenvironment. *Int. J. Mol. Sci.* **2021**, *22* (13).
108. Fabregat, I.; Fernando, J.; Mainez, J.; Sancho, P., TGF-beta signaling in cancer treatment. *Curr. Pharm. Des.* **2014**, *20* (17), 2934-47.
109. Leblond, M. M.; Pérès, E. A.; Helaine, C.; Gérault, A. N.; Moulin, D.; Anfray, C.; Divoux, D.; Petit, E.; Bernaudin, M.; Valable, S., M2 macrophages are more resistant than M1 macrophages following radiation therapy in the context of glioblastoma. *Oncotarget* **2017**, *8* (42), 72597-72612.

110. Castro, B. A.; Flanigan, P.; Jahangiri, A.; Hoffman, D.; Chen, W.; Kuang, R.; De Lay, M.; Yagnik, G.; Wagner, J. R.; Mascharak, S.; Sidorov, M.; Shrivastav, S.; Kohanbash, G.; Okada, H.; Aghi, M. K., Macrophage migration inhibitory factor downregulation: a novel mechanism of resistance to anti-angiogenic therapy. *Oncogene* **2017**, *36* (26), 3749-3759.
111. Dijkgraaf, E. M.; Heusinkveld, M.; Tummers, B.; Vogelpoel, L. T.; Goedemans, R.; Jha, V.; Nortier, J. W.; Welters, M. J.; Kroep, J. R.; van der Burg, S. H., Chemotherapy alters monocyte differentiation to favor generation of cancer-supporting M2 macrophages in the tumor microenvironment. *Cancer Res.* **2013**, *73* (8), 2480-92.
112. Ruffell, B.; Coussens, L. M., Macrophages and therapeutic resistance in cancer. *Cancer Cell* **2015**, *27* (4), 462-72.
113. DeNardo, D. G.; Brennan, D. J.; Rexhepaj, E.; Ruffell, B.; Shiao, S. L.; Madden, S. F.; Gallagher, W. M.; Wadhvani, N.; Keil, S. D.; Junaid, S. A.; Rugo, H. S.; Hwang, E. S.; Jirström, K.; West, B. L.; Coussens, L. M., Leukocyte complexity predicts breast cancer survival and functionally regulates response to chemotherapy. *Cancer Discov.* **2011**, *1* (1), 54-67.
114. Klug, F.; Prakash, H.; Huber, P. E.; Seibel, T.; Bender, N.; Halama, N.; Pfirschke, C.; Voss, R. H.; Timke, C.; Umansky, L.; Klapproth, K.; Schäkel, K.; Garbi, N.; Jäger, D.; Weitz, J.; Schmitz-Winnenthal, H.; Hämmerling, G. J.; Beckhove, P., Low-dose irradiation programs macrophage differentiation to an iNOS⁺/M1 phenotype that orchestrates effective T cell immunotherapy. *Cancer Cell* **2013**, *24* (5), 589-602.
115. Argyle, D.; Kitamura, T., Targeting Macrophage-Recruiting Chemokines as a Novel Therapeutic Strategy to Prevent the Progression of Solid Tumors. *Front. Immunol.* **2018**, *9*, 2629.
116. Canè, S.; Ugel, S.; Trovato, R.; Marigo, I.; De Sanctis, F.; Sartoris, S.; Bronte, V., The Endless Saga of Monocyte Diversity. *Front. Immunol.* **2019**, *10*, 1786.
117. Brana, I.; Calles, A.; LoRusso, P. M.; Yee, L. K.; Puchalski, T. A.; Seetharam, S.; Zhong, B.; de Boer, C. J.; Tabernero, J.; Calvo, E., Carlumab, an anti-C-C chemokine ligand 2 monoclonal antibody, in combination with four chemotherapy regimens for the treatment of patients with solid tumors: an open-label, multicenter phase 1b study. *Target. Oncol.* **2015**, *10* (1), 111-23.
118. Boimel, P. J.; Smirnova, T.; Zhou, Z. N.; Wyckoff, J.; Park, H.; Coniglio, S. J.; Qian, B. Z.; Stanley, E. R.; Cox, D.; Pollard, J. W.; Muller, W. J.; Condeelis, J.; Segall, J. E., Contribution of CXCL12 secretion to invasion of breast cancer cells. *Breast Cancer Res.* **2012**, *14* (1), R23.
119. Ries, C. H.; Cannarile, M. A.; Hoves, S.; Benz, J.; Wartha, K.; Runza, V.; Rey-Giraud, F.; Pradel, L. P.; Feuerhake, F.; Klaman, I.; Jones, T.; Jucknischke, U.; Scheiblich, S.; Kaluza, K.; Gorr, I. H.; Walz, A.; Abiraj, K.; Cassier, P. A.; Sica, A.; Gomez-Roca, C.; de Visser, K. E.; Italiano, A.; Le Tourneau, C.; Delord, J. P.; Levitsky, H.; Blay, J. Y.; Rüttinger, D., Targeting tumor-associated

- macrophages with anti-CSF-1R antibody reveals a strategy for cancer therapy. *Cancer Cell* **2014**, *25* (6), 846-59.
120. Zheng, X.; Turkowski, K.; Mora, J.; Brüne, B.; Seeger, W.; Weigert, A.; Savai, R., Redirecting tumor-associated macrophages to become tumoricidal effectors as a novel strategy for cancer therapy. *Oncotarget* **2017**, *8* (29), 48436-48452.
 121. Yousefzadeh, Y.; Hallaj, S.; Baghi Moornani, M.; Asghary, A.; Azizi, G.; Hojjat-Farsangi, M.; Ghalamfarsa, G.; Jadidi-Niaragh, F., Tumor associated macrophages in the molecular pathogenesis of ovarian cancer. *Int. Immunopharmacol.* **2020**, *84*, 106471.
 122. Zhang, F.; Parayath, N. N.; Ene, C. I.; Stephan, S. B.; Koehne, A. L.; Coon, M. E.; Holland, E. C.; Stephan, M. T., Genetic programming of macrophages to perform anti-tumor functions using targeted mRNA nanocarriers. *Nature communications* **2019**, *10* (1), 3974-16.
 123. Liu, M.; O'Connor, R. S.; Trefely, S.; Graham, K.; Snyder, N. W.; Beatty, G. L., Metabolic rewiring of macrophages by CpG potentiates clearance of cancer cells and overcomes tumor-expressed CD47-mediated 'don't eat me signal'. *Nature immunology* **2019**, *20* (3), 265-275.
 124. Sercombe, L.; Veerati, T.; Moheimani, F.; Wu, S. Y.; Sood, A. K.; Hua, S., Advances and Challenges of Liposome Assisted Drug Delivery. *Front. Pharmacol.* **2015**, *6*, 286.
 125. Cheng, L.; Wang, Y.; Huang, L., Exosomes from M1-Polarized Macrophages Potentiate the Cancer Vaccine by Creating a Pro-inflammatory Microenvironment in the Lymph Node. *Molecular Therapy* **2017**, *25* (7), 1665-1675.
 126. Jang, S. C.; Kim, O. Y.; Yoon, C. M.; Choi, D. S.; Roh, T. Y.; Park, J.; Nilsson, J.; Lötvall, J.; Kim, Y. K.; Gho, Y. S., Bioinspired exosome-mimetic nanovesicles for targeted delivery of chemotherapeutics to malignant tumors. *ACS Nano* **2013**, *7* (9), 7698-710.
 127. Neupane, K. R.; McCorkle, J. R.; Kopper, T. J.; Lakes, J. E.; Aryal, S. P.; Abdullah, M.; Snell, A. A.; Gensel, J. C.; Kolesar, J.; Richards, C. I., Macrophage-Engineered Vesicles for Therapeutic Delivery and Bidirectional Reprogramming of Immune Cell Polarization. *ACS omega* **2021**, *6* (5), 3847-3857.
 128. Goh, W. J.; Zou, S.; Ong, W. Y.; Torta, F.; Alexandra, A. F.; Schiffelers, R. M.; Storm, G.; Wang, J.-W.; Czarny, B.; Pastorin, G., Bioinspired Cell-Derived Nanovesicles versus Exosomes as Drug Delivery Systems: a Cost-Effective Alternative. *Scientific reports* **2017**, *7* (1), 14322-14322.
 129. Brown, S. D.; Nativo, P.; Smith, J.-A.; Stirling, D.; Edwards, P. R.; Venugopal, B.; Flint, D. J.; Plumb, J. A.; Graham, D.; Wheate, N. J., Gold nanoparticles for the improved anticancer drug delivery of the active component of oxaliplatin. *Journal of the American Chemical Society* **2010**, *132* (13), 4678-4684.
 130. Sajid, M. I.; Jamshaid, U.; Jamshaid, T.; Zafar, N.; Fessi, H.; Elaissari, A., Carbon nanotubes from synthesis to in vivo biomedical applications. *International Journal of Pharmaceutics* **2016**, *501* (1-2), 278-299.

131. Estanqueiro, M.; Amaral, M. H.; Conceicao, J.; Sousa Lobo, J. M., Nanotechnological carriers for cancer chemotherapy: the state of the art. *Colloids Surf B Biointerfaces* **2015**, *126*, 631-48.
132. El-Say, K.; El-Sawy, H., Polymeric nanoparticles: Promising platform for drug delivery. *Int. J. Pharm.* **2017**, *528* (1-2), 675-691.
133. Garg, T.; Singh, O.; Arora, S.; Murthy, R., Dendrimer—A novel scaffold for drug delivery. *International Journal of Pharmaceutical Sciences Review and Research* **2011**, *7* (2), 211-220.
134. Akbarzadeh, A.; Rezaei-Sadabady, R.; Davaran, S.; Joo, S. W.; Zarghami, N.; Hanifehpour, Y.; Samiei, M.; Kouhi, M.; Nejati-Koshki, K., Liposome: classification, preparation, and applications. *Nanoscale Res Lett* **2013**, *8* (1), 102.
135. Akbarzadeh, A.; Rezaei-Sadabady, R.; Davaran, S.; Joo, S.; Zarghami, N.; Hanifehpour, Y.; Samiei, M.; Kouhi, M.; Nejati-Koshki, K., Liposome: classification, preparation, and applications. *Nanoscale Research Letters* **2013**, *8* (1), 1-9.
136. Li, M.; Du, C.; Guo, N.; Teng, Y.; Meng, X.; Sun, H.; Li, S.; Yu, P.; Galons, H., Composition design and medical application of liposomes. *European Journal of Medicinal Chemistry* **2019**, *164*, 640-653.
137. Hofheinz, R. D.; Gnad-Vogt, S. U.; Beyer, U.; Hochhaus, A., Liposomal encapsulated anti-cancer drugs. *Anticancer Drugs* **2005**, *16* (7), 691-707.
138. Krauss, A. C.; Gao, X.; Li, L.; Manning, M. L.; Patel, P.; Fu, W.; Janoria, K. G.; Gieser, G.; Bateman, D. A.; Przepioraka, D.; Shen, Y. L.; Shord, S. S.; Sheth, C. M.; Banerjee, A.; Liu, J.; Goldberg, K. B.; Farrell, A. T.; Blumenthal, G. M.; Pazdur, R., FDA Approval Summary: (Daunorubicin and Cytarabine) Liposome for Injection for the Treatment of Adults with High-Risk Acute Myeloid Leukemia. *Clinical Cancer Research* **2018**, clincanres.2990.2018.
139. Sercombe, L.; Veerati, T.; Moheimani, F.; Wu, S. Y.; Sood, A. K.; Hua, S., Advances and Challenges of Liposome Assisted Drug Delivery. *Frontiers in pharmacology* **2015**, *6*, 286-286.
140. Raposo, G.; Stoorvogel, W., Extracellular vesicles: exosomes, microvesicles, and friends. *The Journal of cell biology* **2013**, *200* (4), 373-383.
141. Ha, D.; Yang, N.; Nadithe, V., Exosomes as therapeutic drug carriers and delivery vehicles across biological membranes: current perspectives and future challenges. *Acta Pharmaceutica Sinica B* **2016**, *6* (4), 287-296.
142. Hon, K. W.; Abu, N.; Ab Mutalib, N.-S.; Jamal, R., Exosomes As Potential Biomarkers and Targeted Therapy in Colorectal Cancer: A Mini-Review. *Frontiers in pharmacology* **2017**, *8*, 583-583.
143. Song-Pei, L.; Zhong-Xiao, L.; Xue-Yan, J.; Xi-Yong, Y., Exosomal cargo-loading and synthetic exosome-mimics as potential therapeutic tools. *Acta Pharmacologica Sinica* **2018**, *39* (4).

144. Jang, S. C.; Kim, O. Y.; Yoon, C. M.; Choi, D.-S.; Roh, T.-Y.; Park, J.; Nilsson, J.; Lötvall, J.; Kim, Y.-K.; Gho, Y. S., Bioinspired exosome-mimetic nanovesicles for targeted delivery of chemotherapeutics to malignant tumors. *ACS nano* **2013**, *11* (4), 7698.
145. Zhang, W.; Huang, Q.; Xiao, W.; Zhao, Y.; Pi, J.; Xu, H.; Zhao, H.; Xu, J.; Evans, C. E.; Jin, H., Advances in Anti-Tumor Treatments Targeting the CD47/SIRP α Axis. *Front. Immunol.* **2020**, *11*, 18.
146. Xu, C.; Ju, D.; Zhang, X., Cell Membrane-Derived Vesicle: A Novel Vehicle for Cancer Immunotherapy. *Front. Immunol.* **2022**, *13*, 923598.
147. Zhu, J. Y.; Zheng, D. W.; Zhang, M. K.; Yu, W. Y.; Qiu, W. X.; Hu, J. J.; Feng, J.; Zhang, X. Z., Preferential Cancer Cell Self-Recognition and Tumor Self-Targeting by Coating Nanoparticles with Homotypic Cancer Cell Membranes. *Nano Lett.* **2016**, *16* (9), 5895-901.
148. Song, J.; Jung, H.; You, G.; Mok, H., Cancer-Cell-Derived Hybrid Vesicles from MCF-7 and HeLa Cells for Dual-Homotypic Targeting of Anticancer Drugs. *Macromol. Biosci.* **2021**, *21* (7), e2100067.
149. Liu, B.; Yang, Y.; Chao, Y.; Xiao, Z.; Xu, J.; Wang, C.; Dong, Z.; Hou, L.; Li, Q.; Liu, Z., Equipping Cancer Cell Membrane Vesicles with Functional DNA as a Targeted Vaccine for Cancer Immunotherapy. *Nano Lett.* **2021**, *21* (22), 9410-9418.
150. Fang, R. H.; Hu, C. M.; Luk, B. T.; Gao, W.; Copp, J. A.; Tai, Y.; O'Connor, D. E.; Zhang, L., Cancer cell membrane-coated nanoparticles for anticancer vaccination and drug delivery. *Nano Lett.* **2014**, *14* (4), 2181-8.
151. Ochyl, L. J.; Bazzill, J. D.; Park, C.; Xu, Y.; Kuai, R.; Moon, J. J., PEGylated tumor cell membrane vesicles as a new vaccine platform for cancer immunotherapy. *Biomaterials* **2018**, *182*, 157-166.
152. Cervantes-Villagrana, R. D.; Albores-García, D.; Cervantes-Villagrana, A. R.; García-Acevez, S. J., Tumor-induced neurogenesis and immune evasion as targets of innovative anti-cancer therapies. *Signal Transduct Target Ther* **2020**, *5* (1), 99.
153. Sun, J.; Lu, Q.; Sanmamed, M. F.; Wang, J., Siglec-15 as an Emerging Target for Next-generation Cancer Immunotherapy. *Clin. Cancer Res.* **2021**, *27* (3), 680-688.
154. Yang, R.; Sun, L.; Li, C. F.; Wang, Y. H.; Yao, J.; Li, H.; Yan, M.; Chang, W. C.; Hsu, J. M.; Cha, J. H.; Hsu, J. L.; Chou, C. W.; Sun, X.; Deng, Y.; Chou, C. K.; Yu, D.; Hung, M. C., Galectin-9 interacts with PD-1 and TIM-3 to regulate T cell death and is a target for cancer immunotherapy. *Nat Commun* **2021**, *12* (1), 832.
155. Schäfer, C.; Ascui, G.; Ribeiro, C. H.; López, M.; Prados-Rosales, R.; González, P. A.; Bueno, S. M.; Riedel, C. A.; Baena, A.; Kalergis, A. M.; Carreño, L. J., Innate immune cells for immunotherapy of autoimmune and cancer disorders. *Int. Rev. Immunol.* **2017**, *36* (6), 315-337.

156. Wang, H.; Mooney, D. J., Biomaterial-assisted targeted modulation of immune cells in cancer treatment. *Nature materials* **2018**, *17* (9), 761-772.
157. Lee, D. A., Cellular therapy: Adoptive immunotherapy with expanded natural killer cells. *Immunol. Rev.* **2019**, *290* (1), 85-99.
158. Wilgenhof, S.; Corthals, J.; Heirman, C.; van Baren, N.; Lucas, S.; Kvistborg, P.; Thielemans, K.; Neyns, B., Phase II Study of Autologous Monocyte-Derived mRNA Electroporated Dendritic Cells (TriMixDC-MEL) Plus Ipilimumab in Patients With Pretreated Advanced Melanoma. *J. Clin. Oncol.* **2016**, *34* (12), 1330-8.
159. Xu, R.; Rai, A.; Chen, M.; Suwakulsiri, W.; Greening, D. W.; Simpson, R. J., Extracellular vesicles in cancer - implications for future improvements in cancer care. *Nat. Rev. Clin. Oncol.* **2018**, *15* (10), 617-638.
160. Katsuda, T.; Kosaka, N.; Ochiya, T., The roles of extracellular vesicles in cancer biology: toward the development of novel cancer biomarkers. *Proteomics* **2014**, *14* (4-5), 412-25.
161. Tominaga, N.; Yoshioka, Y.; Ochiya, T., A novel platform for cancer therapy using extracellular vesicles. *Adv Drug Deliv Rev* **2015**, *95*, 50-5.
162. Lai, P.; Weng, J.; Guo, L.; Chen, X.; Du, X., Novel insights into MSC-EVs therapy for immune diseases. *Biomarker Research* **2019**, *7* (1), 6.
163. Del Fattore, A.; Luciano, R.; Pascucci, L.; Goffredo, B. M.; Giorda, E.; Scapaticci, M.; Fierabracci, A.; Muraca, M., Immunoregulatory Effects of Mesenchymal Stem Cell-Derived Extracellular Vesicles on T Lymphocytes. *Cell Transplant.* **2015**, *24* (12), 2615-27.
164. Lee, J. K.; Park, S. R.; Jung, B. K.; Jeon, Y. K.; Lee, Y. S.; Kim, M. K.; Kim, Y. G.; Jang, J. Y.; Kim, C. W., Exosomes derived from mesenchymal stem cells suppress angiogenesis by down-regulating VEGF expression in breast cancer cells. *PLoS One* **2013**, *8* (12), e84256.
165. Du, T.; Ju, G.; Wu, S.; Cheng, Z.; Cheng, J.; Zou, X.; Zhang, G.; Miao, S.; Liu, G.; Zhu, Y., Microvesicles derived from human Wharton's jelly mesenchymal stem cells promote human renal cancer cell growth and aggressiveness through induction of hepatocyte growth factor. *PLoS One* **2014**, *9* (5), e96836.
166. Bruno, S.; Collino, F.; Iavello, A.; Camussi, G., Effects of mesenchymal stromal cell-derived extracellular vesicles on tumor growth. *Front. Immunol.* **2014**, *5*, 382.
167. Xu, J.; Wang, C., Cell-derived vesicles for delivery of cancer immunotherapy. *Exploration of Medicine* **2021**, *2* (1), 39-59.
168. Tung, S. L.; Boardman, D. A.; Sen, M.; Letizia, M.; Peng, Q.; Cianci, N.; Dioni, L.; Carlin, L. M.; Lechler, R.; Bollati, V.; Lombardi, G.; Smyth, L. A., Regulatory T cell-derived extracellular vesicles modify dendritic cell function. *Scientific Reports* **2018**, *8* (1), 6065.
169. Lu, J.; Wu, J.; Xie, F.; Tian, J.; Tang, X.; Guo, H.; Ma, J.; Xu, P.; Mao, L.; Xu, H.; Wang, S., CD4(+) T Cell-Released Extracellular Vesicles Potentiate the

- Efficacy of the HBsAg Vaccine by Enhancing B Cell Responses. *Advanced science (Weinheim, Baden-Wuerttemberg, Germany)* **2019**, *6* (23), 1802219.
170. Zhang, F.; Li, R.; Yang, Y.; Shi, C.; Shen, Y.; Lu, C.; Chen, Y.; Zhou, W.; Lin, A.; Yu, L.; Zhang, W.; Xue, Z.; Wang, J.; Cai, Z., Specific Decrease in B-Cell-Derived Extracellular Vesicles Enhances Post-Chemotherapeutic CD8(+) T Cell Responses. *Immunity* **2019**, *50* (3), 738-750.e7.
 171. Besse, B.; Charrier, M.; Lapiere, V.; Dansin, E.; Lantz, O.; Planchard, D.; Le Chevalier, T.; Livartoski, A.; Barlesi, F.; Laplanche, A.; Ploix, S.; Vimond, N.; Peguillet, I.; Théry, C.; Lacroix, L.; Zoernig, I.; Dhodapkar, K.; Dhodapkar, M.; Viaud, S.; Soria, J. C.; Reiners, K. S.; Pogge von Strandmann, E.; Vély, F.; Rusakiewicz, S.; Eggermont, A.; Pitt, J. M.; Zitvogel, L.; Chaput, N., Dendritic cell-derived exosomes as maintenance immunotherapy after first line chemotherapy in NSCLC. *Oncoimmunology* **2016**, *5* (4), e1071008.
 172. Kowal, J.; Arras, G.; Colombo, M.; Jouve, M.; Morath, J. P.; Primdal-Bengtson, B.; Dingli, F.; Loew, D.; Tkach, M.; Théry, C., Proteomic comparison defines novel markers to characterize heterogeneous populations of extracellular vesicle subtypes. *Proc. Natl. Acad. Sci. U. S. A.* **2016**, *113* (8), E968-77.
 173. Lindenbergh, M. F. S.; Koerhuis, D. G. J.; Borg, E. G. F.; van 't Veld, E. M.; Driedonks, T. A. P.; Wubbolts, R.; Stoorvogel, W.; Boes, M., Bystander T-Cells Support Clonal T-Cell Activation by Controlling the Release of Dendritic Cell-Derived Immune-Stimulatory Extracellular Vesicles. *Front. Immunol.* **2019**, *10*, 448.
 174. Tkach, M.; Kowal, J.; Zucchetti, A. E.; Enserink, L.; Jouve, M.; Lankar, D.; Saitakis, M.; Martin-Jaular, L.; Théry, C., Qualitative differences in T-cell activation by dendritic cell-derived extracellular vesicle subtypes. *EMBO J.* **2017**, *36* (20), 3012-3028.
 175. Larssen, P.; Veerman, R. E.; Akpınar, G. G.; Hiltbrunner, S.; Karlsson, M. C. I.; Gabriellsson, S., Allogenicity Boosts Extracellular Vesicle-Induced Antigen-Specific Immunity and Mediates Tumor Protection and Long-Term Memory In Vivo. *J. Immunol.* **2019**, *203* (4), 825-834.
 176. Cheng, L.; Wang, Y.; Huang, L., Exosomes from M1-Polarized Macrophages Potentiate the Cancer Vaccine by Creating a Pro-inflammatory Microenvironment in the Lymph Node. *Mol. Ther.* **2017**, *25* (7), 1665-1675.
 177. Li, Z.; Suo, B.; Long, G.; Gao, Y.; Song, J.; Zhang, M.; Feng, B.; Shang, C.; Wang, D., Exosomal miRNA-16-5p Derived From M1 Macrophages Enhances T Cell-Dependent Immune Response by Regulating PD-L1 in Gastric Cancer. *Front Cell Dev Biol* **2020**, *8*, 572689.
 178. Żmigrodzka, M.; Witkowska-Piłaszewicz, O.; Winnicka, A., Platelets Extracellular Vesicles as Regulators of Cancer Progression-An Updated Perspective. *Int. J. Mol. Sci.* **2020**, *21* (15).

179. Antich-Rosselló, M.; Forteza-Genestra, M. A.; Monjo, M.; Ramis, J. M., Platelet-Derived Extracellular Vesicles for Regenerative Medicine. *Int. J. Mol. Sci.* **2021**, *22* (16).
180. Wang, C.; Sun, W.; Ye, Y.; Hu, Q.; Bomba, H. N.; Gu, Z., In situ activation of platelets with checkpoint inhibitors for post-surgical cancer immunotherapy. *Nature Biomedical Engineering* **2017**, *1* (2), 0011.
181. Wen, Y.; Fu, Q.; Soliwoda, A.; Zhang, S.; Zheng, M.; Mao, W.; Wan, Y., Cell-derived nanovesicles prepared by membrane extrusion are good substitutes for natural extracellular vesicles. *Extracellular Vesicle* **2022**, *1*, 100004.
182. Lin, Y.-Y.; Chen, C.-Y.; Ma, D.-L.; Leung, C.-H.; Chang, C.-Y.; Wang, H.-M. D., Cell-derived artificial nanovesicle as a drug delivery system for malignant melanoma treatment. *Biomed. Pharmacother.* **2022**, *147*, 112586.
183. Gao, J.; Wang, S.; Wang, Z., High yield, scalable and remotely drug-loaded neutrophil-derived extracellular vesicles (EVs) for anti-inflammation therapy. *Biomaterials* **2017**, *135*, 62-73.
184. Glinsky, G. V.; Kronen-Herzig, A.; Glinskii, A. B.; Gebauer, G., Microarray analysis of xenograft-derived cancer cell lines representing multiple experimental models of human prostate cancer. *Mol. Carcinog.* **2003**, *37* (4), 209-21.
185. Kroll, A. V.; Fang, R. H.; Jiang, Y.; Zhou, J.; Wei, X.; Yu, C. L.; Gao, J.; Luk, B. T.; Dehaini, D.; Gao, W.; Zhang, L., Nanoparticulate Delivery of Cancer Cell Membrane Elicits Multiantigenic Antitumor Immunity. *Adv. Mater.* **2017**, *29* (47).
186. Vader, P.; Breakefield, X. O.; Wood, M. J., Extracellular vesicles: emerging targets for cancer therapy. *Trends Mol Med* **2014**, *20* (7), 385-93.
187. Chowdhury, R.; Webber, J. P.; Gurney, M.; Mason, M. D.; Tabi, Z.; Clayton, A., Cancer exosomes trigger mesenchymal stem cell differentiation into pro-angiogenic and pro-invasive myofibroblasts. *Oncotarget* **2015**, *6* (2), 715-31.
188. Sanchez, C. A.; Andahur, E. I.; Valenzuela, R.; Castellon, E. A.; Fulla, J. A.; Ramos, C. G.; Trivino, J. C., Exosomes from bulk and stem cells from human prostate cancer have a differential microRNA content that contributes cooperatively over local and pre-metastatic niche. *Oncotarget* **2016**, *7* (4), 3993-4008.
189. Gao, J.; Chu, D.; Wang, Z., Cell membrane-formed nanovesicles for disease-targeted delivery. *J. Control. Release* **2016**, *224*, 208-216.
190. Cao, X.; Hu, Y.; Luo, S.; Wang, Y.; Gong, T.; Sun, X.; Fu, Y.; Zhang, Z., Neutrophil-mimicking therapeutic nanoparticles for targeted chemotherapy of pancreatic carcinoma. *Acta pharmaceutica Sinica. B* **2019**, *9* (3), 575-589.
191. Kang, M.; Hong, J.; Jung, M.; Kwon, S. P.; Song, S. Y.; Kim, H. Y.; Lee, J. R.; Kang, S.; Han, J.; Koo, J. H.; Ryu, J. H.; Lim, S.; Sohn, H. S.; Choi, J. M.; Doh, J.; Kim, B. S., T-Cell-Mimicking Nanoparticles for Cancer Immunotherapy. *Adv. Mater.* **2020**, *32* (39), e2003368.

192. Ma, W.; Zhu, D.; Li, J.; Chen, X.; Xie, W.; Jiang, X.; Wu, L.; Wang, G.; Xiao, Y.; Liu, Z.; Wang, F.; Li, A.; Shao, D.; Dong, W.; Liu, W.; Yuan, Y., Coating biomimetic nanoparticles with chimeric antigen receptor T cell-membrane provides high specificity for hepatocellular carcinoma photothermal therapy treatment. *Theranostics* **2020**, *10* (3), 1281-1295.
193. Li, Y.-J.; Wu, J.-Y.; Liu, J.; Xu, W.; Qiu, X.; Huang, S.; Hu, X.-B.; Xiang, D.-X., Artificial exosomes for translational nanomedicine. *Journal of Nanobiotechnology* **2021**, *19* (1), 242.
194. Patty, P. J.; Frisken, B. J., The pressure-dependence of the size of extruded vesicles. *Biophys. J.* **2003**, *85* (2), 996-1004.
195. Olson, F.; Hunt, C. A.; Szoka, F. C.; Vail, W. J.; Papahadjopoulos, D., Preparation of liposomes of defined size distribution by extrusion through polycarbonate membranes. *Biochim. Biophys. Acta* **1979**, *557* (1), 9-23.
196. Jeong, D.; Jo, W.; Yoon, J.; Kim, J.; Gianchandani, S.; Gho, Y. S.; Park, J., Nanovesicles engineered from ES cells for enhanced cell proliferation. *Biomaterials* **2014**, *35* (34), 9302-10.
197. Lunavat, T. R.; Jang, S. C.; Nilsson, L.; Park, H. T.; Repiska, G.; Lässer, C.; Nilsson, J. A.; Gho, Y. S.; Lötvall, J., RNAi delivery by exosome-mimetic nanovesicles - Implications for targeting c-Myc in cancer. *Biomaterials* **2016**, *102*, 231-8.
198. Kalimuthu, S.; Gangadaran, P.; Rajendran, R. L.; Zhu, L.; Oh, J. M.; Lee, H. W.; Gopal, A.; Baek, S. H.; Jeong, S. Y.; Lee, S. W.; Lee, J.; Ahn, B. C., A New Approach for Loading Anticancer Drugs Into Mesenchymal Stem Cell-Derived Exosome Mimetics for Cancer Therapy. *Front. Pharmacol.* **2018**, *9*, 1116.
199. Yang, Z.; Xie, J.; Zhu, J.; Kang, C.; Chiang, C.; Wang, X.; Wang, X.; Kuang, T.; Chen, F.; Chen, Z.; Zhang, A.; Yu, B.; Lee, R. J.; Teng, L.; Lee, L. J., Functional exosome-mimic for delivery of siRNA to cancer: in vitro and in vivo evaluation. *J. Control. Release* **2016**, *243*, 160-171.
200. Tao, S. C.; Rui, B. Y.; Wang, Q. Y.; Zhou, D.; Zhang, Y.; Guo, S. C., Extracellular vesicle-mimetic nanovesicles transport LncRNA-H19 as competing endogenous RNA for the treatment of diabetic wounds. *Drug delivery* **2018**, *25* (1), 241-255.
201. Choo, Y. W.; Kang, M.; Kim, H. Y.; Han, J.; Kang, S.; Lee, J. R.; Jeong, G. J.; Kwon, S. P.; Song, S. Y.; Go, S.; Jung, M.; Hong, J.; Kim, B. S., M1 Macrophage-Derived Nanovesicles Potentiate the Anticancer Efficacy of Immune Checkpoint Inhibitors. *ACS Nano* **2018**, *12* (9), 8977-8993.
202. Wu, J. Y.; Li, Y. J.; Hu, X. B.; Huang, S.; Luo, S.; Tang, T.; Xiang, D. X., Exosomes and biomimetic nanovesicles-mediated anti-glioblastoma therapy: A head-to-head comparison. *J. Control. Release* **2021**, *336*, 510-521.
203. Jo, W.; Kim, J.; Yoon, J.; Jeong, D.; Cho, S.; Jeong, H.; Yoon, Y. J.; Kim, S. C.; Gho, Y. S.; Park, J., Large-scale generation of cell-derived nanovesicles. *Nanoscale* **2014**, *6* (20), 12056-64.

204. Go, G.; Lee, J.; Choi, D. S.; Kim, S. S.; Gho, Y. S., Extracellular Vesicle-Mimetic Ghost Nanovesicles for Delivering Anti-Inflammatory Drugs to Mitigate Gram-Negative Bacterial Outer Membrane Vesicle-Induced Systemic Inflammatory Response Syndrome. *Advanced healthcare materials* **2019**, 8 (4), e1801082.
205. He, Y.; Luo, L.; Liang, S.; Long, M.; Xu, H., Influence of probe-sonication process on drug entrapment efficiency of liposomes loaded with a hydrophobic drug. *International Journal of Polymeric Materials and Polymeric Biomaterials* **2019**, 68 (4), 193-197.
206. Kim, M. S.; Haney, M. J.; Zhao, Y.; Mahajan, V.; Deygen, I.; Klyachko, N. L.; Inskoe, E.; Piroyan, A.; Sokolsky, M.; Okolie, O.; Hingtgen, S. D.; Kabanov, A. V.; Batrakova, E. V., Development of exosome-encapsulated paclitaxel to overcome MDR in cancer cells. *Nanomedicine* **2016**, 12 (3), 655-664.
207. Wallach, D. F.; Soderberg, J.; Bricker, L., The phospholipides of Ehrlich ascites carcinoma cells: composition and intracellular distribution. *Cancer Res.* **1960**, 20, 397-402.
208. Hunter, M. J.; Commerford, S. L., Pressure homogenization of mammalian tissues. *Biochim. Biophys. Acta* **1961**, 47 (3), 580-586.
209. Wallach, D. F.; Kamat, V. B., PLASMA AND CYTOPLASMIC MEMBRANE FRAGMENTS FROM EHRLICH ASCITES CARCINOMA. *Proc. Natl. Acad. Sci. U. S. A.* **1964**, 52 (3), 721-8.
210. Birckbichler, P. J., Preparation of plasma membrane vesicles by nitrogen cavitation. *TCA manual / Tissue Culture Association* **1977**, 3 (3), 653-654.
211. Dowben, R. M.; Gaffey, A.; Lynch, P. M., Isolation of liver and muscle polyribosomes in high yield after cell disruption by nitrogen cavitation. *FEBS Lett.* **1968**, 2 (1), 1-3.
212. Snell, A. A.; Neupane, K. R.; McCorkle, J. R.; Fu, X.; Moonschi, F. H.; Caudill, E. B.; Kolesar, J.; Richards, C. I., Cell-Derived Vesicles for in Vitro and in Vivo Targeted Therapeutic Delivery. *ACS Omega* **2019**, 4 (7), 12657-12664.
213. Zhou, M.; Philips, M. R., Nitrogen Cavitation and Differential Centrifugation Allows for Monitoring the Distribution of Peripheral Membrane Proteins in Cultured Cells. *Journal of visualized experiments : JoVE* **2017**, (126).
214. Gottlieb, R. A.; Adachi, S., Nitrogen cavitation for cell disruption to obtain mitochondria from cultured cells. *Methods Enzymol.* **2000**, 322, 213-21.
215. Mantovani, A.; Biswas, S. K.; Galdiero, M. R.; Sica, A.; Locati, M., Macrophage plasticity and polarization in tissue repair and remodelling. Chichester, UK, 2013; Vol. 229, pp 176-185.
216. Hirayama, D.; Iida, T.; Nakase, H., The Phagocytic Function of Macrophage-Enforcing Innate Immunity and Tissue Homeostasis. *International journal of molecular sciences* **2017**, 19 (1).
217. Arango Duque, G.; Descoteaux, A., Macrophage cytokines: involvement in immunity and infectious diseases. *Frontiers in immunology* **2014**, 5 (491), 491-491.

218. Elhelu, M., The role of macrophages in immunology. *Journal of the National Medical Association* **1983**, 75 (3), 314-317.
219. Stout, R. D.; Suttles, J., Functional plasticity of macrophages: reversible adaptation to changing microenvironments. *Journal of Leukocyte Biology* **2004**, 76 (3), 509-513.
220. Mills, C. D.; Kincaid, K.; Alt, J. M.; Heilman, M. J.; Hill, A. M., M-1/M-2 macrophages and the Th1/Th2 paradigm. *Journal of immunology (Baltimore, Md. : 1950)* **2000**, 164 (12), 6166-6173.
221. Subhra, K. B.; Alberto, M., Macrophage plasticity and interaction with lymphocyte subsets: cancer as a paradigm. *Nature Immunology* **2010**, 11 (10), 889.
222. Sica, A.; Mantovani, A., Macrophage plasticity and polarization: in vivo veritas. *The Journal of clinical investigation* **2012**, 122 (3), 787-795.
223. Zhang, B.; Bailey, W. M.; Kopper, T. J.; Orr, M. B.; Feola, D. J.; Gensel, J. C., Azithromycin Drives Alternative Macrophage Activation and Improves Recovery and Tissue Sparing in Contusion Spinal Cord Injury. **2015**, 12 (217).
224. Cheng, H.; Wang, Z.; Fu, L.; Xu, T., Macrophage Polarization in the Development and Progression of Ovarian Cancers: An Overview. *Frontiers in oncology* **2019**, 9 (MAY), 421-421.
225. Ramanathan, S.; Jagannathan, N., Tumor associated macrophage: a review on the phenotypes, traits and functions. *Iranian journal of cancer prevention* **2014**, 7 (1), 1-8.
226. Sun, L.; He, C.; Nair, L.; Yeung, J.; Egwuagu, C. E., Interleukin 12 (IL-12) family cytokines: Role in immune pathogenesis and treatment of CNS autoimmune disease. *Cytokine* **2015**, 75 (2), 249-255.
227. Lin, Y.; Xu, J.; Lan, H., Tumor-associated macrophages in tumor metastasis: biological roles and clinical therapeutic applications. *Journal of hematology & oncology* **2019**, 12 (1), 76-76.
228. Anestakis, D.; Petanidis, S.; Kalyvas, S.; Nday, C.; Tsave, O.; Kioseoglou, E.; Salifoglou, A., Mechanisms and [Alpha]pplications of [Iota]nterleukins in Cancer Immunotherapy. *International Journal of Molecular Sciences* **2015**, 16 (1), 1691-1710.
229. Sgadari, C.; Angiolillo, A. L.; Tosato, G., Inhibition of Angiogenesis by Interleukin-12 Is Mediated by the Interferon-Inducible Protein 10. *Blood* **1996**, 87 (9), 3877-3882.
230. Sorensen, E. W.; Gerber, S. A.; Frelinger, J. G.; Lord, E. M., IL-12 suppresses vascular endothelial growth factor receptor 3 expression on tumor vessels by two distinct IFN- γ -dependent mechanisms. *The Journal of immunology (1950)* **2010**, 184 (4), 1858-1866.
231. Mantovani, A.; Marchesi, F.; Malesci, A.; Laghi, L.; Allavena, P., Tumour-associated macrophages as treatment targets in oncology. *Nature reviews. Clinical oncology* **2017**, 14 (7), 399-416.

232. Chang, Y.-C.; Chen, T.-C.; Lee, C.-T.; Yang, C.-Y.; Wang, H.-W.; Wang, C.-C.; Hsieh, S.-L., Epigenetic control of MHC class II expression in tumor-associated macrophages by decoy receptor 3. *Blood* **2008**, *111* (10), 5054-5063.
233. Baumgart, M.; Moos, V.; Schuhbauer, D.; Müller, B., Differential expression of major histocompatibility complex class II genes on murine macrophages associated with T cell cytokine profile and protective/suppressive effects. *Proceedings of the National Academy of Sciences of the United States of America* **1998**, *95* (12), 6936-6940.
234. Samuel, D.; Antje, K., Repertoire of microglial and macrophage responses after spinal cord injury. *Nature Reviews Neuroscience* **2011**, *12* (7), 388.
235. Greenhalgh, A. D.; David, S., Differences in the Phagocytic Response of Microglia and Peripheral Macrophages after Spinal Cord Injury and Its Effects on Cell Death. *The Journal of Neuroscience* **2014**, *34* (18), 6316-6322.
236. Kigerl, K. A.; Gensel, J. C.; Ankeny, D. P.; Alexander, J. K.; Donnelly, D. J.; Popovich, P. G., Identification of Two Distinct Macrophage Subsets with Divergent Effects Causing either Neurotoxicity or Regeneration in the Injured Mouse Spinal Cord. *Journal of Neuroscience* **2009**, *29* (43), 13435-13444.
237. Gensel, J. C.; Nakamura, S.; Guan, Z.; Rooijen, v. N.; Ankeny, D. P.; Popovich, P. G., Macrophages Promote Axon Regeneration with Concurrent Neurotoxicity. *Journal of Neuroscience* **2009**.
238. Gensel, J. C.; Zhang, B., Macrophage activation and its role in repair and pathology after spinal cord injury. *Brain Research* **2015**, *1619*, 1-11.
239. Brown, J. M.; Recht, L.; Strober, S., The Promise of Targeting Macrophages in Cancer Therapy. *Clinical cancer research : an official journal of the American Association for Cancer Research* **2017**, *23* (13), 3241-3250.
240. Novak, M. L.; Weinheimer-Haus, E. M.; Koh, T. J., Macrophage activation and skeletal muscle healing following traumatic injury. *Journal of Pathology* **2014**, *232* (3), 344-355.
241. Tariq, M.; Zhang, J.; Liang, G.; Ding, L.; He, Q.; Yang, B., Macrophage Polarization: Anti-Cancer Strategies to Target Tumor-Associated Macrophage in Breast Cancer. *Journal of Cellular Biochemistry* **2017**, *118* (9), 2484-2501.
242. Choo, Y. W.; Kang, M.; Kim, H. Y.; Han, J.; Kang, S.; Lee, J.-R.; Jeong, G.-J.; Kwon, S. P.; Song, S. Y.; Go, S.; Jung, M.; Hong, J.; Kim, B.-S., M1 Macrophage-Derived Nanovesicles Potentiate the Anticancer Efficacy of Immune Checkpoint Inhibitors. *ACS nano* **2018**, *12* (9), 8977-8993.
243. John, C. G.; Timothy, J. K.; Bei, Z.; Michael, B. O.; William, M. B., Predictive screening of M1 and M2 macrophages reveals the immunomodulatory effectiveness of post spinal cord injury azithromycin treatment. *Scientific Reports* **2017**, *7* (1).

244. Pitt, J. M.; André, F.; Amigorena, S.; Soria, J.-C.; Eggermont, A.; Kroemer, G.; Zitvogel, L., Dendritic cell-derived exosomes for cancer therapy. *The Journal of clinical investigation* **2016**, *126* (4), 1224-1232.
245. Antimisiaris, S. G.; Mourtas, S.; Marazioti, A., Exosomes and Exosome-Inspired Vesicles for Targeted Drug Delivery. *Pharmaceutics* **2018**, *10* (4).
246. Dong, X.; Gao, J.; Zhang, C. Y.; Hayworth, C.; Frank, M.; Wang, Z., Neutrophil Membrane-Derived Nanovesicles Alleviate Inflammation To Protect Mouse Brain Injury from Ischemic Stroke. *ACS nano* **2019**, *13* (2), 1272-1283.
247. Yurkin, S. T.; Wang, Z., Cell membrane-derived nanoparticles: emerging clinical opportunities for targeted drug delivery. *Nanomedicine* **2017**, *12* (16), 2007-2019.
248. Gensel, J. C.; Wang, Y.; Guan, Z.; Beckwith, K. A.; Braun, K. J.; Wei, P.; McTigue, D. M.; Popovich, P. G., Toll-Like Receptors and Dectin-1, a C-Type Lectin Receptor, Trigger Divergent Functions in CNS Macrophages. *J Neurosci* **2015**, *35* (27), 9966-76.
249. You, Q.; Gong, Q.; Han, Y.-Q.; Pi, R.; Du, Y.-J.; Dong, S.-Z., Role of miR-124 in the regulation of retinoic acid-induced Neuro-2A cell differentiation. *Neural Regeneration Research* **2020**, *15* (6), 1133-1139.
250. Au - Sandin, J. N.; Au - Aryal, S. P.; Au - Wilkop, T.; Au - Richards, C. I.; Au - Grady, M. E., Near Simultaneous Laser Scanning Confocal and Atomic Force Microscopy (Conpokal) on Live Cells. *JoVE* **2020**, (162), e61433.
251. Doyle, L. M.; Wang, M. Z., Overview of Extracellular Vesicles, Their Origin, Composition, Purpose, and Methods for Exosome Isolation and Analysis. *Cells* **2019**, *8* (7).
252. Choi, D.-S.; Kim, D.-K.; Kim, Y.-K.; Gho, Y. S., Proteomics of extracellular vesicles: Exosomes and ectosomes. Hoboken, 2015; Vol. 34, pp 474-490.
253. Kumar, A.; Dixit, C. K., *3 - Methods for characterization of nanoparticles*. Elsevier Ltd: 2017; p 43-58.
254. Tan, X.; Zhang, Y.; Wang, Q.; Ren, T.; Gou, J.; Guo, W.; Yin, T.; He, H.; Zhang, Y.; Tang, X., Cell-penetrating peptide together with PEG-modified mesostructured silica nanoparticles promotes mucous permeation and oral delivery of therapeutic proteins and peptides. *Biomaterials science* **2019**, *7* (7), 2934-2950.
255. Midekessa, G.; Godakumara, K.; Ord, J.; Viil, J.; Lättekivi, F.; Dissanayake, K.; Kopanchuk, S.; Rinken, A.; Andronowska, A.; Bhattacharjee, S.; Rinken, T.; Fazeli, A., Zeta potential of extracellular vesicles: toward understanding the attributes that determine colloidal stability. **2020**.
256. Gold, E. S.; Underhill, D. M.; Morrisette, N. S.; Guo, J.; McNiven, M. A.; Aderem, A., Dynamin 2 is required for phagocytosis in macrophages. *The Journal of experimental medicine* **1999**, *190* (12), 1849-1856.
257. De Camilli, P.; Takei, K.; McPherson, P. S., The function of dynamin in endocytosis. *Current Opinion in Neurobiology* **1995**, *5* (5), 559-565.

258. Sundborger, A. C.; Hinshaw, J. E., Regulating dynamin dynamics during endocytosis. *F1000prime reports* **2014**, *6*, 85-85.
259. Rappoport, J. Z.; Heyman, K. P.; Kemal, S.; Simon, S. M., Dynamics of Dynamin during Clathrin Mediated Endocytosis in PC12 Cells (Dynamin during Endocytosis). *PLoS ONE* **2008**, *3* (6), e2416.
260. Feng, D.; Zhao, W. L.; Ye, Y. Y.; Bai, X. C.; Liu, R. Q.; Chang, L. F.; Zhou, Q.; Sui, S. F., Cellular internalization of exosomes occurs through phagocytosis. *Traffic* **2010**, *11* (5), 675-87.
261. Kim, H.; Wang, S. Y.; Kwak, G.; Yang, Y.; Kwon, I. C.; Kim, S. H., Exosome-Guided Phenotypic Switch of M1 to M2 Macrophages for Cutaneous Wound Healing. *Advanced Science* **2019**, *6* (20), n/a-n/a.
262. Perry, V.; Teeling, J., Microglia and macrophages of the central nervous system: the contribution of microglia priming and systemic inflammation to chronic neurodegeneration. *Seminars in Immunopathology* **2013**, *35* (5), 601-612.
263. Kanazawa, M.; Ninomiya, I.; Hatakeyama, M.; Takahashi, T.; Shimohata, T., Microglia and Monocytes/Macrophages Polarization Reveal Novel Therapeutic Mechanism against Stroke. *International journal of molecular sciences* **2017**, *18* (10).
264. Kigerl, K. A.; Gensel, J. C.; Ankeny, D. P.; Alexander, J. K.; Donnelly, D. J.; Popovich, P. G., Identification of two distinct macrophage subsets with divergent effects causing either neurotoxicity or regeneration in the injured mouse spinal cord. *J Neurosci* **2009**, *29* (43), 13435-44.
265. Park, K. M.; Bowers, W. J., Tumor necrosis factor-alpha mediated signaling in neuronal homeostasis and dysfunction. *Cellular Signalling* **2010**, *22* (7), 977-983.
266. Williams, A.; Last, V.; Kempster, S.; Bate, C., Interferon- γ increases neuronal death in response to amyloid- β 1-42. *Journal of Neuroinflammation* **2006**, *3* (1), 7.
267. Conroy, S. M.; Nguyen, V.; Quina, L. A.; Blakely-Gonzales, P.; Ur, C.; Netzeband, J. G.; Prieto, A. L.; Gruol, D. L., Interleukin-6 produces neuronal loss in developing cerebellar granule neuron cultures. *Journal of Neuroimmunology* **2004**, *155* (1-2), 43-54.
268. Zhang, B.; Kopper, T. J.; Liu, X.; Cui, Z.; Van Lanen, S. G.; Gensel, J. C., Macrolide Derivatives Reduce Proinflammatory Macrophage Activation and Macrophage-Mediated Neurotoxicity. **2019**, *25* (5).
269. Zhu, L.; Dong, D.; Yu, Z.-L.; Zhao, Y.-F.; Pang, D.-W.; Zhang, Z.-L., Folate-Engineered Microvesicles for Enhanced Target and Synergistic Therapy toward Breast Cancer. *ACS applied materials & interfaces* **2017**, *9* (6), 5100-5108.
270. Théry, C.; Ostrowski, M.; Segura, E., Membrane vesicles as conveyors of immune responses. *Nature Reviews Immunology* **2009**, *9* (8), 581-593.
271. Sharma, S.; Rasool, H. I.; Palanisamy, V.; Mathisen, C.; Schmidt, M.; Wong, D. T.; Gimzewski, J. K., Structural-mechanical characterization of nanoparticle

- exosomes in human saliva, using correlative AFM, FESEM, and force spectroscopy. *ACS Nano* **2010**, *4* (4), 1921-6.
272. Ratajczak, J.; Wysoczynski, M.; Hayek, F.; Janowska-Wieczorek, A.; Ratajczak, M. Z., Membrane-derived microvesicles: important and underappreciated mediators of cell-to-cell communication. *Leukemia* **2006**, *20* (9), 1487-95.
273. Kim, D. K.; Kang, B.; Kim, O. Y.; Choi, D. S.; Lee, J.; Kim, S. R.; Go, G.; Yoon, Y. J.; Kim, J. H.; Jang, S. C.; Park, K. S.; Choi, E. J.; Kim, K. P.; Desiderio, D. M.; Kim, Y. K.; Lötvall, J.; Hwang, D.; Gho, Y. S., EVpedia: an integrated database of high-throughput data for systemic analyses of extracellular vesicles. *J Extracell Vesicles* **2013**, *2*.
274. Valadi, H.; Ekström, K.; Bossios, A.; Sjöstrand, M.; Lee, J. J.; Lötvall, J. O., Exosome-mediated transfer of mRNAs and microRNAs is a novel mechanism of genetic exchange between cells. *Nat. Cell Biol.* **2007**, *9* (6), 654-659.
275. Deng, W.; Chen, W.; Clement, S.; Guller, A.; Zhao, Z.; Engel, A.; Goldys, E. M., Controlled gene and drug release from a liposomal delivery platform triggered by X-ray radiation. *Nature Communications* **2018**, *9* (1), 2713.
276. Liu, P.; Chen, G.; Zhang, J., A Review of Liposomes as a Drug Delivery System: Current Status of Approved Products, Regulatory Environments, and Future Perspectives. *Molecules* **2022**, *27* (4).
277. Shen, J.; Sun, X.; Pan, B.; Cao, S.; Cao, J.; Che, D.; Liu, F.; Zhang, S.; Yu, Y., IL-17 induces macrophages to M2-like phenotype via NF- κ B. *Cancer Manag. Res.* **2018**, *10*, 4217-4228.
278. Zhang, L.; Wu, S.; Qin, Y.; Fan, F.; Zhang, Z.; Huang, C.; Ji, W.; Lu, L.; Wang, C.; Sun, H.; Leng, X.; Kong, D.; Zhu, D., Targeted Codelivery of an Antigen and Dual Agonists by Hybrid Nanoparticles for Enhanced Cancer Immunotherapy. *Nano letters* **2019**, *19* (7), 4237-4249.
279. Smith, A. A. A.; Gale, E. C.; Roth, G. A.; Maikawa, C. L.; Correa, S.; Yu, A. C.; Appel, E. A., Nanoparticles Presenting Potent TLR7/8 Agonists Enhance Anti-PD-L1 Immunotherapy in Cancer Treatment. *Biomacromolecules* **2020**, *21* (9), 3704-3712.
280. Moonschi, F. H.; Effinger, A. K.; Zhang, X.; Martin, W. E.; Fox, A. M.; Heidary, D. K.; DeRouchey, J. E.; Richards, C. I., Cell-Derived Vesicles for Single-Molecule Imaging of Membrane Proteins. *Angewandte Chemie (International ed.)* **2015**, *54* (2), 481-484.
281. Dostert, C.; Grusdat, M.; Letellier, E.; Brenner, D., The TNF family of ligands and receptors: Communication modules in the immune system and beyond. *Physiol. Rev.* **2019**, *99* (1), 115-160.
282. Deora, A.; Hegde, S.; Lee, J.; Choi, C. H.; Chang, Q.; Lee, C.; Eaton, L.; Tang, H.; Wang, D.; Lee, D.; Michalak, M.; Tomlinson, M.; Tao, Q.; Gaur, N.; Harvey, B.; McLoughlin, S.; Labkovsky, B.; Ghayur, T., Transmembrane TNF-dependent uptake of anti-TNF antibodies. *MAbs* **2017**, *9* (4), 680-695.

283. Liu, T.; Zhang, L.; Joo, D.; Sun, S.-C., NF- κ B signaling in inflammation. *Signal Transduction and Targeted Therapy* **2017**, 2 (1), 17023.
284. Maguire, O.; Collins, C.; O'Loughlin, K.; Miecznikowski, J.; Minderman, H., Quantifying nuclear p65 as a parameter for NF- κ B activation: Correlation between ImageStream cytometry, microscopy, and Western blot. *Cytometry. Part A : the journal of the International Society for Analytical Cytology* **2011**, 79 (6), 461-9.
285. Fantuzzi, L.; Belardelli, F.; Gessani, S., Monocyte/macrophage-derived CC chemokines and their modulation by HIV-1 and cytokines: A complex network of interactions influencing viral replication and AIDS pathogenesis. *Journal of leukocyte biology* **2003**, 74 (5), 719-725.
286. Gosset, P.; Tillie-Leblond, I.; Oudin, S.; Parmentier, O.; Wallaert, B.; Joseph, M.; Tonnel, A. B., Production of chemokines and proinflammatory and antiinflammatory cytokines by human alveolar macrophages activated by IgE receptors. *J. Allergy Clin. Immunol.* **1999**, 103 (2 Pt 1), 289-97.
287. Ruytinx, P.; Proost, P.; Van Damme, J.; Struyf, S., Chemokine-Induced Macrophage Polarization in Inflammatory Conditions. *Frontiers in Immunology* **2018**, 9.
288. Gschwandtner, M.; Derler, R.; Midwood, K. S., More Than Just Attractive: How CCL2 Influences Myeloid Cell Behavior Beyond Chemotaxis. *Frontiers in Immunology* **2019**, 10.
289. Li, M.; Sun, X.; Zhao, J.; Xia, L.; Li, J.; Xu, M.; Wang, B.; Guo, H.; Yu, C.; Gao, Y.; Wu, H.; Kong, X.; Xia, Q., CCL5 deficiency promotes liver repair by improving inflammation resolution and liver regeneration through M2 macrophage polarization. *Cell. Mol. Immunol.* **2020**, 17 (7), 753-764.
290. Wang, Q.; Ren, J.; Morgan, S.; Liu, Z.; Dou, C.; Liu, B., Monocyte Chemoattractant Protein-1 (MCP-1) regulates macrophage cytotoxicity in abdominal aortic aneurysm. *PloS one* **2014**, 9 (3), e92053-e92053.
291. Tokunaga, R.; Zhang, W.; Naseem, M.; Puccini, A.; Berger, M. D.; Soni, S.; McSkane, M.; Baba, H.; Lenz, H.-J., CXCL9, CXCL10, CXCL11/CXCR3 axis for immune activation – A target for novel cancer therapy. *Cancer Treat. Rev.* **2018**, 63, 40-47.
292. Yang, M.; Liu, J.; Piao, C.; Shao, J.; Du, J., ICAM-1 suppresses tumor metastasis by inhibiting macrophage M2 polarization through blockade of efferocytosis. *Cell Death Dis.* **2015**, 6 (6), e1780.
293. Krishnamachari, Y.; Salem, A. K., Innovative strategies for co-delivering antigens and CpG oligonucleotides. *Advanced drug delivery reviews* **2009**, 61 (3), 205-217.
294. Lai, C. Y.; Yu, G. Y.; Luo, Y.; Xiang, R.; Chuang, T. H., Immunostimulatory Activities of CpG-Oligodeoxynucleotides in Teleosts: Toll-Like Receptors 9 and 21. *Front. Immunol.* **2019**, 10, 179.

295. Bauer, S.; Kirschning, C. J.; Häcker, H.; Redecke, V.; Hausmann, S.; Akira, S.; Wagner, H.; Lipford, G. B., Human TLR9 confers responsiveness to bacterial DNA via species-specific CpG motif recognition. *2001*, 98 (16), 9237-9242.
296. Hemmi, H.; Takeuchi, O.; Kawai, T.; Kaisho, T.; Sato, S.; Sanjo, H.; Matsumoto, M.; Hoshino, K.; Wagner, H.; Takeda, K.; Akira, S., A Toll-like receptor recognizes bacterial DNA. *Nature* **2000**, 408 (6813), 740-5.
297. Sands, H.; Gorey-Feret, L. J.; Cocuzza, A. J.; Hobbs, F. W.; Chidester, D.; Trainor, G. L., Biodistribution and metabolism of internally 3H-labeled oligonucleotides. I. Comparison of a phosphodiester and a phosphorothioate. *Mol. Pharmacol.* **1994**, 45 (5), 932-943.
298. Wang, X.; Zhang, H.; Bai, M.; Ning, T.; Ge, S.; Deng, T.; Liu, R.; Zhang, L.; Ying, G.; Ba, Y., Exosomes Serve as Nanoparticles to Deliver Anti-miR-214 to Reverse Chemoresistance to Cisplatin in Gastric Cancer. *Molecular Therapy* **2018**, 26 (3), 774-783.
299. Théry, C.; Zitvogel, L.; Amigorena, S., Exosomes: composition, biogenesis and function. *Nature Reviews Immunology* **2002**, 2 (8), 569-579.
300. Kalluri, R.; LeBleu, V. S., The biology, function, and biomedical applications of exosomes. *Science* **2020**, 367 (6478).
301. van Niel, G.; D'Angelo, G.; Raposo, G., Shedding light on the cell biology of extracellular vesicles. *Nature Reviews Molecular Cell Biology* **2018**, 19 (4), 213-228.
302. Wang, J.; Chen, D.; Ho, E. A., Challenges in the development and establishment of exosome-based drug delivery systems. *J. Control. Release* **2021**, 329, 894-906.
303. Ye, J.; Yang, Y.; Dong, W.; Gao, Y.; Meng, Y.; Wang, H.; Li, L.; Jin, J.; Ji, M.; Xia, X.; Chen, X.; Jin, Y.; Liu, Y., Drug-free mannoseylated liposomes inhibit tumor growth by promoting the polarization of tumor-associated macrophages. *International journal of nanomedicine* **2019**, 14, 3203-3220.
304. Mout, R.; Ray, M.; Tay, T.; Sasaki, K.; Yesilbag Tonga, G.; Rotello, V. M., General Strategy for Direct Cytosolic Protein Delivery via Protein-Nanoparticle Co-engineering. *ACS Nano* **2017**, 11 (6), 6416-6421.
305. Mitragotri, S.; Burke, P. A.; Langer, R., Overcoming the challenges in administering biopharmaceuticals: formulation and delivery strategies. *Nature reviews. Drug discovery* **2014**, 13 (9), 655-72.
306. Gu, Z.; Biswas, A.; Zhao, M.; Tang, Y., Tailoring nanocarriers for intracellular protein delivery. *Chem. Soc. Rev.* **2011**, 40 (7), 3638-55.
307. Moonschi, F. H.; Hughes, C. B.; Mussman, G. M.; Fowlkes, J. L.; Richards, C. I.; Popescu, I., Advances in micro- and nanotechnologies for the GLP-1-based therapy and imaging of pancreatic beta-cells. *Acta Diabetol.* **2018**, 55 (5), 405-418.
308. Xiong, Q.; Lee, G. Y.; Ding, J.; Li, W.; Shi, J., Biomedical applications of mRNA nanomedicine. *Nano research* **2018**, 11 (10), 5281-5309.

309. Wang, Z.; Ling, L.; Du, Y.; Yao, C.; Li, X., Reduction responsive liposomes based on paclitaxel-ss-lysophospholipid with high drug loading for intracellular delivery. *Int. J. Pharm.* **2019**, *564*, 244-255.
310. Patel, S. G.; Sayers, E. J.; He, L.; Narayan, R.; Williams, T. L.; Mills, E. M.; Allemann, R. K.; Luk, L. Y. P.; Jones, A. T.; Tsai, Y. H., Cell-penetrating peptide sequence and modification dependent uptake and subcellular distribution of green florescent protein in different cell lines. *Sci. Rep.* **2019**, *9* (1), 6298.
311. Stewart, M. P.; Sharei, A.; Ding, X.; Sahay, G.; Langer, R.; Jensen, K. F., In vitro and ex vivo strategies for intracellular delivery. *Nature* **2016**, *538* (7624), 183-192.
312. Allen, T. M., Long-circulating (sterically stabilized) liposomes for targeted drug delivery. *Trends Pharmacol. Sci.* **1994**, *15* (7), 215-20.
313. Ha, D.; Yang, N.; Nadithe, V., Exosomes as therapeutic drug carriers and delivery vehicles across biological membranes: current perspectives and future challenges. *Acta pharmaceutica Sinica. B* **2016**, *6* (4), 287-96.
314. Green, A. E.; Rose, P. G., Pegylated liposomal doxorubicin in ovarian cancer. *International journal of nanomedicine* **2006**, *1* (3), 229-39.
315. Li, S. P.; Lin, Z. X.; Jiang, X. Y.; Yu, X. Y., Exosomal cargo-loading and synthetic exosome-mimics as potential therapeutic tools. *Acta Pharmacol. Sin.* **2018**, *39* (4), 542-551.
316. Wang, P.; Wang, H.; Huang, Q.; Peng, C.; Yao, L.; Chen, H.; Qiu, Z.; Wu, Y.; Wang, L.; Chen, W., Exosomes from M1-Polarized Macrophages Enhance Paclitaxel Antitumor Activity by Activating Macrophages-Mediated Inflammation. *Theranostics* **2019**, *9* (6), 1714-1727.
317. Zhao, Y.; Zheng, Y.; Zhu, Y.; Li, H.; Zhu, H.; Liu, T., Docetaxel-loaded M1 macrophage-derived exosomes for a safe and efficient chemoimmunotherapy of breast cancer. *Journal of Nanobiotechnology* **2022**, *20* (1), 359.
318. Aslan, C.; Kiaie, S. H.; Zolbanin, N. M.; Lotfinejad, P.; Ramezani, R.; Kashanchi, F.; Jafari, R., Exosomes for mRNA delivery: a novel biotherapeutic strategy with hurdles and hope. *BMC Biotechnol.* **2021**, *21* (1), 20.
319. Zhai, Y.; Su, J.; Ran, W.; Zhang, P.; Yin, Q.; Zhang, Z.; Yu, H.; Li, Y., Preparation and Application of Cell Membrane-Camouflaged Nanoparticles for Cancer Therapy. *Theranostics* **2017**, *7* (10), 2575-2592.
320. Gao, J.; Chu, D.; Wang, Z., Cell membrane-formed nanovesicles for disease-targeted delivery. *Journal of Controlled Release* **2016**, *224*, 208-216.
321. Parker, N.; Turk, M. J.; Westrick, E.; Lewis, J. D.; Low, P. S.; Leamon, C. P., Folate receptor expression in carcinomas and normal tissues determined by a quantitative radioligand binding assay. *Analytical Biochemistry* **2005**, *338* (2), 284-293.
322. Sudimack, J.; Lee, R. J., Targeted drug delivery via the folate receptor. *Advanced Drug Delivery Reviews* **2000**, *41* (2), 147-162.

323. Low, P. S.; Kularatne, S. A., Folate-targeted therapeutic and imaging agents for cancer. *Current Opinion in Chemical Biology* **2009**, *13* (3), 256-262.
324. Lu, Y.; Low, P. S., Folate-mediated delivery of macromolecular anticancer therapeutic agents. *Advanced Drug Delivery Reviews* **2012**, *64* (sS), 342-352.
325. Zhu, L.; Dong, D.; Yu, Z. L.; Zhao, Y. F.; Pang, D. W.; Zhang, Z. L., Folate-Engineered Microvesicles for Enhanced Target and Synergistic Therapy toward Breast Cancer. *ACS Appl Mater Interfaces* **2017**, *9* (6), 5100-5108.
326. Ceci, C.; Atzori, M. G.; Lacal, P. M.; Graziani, G., Targeting Tumor-Associated Macrophages to Increase the Efficacy of Immune Checkpoint Inhibitors: A Glimpse into Novel Therapeutic Approaches for Metastatic Melanoma. *Cancers (Basel)* **2020**, *12* (11).
327. Solinas, C.; Aiello, M.; Rozali, E.; Lambertini, M.; Willard-Gallo, K.; Migliori, E., Programmed cell death-ligand 2: A neglected but important target in the immune response to cancer? *Transl. Oncol.* **2020**, *13* (10), 100811.
328. Gordon, S. R.; Maute, R. L.; Dulken, B. W.; Hutter, G.; George, B. M.; McCracken, M. N.; Gupta, R.; Tsai, J. M.; Sinha, R.; Corey, D.; Ring, A. M.; Connolly, A. J.; Weissman, I. L., PD-1 expression by tumour-associated macrophages inhibits phagocytosis and tumour immunity. *Nature* **2017**, *545* (7655), 495-499.
329. Peng, P.; Yu, H.; Xing, C.; Tao, B.; Li, C.; Huang, J.; Ning, G.; Zhang, B.; Feng, S., Exosomes-mediated phenotypic switch of macrophages in the immune microenvironment after spinal cord injury. *Biomed. Pharmacother.* **2021**, *144*, 112311.
330. Liang, Z.-Y.; Xu, X.-J.; Rao, J.; Yang, Z.-L.; Wang, C.-H.; Chen, C.-M., Mesenchymal Stem Cell-Derived Exosomal MiRNAs Promote M2 Macrophages Polarization: Therapeutic Opportunities for Spinal Cord Injury. **2022**, *15*.
331. Cheng, Q.; Shi, X.; Han, M.; Smbatyan, G.; Lenz, H.-J.; Zhang, Y., Reprogramming Exosomes as Nanoscale Controllers of Cellular Immunity. *Journal of the American Chemical Society* **2018**, *140* (48), 16413-16417.
332. Romero, A.; Peri, F., Increasing the Chemical Variety of Small-Molecule-Based TLR4 Modulators: An Overview. **2020**, *11*.
333. Kelly, C.; Jefferies, C.; Cryan, S. A., Targeted liposomal drug delivery to monocytes and macrophages. *Journal of drug delivery* **2011**, *2011*, 727241.
334. Akuma, P.; Okagu, O. D.; Udenigwe, C. C., Naturally Occurring Exosome Vesicles as Potential Delivery Vehicle for Bioactive Compounds. **2019**, *3*.
335. Kibria, G.; Ramos, E. K.; Wan, Y.; Gius, D. R.; Liu, H., Exosomes as a Drug Delivery System in Cancer Therapy: Potential and Challenges. *Mol. Pharm.* **2018**, *15* (9), 3625-3633.
336. Altun, İ.; Sonkaya, A., The Most Common Side Effects Experienced by Patients Were Receiving First Cycle of Chemotherapy. *Iran J. Public Health* **2018**, *47* (8), 1218-1219.

VITA

Khaga Raj Neupane

Education

01/2013 – 01/2015 Tribhuvan University
 Kathmandu, Nepal
 Master of Science in Chemistry

Awards and Scholarships

08/2022 – 12/2022 Research Challenge Trust Fund Fellowship
08/2021 – 08/2022 100% Plus Award
01/2022 – 06/2022 Graduate Student Congress Research Award
01/2015 – 01/2016 Dr. Basant Bikram Gyana Shah Research Award

Scientific Publications

1. Schweer, D., Annabel, M., **Neupane, K.R.**, Richards, C.I., Ueland, F., Kolesar, J., “Tumor Associated Macrophages & Ovarian Cancer: Implications for Therapy” *Cancers*, 2022.
2. **Neupane, K. R.**, McCorkle, J.R., Kopper, T.J., Lakes, J., Aryal, S.P., Masud, A.A., Snell, A.A., Gensel, J.C., Kolesar, J., Richards, C.I., “Macrophage-Engineered vesicles for Therapeutic Delivery and Bidirectional Reprogramming of Immune Cell Polarization” *ACS Omega*, 6, no. 5, 2021, 3847 – 3857.
3. Aryal, S. P., Xu, F., Masud, A.A., **Neupane, K.R.**, Richards, C.I., “Characterization of Astrocyte Morphology and Function Using a Fast and Reliable Tissue Clearing Technique” *Bio-protocol*, 1, 2021, e279.
4. Masud, A. A., Moonschi, F., Xu, F., Calabro, R.L., Bernadeta, S., Collier, P., **Neupane, K.R.**, Kim, D.Y., and Richards, C.I., “Photoluminescence Enhancement, Blinking Suppression, and Improved Biexciton Quantum Yield of Single Quantum Dots in Zero Mode Waveguides” *The Journal of Physical Chemistry Letters*, 12, 13, 2021, 3303-3311.

5. Aryal, S. P., Xu, F., Masud A.A, **Neupane, K.R.**, Richards, C.I., “Single- Molecule Studies of Membrane Receptors from Brain Region Specific Nanovesicles” *Bio-protocol*, 11, 10, 2021, e4018.
6. Aryal, S.P., Xu, F., Sandin, J.N., **Neupane, K.R.**, Lakes, J.E., Grady, M.E., Richards, C.I., “Nicotine Induces Morphological and Functional Changes in Astrocytes via Nicotinic Receptor Activity”. *Glia*, 2021
7. Snell, A.A., **Neupane, K.R.**, McCorkle, J.R., Xu, F., Moonschi, F.H., Caudill, E.B., Kolesar J., and Richards C.I., “Cell-Derived Vesicles for in Vitro and in Vivo Targeted Therapeutic Delivery”. *ACS Omega*, 2019. 12657-12664